

The q_T and $\Delta\phi_{t\bar{t}}$ spectra in top-antitop hadroproduction at N^2LL+N^2LO :

the interplay of soft-collinear resummation and Coulomb singularities

Wan-Li Ju^(a,c), Marek Schönherr^(b)

^(a) INFN, Sezione di Milano, Via Celoria 16, 20133 Milano, Italy

^(b) Institute for Particle Physics Phenomenology, Durham University, Durham DH1 3LE, United Kingdom

^(c) Department of Physics, University of Alberta, Edmonton AB T6G 2J1, Canada

Emails: wju@ualberta.ca, marek.schoenherr@durham.ac.uk

Abstract: In this paper, we present the resummation-improved differential transverse momentum and azimuthal decorrelation cross sections, $d\sigma_{t\bar{t}}/dq_T$ and $d\sigma_{t\bar{t}}/d\Delta\phi_{t\bar{t}}$, in top-antitop pair production at the LHC. Our calculation is based on the observation that both cross sections are dominated by topologies where the top-quark pair is well separated, expressed in their relative velocity $\beta_{t\bar{t}} \sim \mathcal{O}(1)$, at colliding energies of $\sqrt{s} = 13$ TeV or higher. Therefore, the asymptotic behaviour in the limits $q_T \rightarrow 0$ and $\Delta\phi_{t\bar{t}} \rightarrow 0$ can mostly be captured by the soft and collinear resummation in the HQET+SCT framework. Nevertheless, starting at N²LL, Coulomb singularities emerge in the threshold regime, $\beta_{t\bar{t}} \rightarrow 0$, in both the hard sector and its evolution kernels, leading to unphysical results upon integration over the entire $\beta_{t\bar{t}}$ range. To this end, two prescriptions, dubbed the D- and R-prescription, are introduced to regularise these Coulomb singularities. They embody two fundamentally different methods to truncate the threshold enhanced terms, rendering their contribution finite. In the absence of a combined threshold and small-transverse-momentum resummation, we present a quantitative assessment of the ambiguity introduced by the choice of prescription, itself a test of the sensitivity of our calculation to such threshold enhancements, for both the $d\sigma_{t\bar{t}}/dq_T$ and $d\sigma_{t\bar{t}}/d\Delta\phi_{t\bar{t}}$ spectra.

Contents

1	Introduction	3
2	Theoretical details	5
2.1	Soft and collinear resummation in the domain $\Delta E_{t\bar{t}} \sim \mathcal{O}(m_t)$	5
2.2	Extending the resummation region – properties and caveats	9
2.3	Prescriptions to extend the resummation region	17
2.3.1	D-prescription: Resummation with a decomposed Sudakov factor	17
2.3.2	R-prescription: Resummation with a re-exponentiated anomalous dimension	20
2.4	Matching to fixed-order QCD	24
3	Numerical Results	24
3.1	Input parameters	24
3.2	Validation	25
3.3	Resummation-improved q_T and $\Delta\phi_{t\bar{t}}$ distributions	29
4	Conclusions	31
A	Comparison of D- and R-prescriptions in the double differential distributions	32
B	Numerical results of hard-scale evolution kernel	33
C	Definitions of the color and helicity bases	35

1 Introduction

The investigation of top-antitop pair ($t\bar{t}$) production at hadron colliders has drawn both experimental and theoretical attention in the past decades. This has facilitated the precise determination of the top quark mass m_t as an input parameter of the Standard Model (SM) as well as the exploration of many possible new physics scenarios. In the recent experiments carried out at Large Hadron Collider (LHC), the total cross sections of the top-antitop pair hadroproduction have been measured at a variety of colliding energies, for instance, $\sqrt{s} = 5.02$ TeV [1–4], 7 TeV [5–12], 8 TeV [6, 8, 9, 11–16], 13 TeV [17–25], and 13.6 TeV [26, 27]. In addition, many properties of the final state have been measured in single and double-differential distributions [14, 15, 17, 21, 28–49], among them the transverse momentum q_T of the $t\bar{t}$ system, its invariant mass $M_{t\bar{t}}$ or the separation in the azimuthal plane $\Delta\Phi_{t\bar{t}}$. Simultaneously, precise theoretical predictions were developed and the first NLO accurate calculations, including first-order QCD corrections, became available over 30 years ago [50–53]. More recently, the precision of the theoretical predictions has been further increased by including second-order corrections at N²LO accuracy in QCD [54–64] and first-order NLO electroweak (EW) effects [58, 65–74]. Alongside, corrections to top-quark decays and off-shell corrections were included [63, 75–81]. Even though these fixed-order results are able to describe the production cross sections in the majority of the phase space, considerable corrections can emerge in particular kinematic limits from all orders in the perturbative series underpinning these calculations, calling for resummation techniques to improve the perturbative convergence and, in turn, provide reliable theoretical predictions. Existing research in this context comprises soft-gluon resummation in $t\bar{t}$ production [82–94], the Coulomb resummation around $M_{t\bar{t}} \rightarrow 2m_t$ [95–98] with a generic transverse recoil against the $t\bar{t}$ system, the combined resummation of Coulomb and soft-gluon corrections [99–103], and the resummation of soft and collinear parton emissions [104–110] in the small transverse recoil region. Parton-shower matched predictions at the highest fixed-order precision can be found in [111–113].

In this work we will continue to study the resummation of QCD logarithms in the process $pp \rightarrow t\bar{t} + X$ and put particular emphasis on the asymptotic regions $q_T \rightarrow 0$ and $\Delta\Phi_{t\bar{t}} \rightarrow \pi$. The azimuthally averaged distribution $d\sigma_{t\bar{t}}/dq_T$ is an observable that is free of any azimuthally asymmetric divergences [107]. It thus allows for a systematic resummation of the asymptotic behaviour of each perturbative order by means of exponentiating

the logarithmic contributions in impact-parameter space, akin to the corresponding procedure in the Drell-Yan process [114–134] or Higgs hadroproduction [124, 127, 135–146]. In the existing literature, focusing on the leading singular contributions in low q_T domain, such a logarithmic exponentiation has been presented in [104, 105], through a combination of the Soft-Collinear Effective Theory (SCET) [147–156] with the Heavy-Quark Effective Theory (HQET) [157–160], as well as using a generalised CSS approach in [106–108]. Moreover, a second class of observables, the projected transverse momentum spectra $d\sigma_{t\bar{t}}/dq_T$, were proposed in [110] to remove any azimuthally asymmetric contributions, where $q_T \equiv |\vec{q}_T \cdot \vec{\tau}|$ represents the magnitude of the projection of \vec{q}_T onto a reference unit vector $\vec{\tau}$ in the transverse plane. Choosing this reference vector $\vec{\tau}$ perpendicular to the top quark spatial momentum, $d\sigma_{t\bar{t}}/dq_T$ can be related to the azimuthal decorrelation $d\sigma_{t\bar{t}}/d\Delta\Phi_{t\bar{t}}$ between the top and antitop quarks. This observable has been of particular interest in recent measurements at the LHC [36, 37], where it was observed that fixed-order calculations generally exhibited significant theoretical uncertainties in the vicinity of $\Delta\Phi_{t\bar{t}} \rightarrow \pi$, demanding the inclusion and resummation of the dominant higher-order corrections.

In addition, Coulomb divergences appear in the physical region of top-quark pair production in the vicinity of their production threshold [95–103], characterised through $\beta_{t\bar{t}} = 0$ or $\Delta E_{t\bar{t}} = 0$, with the relative velocity $\beta_{t\bar{t}} \equiv \sqrt{1 - 4m_t^2/M_{t\bar{t}}^2}$ and the energy separation $\Delta E_{t\bar{t}} \equiv M_{t\bar{t}} - 2m_t$. This Coulomb divergence has the potential to formally spoil the perturbative convergence of the above SCET+HQET resummed calculation. In [110], in order to remove the thus afflicted region from our consideration, a lower bound on the top-antitop-pair invariant mass, $M_{t\bar{t}} \geq 400 \text{ GeV}$, was introduced. In the following, we will explore methods to lift this kinematic constraint, so as to extend our resummation to encompass the whole $t\bar{t}$ production phase space. Meanwhile, as the leading singular terms as $q_T \rightarrow 0$ and $\Delta\Phi_{t\bar{t}} \rightarrow \pi$ are driven by the same dynamic modes, we will also generalise the resummation formalism in [110] through an adapted multipole expansion procedure to access $d\sigma_{t\bar{t}}/dq_T$ itself.

Ideally, the overlap of Coulomb divergences and divergences of soft-collinear origin calls for a combined resummation to study the q_T and $\Delta\Phi_{t\bar{t}}$ spectra near the threshold regime. In terms of combining SCET and potential non-relativistic QCD (pNRQCD) [161–164] (or, alternatively, velocity non-relativistic QCD, vNRQCD [165–169]), such a resummation at leading-logarithmic (LL) accuracy primarily entails the products of LO Green function [101, 163, 164, 170], the tree-level amplitudes for the hard processes, and the Sudakov factor consisting of the cusp anomalous dimensions at LO. Even though the leading threshold enhancements induced by Coulomb interactions can be resummed at such an accuracy, it limits the perturbative corrections of soft and collinear radiation to its lowest order at leading power, thereby neglecting crucial known higher-order corrections that have been embedded in the earlier works [104, 105, 110]. Owing to the superrenormalisable nature of the Coulomb vertices [99, 171], beyond-LL precision involves both leading and sub-leading power perturbative contributions from the soft-collinear sector, in analogy with the combination of soft and Coulomb resummation [100, 101, 103, 172]. In recent years, a lot of effort has been devoted to calculate subleading power contributions to the q_T spectrum in colour-singlet hadroproduction [173–188], while results for coloured heavy partons processes have still to appear. In addition, off-shell top quarks effects will become relevant if the top-antitop quark pair invariant mass is lowered further, $M_{t\bar{t}} \leq 2m_t$. They have been investigated in lepton collider environments in the vicinity of the $t\bar{t}$ production threshold [189–196]. Generalising these calculations to a hadron collider, however, involves further complexity due to the jet-like nature of the final state, necessitating the use of jet algorithms for event selection. This introduces the non-global dynamics [197–199] into the problem, structurally changing the factorisation formulae derived in [110].

Therefore, choosing a pragmatic approach aiming for a phenomenological appraisal of both the q_T and $\Delta\Phi_{t\bar{t}}$ spectra, we will employ ad hoc prescriptions to achieve a meaningful soft-collinear resummation in the presence of Coulomb divergences. The expectation is that for the process $pp \rightarrow t\bar{t} + X$ taking place at a colliding energy $\sqrt{s} = 13 \text{ TeV}$, the bulk of events are produced well above the $t\bar{t}$ production threshold in the domain $M_{t\bar{t}} \geq 400 \text{ GeV}$ where $\beta_{t\bar{t}} \sim \mathcal{O}(1)$ or $\Delta E_{t\bar{t}} \sim \mathcal{O}(m_t)$. Here, the top and antitop quarks are kinematically well separated and the dynamics behind the asymptotic behaviour are captured entirely by SCET and HQET. Then, extending the coverage of the QCD resummation established in this domain to the whole phase space including the threshold region, using such an ad hoc prescription, can serve as a rapid and reasonable estimation for the single differential observables $d\sigma_{t\bar{t}}/dq_T$ and $d\sigma_{t\bar{t}}/d\Delta\Phi_{t\bar{t}}$ without its details having a major impact when integrated over the entire invariant mass range. Such a methodology has been extensively applied in existing calculations on the total cross section of the processes $pp \rightarrow t\bar{t} + X$ [88, 92, 200–202], $pp \rightarrow t\bar{t}B(B = H, Z, W^\pm) + X$ [203–208], and $pp \rightarrow t\bar{t}t\bar{t} + X$ [209].

However, extending the resummation phase space to include the threshold regime, $M_{t\bar{t}} \geq 2m_t$, is not always straightforward in a SCET+HQET based resummation. To be precise, the resummation in the well-separated region [110] features the products of the fixed-order sectors, including hard, soft, and beam-collinear functions, as well as their corresponding scale evolution kernels. In this work, we will demonstrate that, starting from next-to-next-to leading logarithmic order (N²LL), taking the threshold limit $\beta_{t\bar{t}} \rightarrow 0$ of those ingredients will develop cubic and quadratic divergences in the triple differential cross sections $d^3\sigma_{t\bar{t}}/(d\beta_{t\bar{t}}dY_{t\bar{t}}dq_T)$ and $d^3\sigma_{t\bar{t}}/(d\beta_{t\bar{t}}dY_{t\bar{t}}d\Delta\Phi_{t\bar{t}})$, respectively. This, in turn, leads to a diverging phase space integration in evaluating $d\sigma_{t\bar{t}}/dq_T$ and $d\sigma_{t\bar{t}}/d\Delta\Phi_{t\bar{t}}$ without further regularisation on the threshold enhancements.

To this end, in this paper, we introduce two ad hoc prescriptions to treat this problem. Their derivation is based on the observation that in using the expanded solution of the hard RGE [210,211] the main driver for the threshold divergences are the non-logarithmic products of the hard scale evolution kernels, contributing $\mathcal{O}(\beta_{t\bar{t}}^{-4})$ in the limit of $\beta_{t\bar{t}} \rightarrow 0$. Ideally, this behaviour can be mitigated by implementing the exact solution of the hard RGE. However, in presence of soft colour correlations, such an exact solution necessitates the path-ordered integration over a set of threshold-enhanced colour matrices. Unfortunately, neither an analytically compact expression nor a numerical approximation via Taylor expansion is straightforward. Hence, akin to [88, 104, 105, 109, 206], we first introduce the ‘‘decomposition (D) prescription’’, in which the threshold-singular contributions at N²LL are, in part, shifted to a higher logarithmic accuracy at the cost of mild corrections in the domain $\beta_{t\bar{t}} \sim \mathcal{O}(1)$. It allows a smooth and consistent extrapolation to the threshold area $\beta_{t\bar{t}} \rightarrow 0$. On the other hand, we will also introduce the ‘‘re-exponentiation (R) prescription’’. In spite of the difficulties in determining a rigorous solution of hard RGE for a generic $\beta_{t\bar{t}}$, we will demonstrate that solving hard RGE can be substantially simplified in the vicinity of $\beta_{t\bar{t}} = 0$. This is thanks to the fact that up to two-loop level the leading threshold divergences all reside in the diagonal entries of the hard anomalous dimensions [212, 213]. Consequently, the leading singular behaviour of the hard anomalous dimensions can be exponentiated by solving an approximate hard RGE. The resulting resummation kernels in the R-prescription present intensively oscillatory but integrable behaviour in the limit $\beta_{t\bar{t}} \rightarrow 0$. Due to the fact that in these prescriptions, the threshold enhanced series are truncated in two radically different approaches, comparing their outcome can deliver a quantitative assessment on the dependence of $d\sigma_{t\bar{t}}/dq_T$ and $d\sigma_{t\bar{t}}/d\Delta\Phi_{t\bar{t}}$ on the ad hoc prescriptions and in turn unveil their sensitivity to the higher order Coulomb interactions.

The paper is structured as follows. In Sec. 2 we start with a brief review of the soft-collinear resummation on the q_T and $\Delta\Phi_{t\bar{t}}$ spectra for the well-separated region, thereby specifying the fixed-order ingredients and anomalous dimensions comprised up to N²LL. Then, Sec. 2.2 is devoted to an analysis of the asymptotic behaviour of HQET and SCET based resummation in the vicinity of $\beta_{t\bar{t}} \rightarrow 0$, from which we raise the concern over the integrability of the resummation kernel at N²LL. In turn, we propose the two ad hoc prescriptions discussed above in Sec. 2.3 to mitigate the arising threshold singularities before we match the resummed q_T and $\Delta\Phi_{t\bar{t}}$ distributions to the exact fixed-order calculations in Sec. 2.4. With our framework in place, we deliver a numeric evaluation in Sec. 3. Therein, we will at first validate the perturbative expansion of our resummed results by comparing against the q_T and $\Delta\Phi_{t\bar{t}}$ distribution computed in the full theory in three different $M_{t\bar{t}}$ slices, i.e. the threshold domain $M_{t\bar{t}} \in [2m_t, 360]$ GeV, the transitional region $M_{t\bar{t}} \in [360, 400]$ GeV, and the well-separated realm $M_{t\bar{t}} \geq 400$ GeV. Finally, we present our final resummation improved q_T and $\Delta\Phi_{t\bar{t}}$ distributions at N²LL+N²LO accuracy using both the D- and R-schemes before concluding this work in Sec. 4.

2 Theoretical details

2.1 Soft and collinear resummation in the domain $\Delta E_{t\bar{t}} \sim \mathcal{O}(m_t)$

From the QCD factorisation theorem [214], the differential cross section of a generic observable \mathcal{Q} for the process $pp \rightarrow t\bar{t} + X$ can be expressed as,

$$\frac{d^3\sigma_{t\bar{t}}}{dM_{t\bar{t}}^2 dY_{t\bar{t}} d\mathcal{Q}} = \sum_{\text{sign}[P_t^z]} \frac{1}{16s(2\pi)^6} \int d^2\vec{P}_t^\perp d^2\vec{q}_T \delta[\mathcal{Q} - \mathcal{F}_{\mathcal{Q}}] \frac{\Sigma_{t\bar{t}}}{M_T^{t\bar{t}} |P_t^z|}, \quad (2.1)$$

where s denotes collider energy and will be taken to be 13 TeV throughout our investigation. \vec{P}_t^\perp stands for the transverse momentum of the top quark measured in the laboratory reference frame (LRF), while P_t^z

marks its longitudinal components detected from the z -direction rest frame (z RF) of the top-antitop pair. Further, \vec{q}_T , $M_{t\bar{t}}$, and $Y_{t\bar{t}}$ represent the transverse momentum, invariant mass and pseudo-rapidity of the $t\bar{t}$ system in LRF, respectively, from which the transverse mass of the top-antitop pair can be expressed as

$$M_{t\bar{t}}^T = \sqrt{M_{t\bar{t}}^2 + q_T^2}. \quad (2.2)$$

\mathcal{Q} in Eq. (2.1) refers to the observable, which can be evaluated via its definition function $\mathcal{F}_{\mathcal{Q}}$. $\mathcal{F}_{\mathcal{Q}}$ takes the following form for the observables of interest in the present paper,

$$\begin{aligned} \mathcal{Q} &= q_T, & \mathcal{F}_{\mathcal{Q}} &= |\vec{q}_T|, \\ \mathcal{Q} &= \Delta\phi_{t\bar{t}} \equiv \pi - \Delta\Phi_{t\bar{t}}, & \mathcal{F}_{\mathcal{Q}} &= \pi - \arccos \left[\frac{\vec{P}_t^\perp \cdot \vec{P}_{\bar{t}}^\perp}{|\vec{P}_t^\perp| |\vec{P}_{\bar{t}}^\perp|} \right]. \end{aligned} \quad (2.3)$$

Here, \vec{P}_t^\perp stands for the transverse momenta of the antitop quark in the LRF, satisfying $\vec{P}_{\bar{t}}^\perp = \vec{q}_T - \vec{P}_t^\perp$. $\Delta\Phi_{t\bar{t}}$ measures the azimuthal separation of the top and antitop quarks in the transverse plane.

At last, $\Sigma_{t\bar{t}}$ in Eq. (2.1) collects the contributions from all participating partonic processes,

$$\begin{aligned} \Sigma_{t\bar{t}} &= \sum_{i,j} \int_0^1 \frac{dx_n}{x_n} \frac{dx_{\bar{n}}}{x_{\bar{n}}} f_{i/N}(x_n) f_{j/\bar{N}}(x_{\bar{n}}) \sum_{r=0}^{\infty} \int \left[\prod_{m=1}^r \frac{d^3\vec{k}_m}{(2\pi)^3 2E_{k_m}} \right] \overline{\sum_{\text{hel,col}}} |\mathcal{M}(i+j \rightarrow t+\bar{t}+X)|^2 \\ &\quad \times (2\pi)^4 \delta^4 \left(p_i + p_j - P_t - P_{\bar{t}} - \sum_{m=0}^r k_m \right), \end{aligned} \quad (2.4)$$

where the $f_{i/N}(x)$ is the parton distribution function (PDF) for parton i with the momentum fraction x from proton N , and E_{k_m} and \vec{k}_m are the energy and spatial momentum of the m -th emitted parton, respectively. \mathcal{M} evaluates the transition amplitude of the occurring partonic scattering $i+j \rightarrow t+\bar{t}+X$, with $\{i, j\} \in [u, \bar{u}, d, \bar{d}, s, \bar{s}, c, \bar{c}, b, \bar{b}, g]$, in line with the 5 active flavour scheme.

Substituting Eq. (2.4) into Eq. (2.1), we can now appraise the q_T and $\Delta\phi_{t\bar{t}}$ spectra on the fixed-order level. Although such a calculation delivers satisfactory predictions in most phase space regions, it converges poorly as $q_T \rightarrow 0$ or $\Delta\phi_{t\bar{t}} \rightarrow 0$ due to the occurrence of large logarithmic corrections to all orders. Thus, a resummation of this asymptotic behaviour is mandated.

In the domain where the top and antitop quarks are kinematically well-separated, i.e.

$$\Delta E_{t\bar{t}} \equiv M_{t\bar{t}} - 2m_t \sim \mathcal{O}(m_t), \quad (2.5)$$

the factorisation and resummation of the azimuthally averaged distribution $d\sigma_{t\bar{t}}/dq_T$ have been investigated in different approaches, including the EFT-based analysis [104, 105] and the generalized CSS framework [106–108, 215]. It is demonstrated that (at least) the leading singular behaviour of the q_T distribution is predominantly driven by the hard, soft and beam-collinear domains in the loop and phase space integrations. This conclusion has been extensively applied in fixed order calculations [59, 60, 63, 64, 215–220] and also their combination with parton showers [111, 112, 221, 222].

Recently, to further investigate the top-antitop-pair dynamics, the differential distribution of the projected transverse momentum $d\sigma_{t\bar{t}}/dq_\tau$ was computed in [110], where q_τ signifies the projection of \vec{q}_T onto a reference unit vector $\vec{\tau}$ on the azimuthal plane, from which the $\Delta\phi_{t\bar{t}}$ spectrum can be derived by choosing $\vec{\tau}$ perpendicular to the flight direction of (anti)top quark. At variance with the small q_T region, which imposes constraints on both components of \vec{q}_T , the asymptotic regime $q_\tau \rightarrow 0$ or $\Delta\phi_{t\bar{t}} \rightarrow 0$ concerns only the longitudinal projection $q_\tau = |\vec{q}_T \cdot \vec{\tau}|$, leaving the transverse part unresolved. To probe the dynamic modes for the transverse component, in [110], employing the method of expansion of dynamic regions [223–226] as well as the SCET formalism [147–156], we enumerate the possible regions that can prompt energetic recoil against the top-antitop system, finding that assigning the label momenta to the transverse direction will incur an additional suppression from the phase space by at least one power of $\lambda_\tau \equiv q_\tau/M_{t\bar{t}}$, such that the leading singular behaviour of $d\sigma_{t\bar{t}}/dq_\tau$ is also captured by the hard, soft and beam-collinear regions, akin to the q_T resummation in [104–106].

Given their common dynamic regions that preside over the leading singular contributions¹, we can utilise a uniform framework to compute the resummed expressions for both the q_T and $\Delta\phi_{t\bar{t}}$ distributions. Within the

¹As far as we know, this coincidence only takes place in the leading power factorisation and resummation, since without

context of SCET_{II} [154–156] and HQET [157–160], both of them comprise the resummed partonic function,

$$\Sigma_{t\bar{t}}^{\text{res}} = \frac{8\pi^2}{M_{t\bar{t}}^2} \sum_{\kappa} \int d^2\vec{b}_T \exp\left(i\vec{b}_T \cdot \vec{q}_T\right) \tilde{\Sigma}_{t\bar{t}}^{\text{res},[\kappa]}(\vec{b}_T, Y_{t\bar{t}}, M_{t\bar{t}}, \Omega_t), \quad (2.6)$$

where κ runs over $\{g_n g_{\bar{n}}, q_n^i \bar{q}_{\bar{n}}^j, \bar{q}_{\bar{n}}^i q_n^j\}$, enumerating the active initial-state parton-pairs contributing to the hard kernels, with $i, j \in \{u, d, c, s, b\}$ specifying the flavour of the quark fields. $\tilde{\Sigma}_{t\bar{t}}^{\text{res},[\kappa]}$ collects the partonic contribution after Fourier transforming it into impact-parameter space, which is in general a function of the impact parameter \vec{b}_T , the pseudorapidity $Y_{t\bar{t}}$, the invariant mass $M_{t\bar{t}}$, and the solid angle Ω_t of the top quark measured in the rest reference frame of $t\bar{t}$ system. $\tilde{\Sigma}_{t\bar{t}}^{\text{res},[\kappa]}$ is formally related to the choice of the scheme regularising the rapidity divergences. In the following, we will use the soft and beam functions evaluated within the exponential regulator as proposed in [238, 239]. Alternative choices can also be found in [104, 105, 240–242] calculated via analytic rapidity regulator [243], and in [216, 244–246] using a generalised CSS method [106]. It follows that,

$$\begin{aligned} & \tilde{\Sigma}_{t\bar{t}}^{\text{res},[q_n^i \bar{q}_{\bar{n}}^j]}(\vec{b}_T, Y_{t\bar{t}}, M_{t\bar{t}}, \Omega_t) \\ &= \left(\frac{1}{2N_c}\right)^2 \mathcal{D}_{[q_n^i \bar{q}_{\bar{n}}^j]}^{\text{res}}(b_T, M_{t\bar{t}}, \mu_h, \mu_b, \mu_s, \nu_b, \nu_s) \mathcal{B}_n^{[q_n^i]}(\eta_n, b_T, \mu_b, \nu_b) \mathcal{B}_{\bar{n}}^{[\bar{q}_{\bar{n}}^j]}(\eta_{\bar{n}}, b_T, \mu_b, \nu_b) \\ & \sum_{\{\alpha, \beta, h\}} \left\{ \mathcal{S}_{[q_n \bar{q}_{\bar{n}}]}^{\alpha\beta}(\vec{b}_T, v_t, v_{\bar{t}}, \mu_s, \nu_s) \left[\mathcal{V}_{\alpha_1 \alpha_2}^{[q_n \bar{q}_{\bar{n}}]}(v_t, v_{\bar{t}}, \mu_s, \mu_h) \mathcal{C}_{\alpha_2; h_n h_{\bar{n}} h_t h_{\bar{t}}}^{[q_n \bar{q}_{\bar{n}}]} \right]^* \mathcal{V}_{\beta_1 \beta_2}^{[q_n \bar{q}_{\bar{n}}]}(v_t, v_{\bar{t}}, \mu_s, \mu_h) \right. \\ & \left. \mathcal{C}_{\beta_2; h_n h_{\bar{n}} h_t h_{\bar{t}}}^{[q_n \bar{q}_{\bar{n}}]} \right\}, \end{aligned} \quad (2.7)$$

and

$$\begin{aligned} & \tilde{\Sigma}_{t\bar{t}}^{\text{res},[g_n g_{\bar{n}}]}(\vec{b}_T, Y_{t\bar{t}}, M_{t\bar{t}}, \Omega_t) \\ &= \left(\frac{1}{N_c^2 - 1}\right)^2 \mathcal{D}_{[g_n g_{\bar{n}}]}^{\text{res}}(b_T, M_{t\bar{t}}, \mu_h, \mu_b, \mu_s, \nu_b, \nu_s) \sum_{\{\alpha, \beta, h, h'\}} \left\{ \mathcal{S}_{[g_n g_{\bar{n}}]}^{\alpha\beta}(\vec{b}_T, v_t, v_{\bar{t}}, \mu_s, \nu_s) \right. \\ & \times \mathcal{B}_{n, h'_n h_n}^{[g_n]}(\eta_n, \vec{b}_T, \mu_b, \nu_b) \mathcal{B}_{\bar{n}, h'_n h_{\bar{n}}}^{[g_{\bar{n}}]}(\eta_{\bar{n}}, \vec{b}_T, \mu_b, \nu_b) \left[\mathcal{V}_{\alpha_1 \alpha_2}^{[g_n g_{\bar{n}}]}(v_t, v_{\bar{t}}, \mu_s, \mu_h) \mathcal{C}_{\alpha_2; h'_n h'_n h_t h_{\bar{t}}}^{[g_n g_{\bar{n}}]} \right]^* \\ & \left. \times \mathcal{V}_{\beta_1 \beta_2}^{[g_n g_{\bar{n}}]}(v_t, v_{\bar{t}}, \mu_s, \mu_h) \mathcal{C}_{\beta_2; h_n h_{\bar{n}} h_t h_{\bar{t}}}^{[g_n g_{\bar{n}}]} \right\}, \end{aligned} \quad (2.8)$$

where the soft function is given by $\mathcal{S}_{[\kappa]}^{\alpha\beta}$ as a function of the impact parameter \vec{b}_T , the velocity $v_{t(\bar{t})}$ of the (anti)top quark, and the soft virtuality (rapidity) scale $\mu_s(\nu_s)$. To facilitate our calculations, we have projected the colour states of the soft function onto the orthonormal bases $c_{\{a_i\}}^{qq}$ and $c_{\{a_i\}}^{gg}$ of [247], leading to the colour indices $\{\alpha, \beta\}$ emerging as superscripts. Their expressions are presented in App. C. It is important to note that, heretofore, while the azimuthally averaged soft function have been calculated up to N²LO [240, 246], its fully azimuthal-angle-dependent form that are essential to compute the $\phi_{t\bar{t}}$ resummation are only available at NLO [110, 216].

Furthermore, Eqs. (2.7-2.8) include the hard functions $\mathcal{C}_{\alpha; h_n h_{\bar{n}} h_t h_{\bar{t}}}^{[q_n^i \bar{q}_{\bar{n}}^j]}$ and $\mathcal{C}_{\beta; h_n h_{\bar{n}} h_t h_{\bar{t}}}^{[g_n g_{\bar{n}}]}$ which consist of the UV-renormalized and IRC-subtracted amplitudes of the relevant hard partonic processes. Again, the $\{\alpha, \beta\}$ encode the colour states as in the soft function, while the tuple $\{h_n, h_{\bar{n}}, h_t, h_{\bar{t}}\}$ is introduced to specify the helicity states of the external particles. Throughout this work, the helicity bases of [248, 249] are taken as our default choice to evaluate the helicity projections and we present their expression in App. C. In calculating $\mathcal{C}_{\alpha; h_n h_{\bar{n}} h_t h_{\bar{t}}}^{[q_n^i \bar{q}_{\bar{n}}^j]}$ and $\mathcal{C}_{\beta; h_n h_{\bar{n}} h_t h_{\bar{t}}}^{[g_n g_{\bar{n}}]}$, the $\overline{\text{MS}}$ scheme is utilised to renormalise the UV divergences associated with the massless partons and the zero-momentum subtraction prescription [250] is employed to cope with those

accidental cancellations the central collinear mode can be relevant for $d\sigma_{t\bar{t}}/d\Delta\phi_{t\bar{t}}$ starting from the subleading power [110], whereas its participation in $d\sigma_{t\bar{t}}/dq_T$ is postponed to the sub-subleading power by its kinematics [110, 227, 228]. Analogously, structural similarities between Eqs. (2.6-2.8) and those governing resummation-improved azimuthal decorrelation of the jet-boson [229–233] and dijet [234–237] processes may also be limited to leading power, especially when the jets therein are defined exclusively.

pertaining to the (anti)top quarks. The remaining IRC singularities are removed following the procedures in [212]. Up to NLO, the automated program RECOLA [248, 249] is employed in this paper to extract the amplitudes of $q\bar{q} \rightarrow t\bar{t}$ and $gg \rightarrow t\bar{t}$ in all the helicity and colour configurations. The N²LO calculation are more involved. For now, the grid-based numerical results have been presented in [251], while the progress towards the full analytic evaluations are made in [252–255].

Next, Eqs. (2.7-2.8) also comprise the beam functions $\mathcal{B}_{n(\bar{n})}^{[q_n^i(\bar{n})]}$ and $\mathcal{B}_{n(\bar{n})}^{[g_n(\bar{n})]}$ governing the beam-collinear contributions along the $n(\bar{n})$ -direction. They are the functions of the virtuality (rapidity) scale $\mu_b(\nu_b)$ and the momentum fractions $\eta_n = M_{t\bar{t}} e^{Y_{t\bar{t}}}/\sqrt{s}$ and $\eta_{\bar{n}} = M_{t\bar{t}} e^{-Y_{t\bar{t}}}/\sqrt{s}$. In comparison with the quark beam function $\mathcal{B}_{n(\bar{n})}^{[q_n^i(\bar{n})]}$, the gluon case additionally depends on the gluon helicities $\{h_{n(\bar{n})}, h'_{n(\bar{n})}\} \in \{+, -\}$ to accommodate the helicity-flipping and helicity-conserving contributions. At present, the quark beam function, $\mathcal{B}_{n(\bar{n})}^{[q_n^i(\bar{n})]}$, and the helicity-conserving components of the gluon beam function, $\mathcal{B}_{n(\bar{n}),++}^{[g_n(\bar{n})]}$ and $\mathcal{B}_{n(\bar{n}),--}^{[g_n(\bar{n})]}$, have been calculated up to N³LO [256, 256–258], while the helicity-flipping entries $\mathcal{B}_{n(\bar{n}),+-}^{[g_n(\bar{n})]}$ and $\mathcal{B}_{n(\bar{n}),-+}^{[g_n(\bar{n})]}$ are only known on the N²LO level [143, 245, 258].

Finally, in addition to the above fixed-order contributions, Eqs. (2.7-2.8) contain the evolution kernels $\mathcal{D}_{[\kappa]}^{\text{res}}$ and $\mathcal{V}_{\alpha\beta}^{[\kappa]}$ as well. They bridge the gap between the intrinsic scales in the hard, soft, and beam-collinear contributions by resumming the occurring large logarithms and are derived by solving the respective R(a)GEs of the corresponding constituents [238, 239, 259, 260]. For instance, $\mathcal{D}_{[\kappa]}^{\text{res}}$ consists of the solutions of the beam-collinear R(a)GEs and the diagonal part of the hard RGEs, see [110],

$$\begin{aligned} & \ln \mathcal{D}_{[\kappa]}^{\text{res}}(b_T, M_{t\bar{t}}, \mu_h, \mu_b, \mu_s, \nu_b, \nu_s) \\ &= \int_{\mu_b^2}^{\mu_s^2} \frac{d\bar{\mu}^2}{\bar{\mu}^2} \left\{ C_{[\kappa]} \Gamma_{\text{cusp}}[\alpha_s(\bar{\mu})] \ln \left[\frac{\nu_b^2}{M_{t\bar{t}}^2} \right] + 2\gamma_b^{[\kappa]}[\alpha_s(\bar{\mu})] \right\} - \int_{\mu_h^2}^{\mu_s^2} \frac{d\bar{\mu}^2}{\bar{\mu}^2} \left\{ C_{[\kappa]} \Gamma_{\text{cusp}}[\alpha_s(\bar{\mu})] \ln \left[\frac{\bar{\mu}^2}{M_{t\bar{t}}^2} \right] \right\} \\ &+ C_{[\kappa]} \ln \left[\frac{\nu_s^2}{\nu_b^2} \right] \int_{\frac{b_0^2}{b_T^2}}^{\mu_s^2} \frac{d\bar{\mu}^2}{\bar{\mu}^2} \Gamma_{\text{cusp}}[\alpha_s(\bar{\mu})] - C_{[\kappa]} \ln \left[\frac{\nu_s^2}{\nu_b^2} \right] \gamma_r \left[\alpha_s \left(\frac{b_0}{b_T} \right) \right]. \end{aligned} \quad (2.9)$$

Therein, Γ_{cusp} , $\gamma_b^{[\kappa]}$, and γ_r denote the cusp anomalous dimension, the non-cusp anomalous dimension associated with the virtuality divergences in the beam functions, and the non-cusp anomalous dimension of the rapidity renormalisation. All their expressions up to N⁴LO are already available in the literature [261–264] and [238, 239, 256–258, 265–271], respectively. In writing Eq. (2.9), the following abbreviations are employed for the corresponding colour factor in QCD,

$$\kappa \in \{g_n g_{\bar{n}}\} : C_{[\kappa]} = C_A, \quad \kappa \in \{q_n^i \bar{q}_{\bar{n}}^j, q_{\bar{n}}^i \bar{q}_n^j\} : C_{[\kappa]} = C_F, \quad (2.10)$$

as well as the non-cusp anomalous dimensions,

$$\kappa \in \{g_n g_{\bar{n}}\} : \gamma_b^{[\kappa]} = \gamma_b^{[g]}, \quad \kappa \in \{q_n^i \bar{q}_{\bar{n}}^j, q_{\bar{n}}^i \bar{q}_n^j\} : \gamma_b^{[\kappa]} = \gamma_b^{[q]}. \quad (2.11)$$

Complementarily, the $\mathcal{V}_{\alpha\beta}^{[\kappa]}$ are in charge of the non-cusp hard anomalous dimension $\gamma_h^{[\kappa]}$ [212, 213]. Up to NLL, the $\mathcal{V}_{\alpha\beta}^{[\kappa]}$ can be derived by solving the RGE of the hard function in the diagonal colour space [88, 210, 211],

$$\mathbf{V}_h^{[\kappa]}(v_t, v_{\bar{t}}, \mu_s, \mu_h) \Big|_{\text{NLL}} = \mathbf{R}_{[\kappa]}^{-1} \exp \left\{ \frac{\mathbf{r}_h^{[\kappa],(0)}}{2\beta_0} \ln \left[\frac{\alpha_s(\mu_h)}{\alpha_s(\mu_s)} \right] \right\} \mathbf{R}_{[\kappa]}, \quad (2.12)$$

where $\mathbf{V}_h^{[\kappa]}$ is the matrix representation of $\mathcal{V}_{\alpha\beta}^{[\kappa]}$. $\mathbf{r}_h^{[\kappa],(0)}$ stands for the diagonalised one-loop non-cusp anomalous dimension of the hard function, by means of the invertible transformation matrix $\mathbf{R}_{[\kappa]}$. α_s denotes the strong coupling evaluated in the $N_F = 5$ flavour scheme, with the according anomalous dimension β_k at $(k+1)$ -loop accuracy.

This approach can also be generalized to N²LL by including the off-diagonal entries of the two-loop hard

anomalous dimensions as appropriate [210, 211], i.e.,

$$\begin{aligned} & \mathbf{V}_h^{[\kappa]}(v_t, v_{\bar{t}}, \mu_s, \mu_h) \Big|_{\text{N}^2\text{LL}} \\ &= \mathbf{R}_{[\kappa]}^{-1} \left[\mathbf{I} + \frac{\alpha_s(\mu_s)}{4\pi} \mathbf{J}^{[\kappa]} \right] \exp \left\{ \frac{\mathbf{r}_h^{[\kappa],(0)}}{2\beta_0} \ln \left[\frac{\alpha_s(\mu_h)}{\alpha_s(\mu_s)} \right] \right\} \left[\mathbf{I} - \frac{\alpha_s(\mu_h)}{4\pi} \mathbf{J}^{[\kappa]} \right] \mathbf{R}_{[\kappa]}, \end{aligned} \quad (2.13)$$

where the matrix $\mathbf{J}^{[\kappa]}$ is introduced here to take in the two loop ingredients,

$$\mathbf{J}_{ij}^{[\kappa]} = \mathbf{r}_{h,ii}^{[\kappa],(0)} \delta_{ij} \frac{\beta_1}{2\beta_0^2} - \frac{\mathbf{r}_{h,ij}^{[\kappa],(1)}}{2\beta_0 + \mathbf{r}_{h,ii}^{[\kappa],(0)} - \mathbf{r}_{h,jj}^{[\kappa],(0)}}. \quad (2.14)$$

Herein, δ_{ij} represents the Kronecker delta function carrying the indices $\{i, j\} \in \{1, 2\}$ ($\{1, 2, 3\}$) for the quark (gluon) channel. $\mathbf{r}_h^{[\kappa],(1)}$ is defined analogously to $\mathbf{r}_h^{[\kappa],(0)}$ in terms of the two-loop non-cusp anomalous dimension $\gamma_h^{(1)}$ within the diagonal space of $\gamma_h^{(0)}$.

Reinserting the results of Eqs. (2.7-2.8) into Eq. (2.1) and expanding the kinematic variables to leading power, we arrive at the resummed q_T and $\Delta\phi_{t\bar{t}}$ spectra [110],

$$\begin{aligned} \frac{d\sigma_{t\bar{t}}^{\text{res}}}{dq_T} &= \frac{q_T}{64\pi^3 s} \sum_{\kappa, \text{sign}[\tilde{P}_t^z]} \int dM_{t\bar{t}}^2 dY_{t\bar{t}} d^2\tilde{P}_t^\perp \frac{\theta(M_{t\bar{t}} - M_{t\bar{t}}^{\text{min}})}{M_{t\bar{t}}^3 |\tilde{P}_t^z|} \int d^2\vec{b}_T J_0(b_T q_T) \tilde{\Sigma}_{t\bar{t}}^{\text{res},[\kappa]}(\vec{b}_T, Y_{t\bar{t}}, M_{t\bar{t}}, \Omega_t), \\ \frac{d\sigma_{t\bar{t}}^{\text{res}}}{d\Delta\phi_{t\bar{t}}} &= \frac{1}{32\pi^3 s} \sum_{\kappa, \text{sign}[\tilde{P}_t^z]} \int dM_{t\bar{t}}^2 dY_{t\bar{t}} d^2\tilde{P}_t^\perp \frac{\theta(M_{t\bar{t}} - M_{t\bar{t}}^{\text{min}})}{M_{t\bar{t}}^3} \frac{|\tilde{P}_t^\perp|}{|\tilde{P}_t^z|} \\ &\quad \times \int db_\tau \cos(b_\tau |\tilde{P}_t^\perp| \Delta\phi_{t\bar{t}}) \tilde{\Sigma}_{t\bar{t}}^{\text{res},[\kappa]}(\vec{b}_\tau^\parallel, Y_{t\bar{t}}, M_{t\bar{t}}, \Omega_t), \end{aligned} \quad (2.15)$$

where \tilde{P}_t^z and \tilde{P}_t^\perp are the longitudinal and transverse momenta of the top quark measured in the rest frame of the top and antitop pair. A lower cutoff $M_{t\bar{t}}^{\text{min}}$, which was chosen to be 400 GeV in [110], is introduced to avoid any threshold enhanced contributions, thereby ensuring the applicability of HQET. $J_0(x)$ represents the zeroth-rank Bessel function. \vec{b}_τ refers to the projected component of the impact parameter \vec{b}_T ,

$$\vec{b}_T = \vec{b}_\tau^\perp + \vec{b}_\tau^\parallel \equiv b_\tau^\perp \vec{\tau} \times \vec{n} + b_\tau \vec{\tau}. \quad (2.16)$$

Here \vec{n} stands for a unit vector pointing to one of beam directions in the laboratory reference frame, whilst in calculating $\Delta\phi_{t\bar{t}}$ distribution, $\vec{\tau}$ is always chosen to be perpendicular to the flight direction of top quark. Before closing this subsection, we want to discuss the choice of the auxiliary scales in Eqs. (2.7-2.8). Therein, two sets of auxiliary scales $\{\mu_h, \mu_b, \mu_s\}$ and $\{\nu_b, \nu_s\}$ are introduced during the virtuality and rapidity renormalisation in the relevant sectors. An appropriate choice of their values can minimise the logarithmic dependences in the fixed-order functions, and in turn improve the convergence of the resummation. To this end, the following values will be taken by default in this paper [110, 140, 260],

$$\begin{aligned} \mathcal{Q} &= q_T, & \mu_h^{\text{def}} &= \nu_b^{\text{def}} = M_{t\bar{t}}, & \mu_b^{\text{def}} &= \mu_s^{\text{def}} = \nu_s^{\text{def}} = b_0/b_T, \\ \mathcal{Q} &= \Delta\phi_{t\bar{t}}, & \mu_h^{\text{def}} &= \nu_b^{\text{def}} = M_{t\bar{t}}, & \mu_b^{\text{def}} &= \mu_s^{\text{def}} = \nu_s^{\text{def}} = b_0/b_\tau, \end{aligned} \quad (2.17)$$

where $b_0 = 2 \exp(-\gamma_E)$ with γ_E being the Euler constant. With the choice of Eq. (2.17), the evaluation of Eq. (2.15) can encounter the Landau singularity of the strong coupling α_s during the impact parameter space integration, which we regularise using the cutoff prescription proposed in [140].

2.2 Extending the resummation region – properties and caveats

In the last subsection, we introduced the resummed q_T and $\Delta\phi_{t\bar{t}}$ spectra in the domain where the top and antitop quarks are kinematically well-separated, i.e. $\Delta E_{t\bar{t}} \sim \mathcal{O}(m_t)$ or larger. In this regime, thanks to HQET [157–160], the (anti)top quark field will not interact with the other particles at leading power accuracy after applying the decoupling transformation [100, 147]. In consequence, at least up to leading

power, the hard, soft and beam-collinear regions are sufficient to describe the asymptotic behaviour of the q_T and $\Delta\phi_{t\bar{t}}$ spectra.

We are now interested in exploring the possibility to lift this kinematic restriction, $\theta(M_{t\bar{t}} - M_{t\bar{t}}^{\min})$, in Eq. (2.15) and extend the single differential observables $d\sigma_{t\bar{t}}/dq_T$ and $d\sigma_{t\bar{t}}/d\Delta\phi_{t\bar{t}}$ over the full $M_{t\bar{t}}$ range. Such an approach is motivated by the anticipation that for top-quark pair production at the LHC at 13 TeV the kinematic region $\Delta E_{t\bar{t}} \sim \mathcal{O}(m_t)$ accounts for the bulk of the total production cross section. Hence, the asymptotic behaviour in the $q_T \rightarrow 0$ and $\Delta\phi_{t\bar{t}} \rightarrow 0$ limits of the unconstrained cross section is expected to be mostly governed by the dynamics in HQET and SCET, in analogy to the methodology used in [88, 92, 200–209].

Nonetheless, we will discuss in the following the implications of removing the phase space restriction $M_{t\bar{t}}^{\min}$ in Eq. (2.15). In particular, we will show that the integrand $\tilde{\Sigma}_{t\bar{t}}^{\text{res},[\kappa]}$, in particular the amplitudes $\mathcal{C}_{\alpha;\{h_i\}}^{[\kappa]}$ of the hard sector as well as the evolution kernels $\mathbf{V}_h^{[\kappa]}$ it comprises, develops power-like divergences $\sim (\alpha_s/\beta_{t\bar{t}})^n$ as the Coulomb interactions manifest themselves in the threshold limit as $\Delta E_{t\bar{t}} \rightarrow 0$, or more conventionally

$$\beta_{t\bar{t}} \equiv \sqrt{1 - \frac{4m_t^2}{M_{t\bar{t}}^2}} \rightarrow 0. \quad (2.18)$$

Beam function and the evolution kernel $\mathcal{D}_{[\kappa]}^{\text{res}}$

As illustrated in Eqs. (2.7-2.8), $\tilde{\Sigma}_{t\bar{t}}^{\text{res},[\kappa]}$ contains the fixed-order contribution functions $\mathcal{B}_{n(\bar{n})}^{[\kappa]}$, $\mathcal{S}_{[\kappa]}^{\alpha\beta}$, and $\mathcal{C}_{\alpha,\{h\}}^{[\kappa]}$ as well as the evolution kernels $\mathcal{D}_{[\kappa]}^{\text{res}}$ and $\mathcal{V}_{\alpha\beta}^{[\kappa]}$. Here, we start with an analysis of the threshold limit of the beam sector $\mathcal{B}_{n(\bar{n})}^{[\kappa]}$ and the evolution kernel $\mathcal{D}_{[\kappa]}^{\text{res}}$. Given the fact that both are functions of $M_{t\bar{t}}$, $Y_{t\bar{t}}$, and the magnitude of impact parameters b_T and b_τ , taking the threshold limit is straightforward and does not incur any singular behaviour at any perturbative order. It follows that,

$$\mathcal{B}_{n(\bar{n})}^{[\kappa]} \xrightarrow{\beta_{t\bar{t}} \rightarrow 0} \sum_{m=0}^{\infty} \left(\frac{\alpha_s(\mu_b)}{4\pi} \right)^m \underbrace{\mathcal{B}_{n(\bar{n}),\text{thr}}^{[\kappa],(m)}}_{\mathcal{O}(\beta_{t\bar{t}}^0)} + \mathcal{O}(\beta_{t\bar{t}}), \quad (2.19)$$

$$\mathcal{D}_{[\kappa]}^{\text{res}} \xrightarrow{\beta_{t\bar{t}} \rightarrow 0} \underbrace{\mathcal{D}_{\text{thr},[\kappa]}^{\text{res}}}_{\mathcal{O}(\beta_{t\bar{t}}^0)} + \mathcal{O}(\beta_{t\bar{t}}). \quad (2.20)$$

Herein, to facilitate the later discussion, the functions $\mathcal{B}_{n(\bar{n}),\text{thr}}^{[\kappa],(m)}$ and $\mathcal{D}_{\text{thr},[\kappa]}^{\text{res}}$, that represent leading contributions of the beam-collinear sector and the cusp evolution kernel in the vicinity of $M_{t\bar{t}} = 2m_t$, respectively, are introduced, with the corresponding scalings indicated in the underbraces.

Hard function

Approaching the limit $\beta_{t\bar{t}} \rightarrow 0$ can induce a distinct asymptotic behaviour in the hard function $\mathcal{C}_{\alpha,\{h\}}^{[\kappa]}$. Within the context of the expansion by regions [223–226], we can perform the asymptotic expansion of $\mathcal{C}_{\alpha,\{h\}}^{[\kappa]}$ in $\beta_{t\bar{t}}$ via a set of dynamic regions in the loop integrals, which in general includes the hard, collinear, soft, ultrasoft, and Coulomb regions [100]. In the following, we will use the soft-collinear effective field theory (SCET) [147, 149, 150, 152, 153] and potential non-relativistic QCD (pNRQCD) [161–164] frameworks to capture their contributions.

At leading power, the SCET and pNRQCD effective Lagrangians can be expressed as [152, 153, 163, 164, 272]

$$\mathcal{L}_{\text{SCET}} = \bar{\varphi}_n \left(in \cdot D_n + i\not{D}_{n\perp} \frac{1}{i\bar{n} \cdot D_n} i\not{D}_{n\perp} \right) \frac{\not{n}}{2} \varphi_n - \frac{1}{2} \text{Tr} \left\{ F_n^{\mu\nu} F_{\mu\nu}^n \right\} + (n \leftrightarrow \bar{n}) - \frac{1}{2} \text{Tr} \left\{ F_{\text{us}}^{\mu\nu} F_{\mu\nu}^{\text{us}} \right\}, \quad (2.21)$$

$$\mathcal{L}_{\text{pNR}} = \psi^\dagger \left(i\partial^0 + \frac{\vec{\partial}^2}{2m_t} \right) \psi + \chi^\dagger \left(i\partial^0 - \frac{\vec{\partial}^2}{2m_t} \right) \chi - \int d^3\vec{r} \psi^\dagger T^a \psi(x^0, \vec{x} + \vec{r}) \left(\frac{\alpha_s}{r} \right) \chi^\dagger T^a \chi(x^0, \vec{x}), \quad (2.22)$$

where φ_n denotes the collinear quark field, while $F_n^{\mu\nu}$ is the collinear gluon field strength tensor. Likewise, $F_{\text{us}}^{\mu\nu}$ represents the field strength tensor for the ultrasoft gluons. $\psi^\dagger(\chi)$ stands for the heavy quark field

creating the (anti)top quark. The T^a are the usual generators of QCD. In writing Eqs. (2.21) and (2.22), the decoupling transformation [100] has been carried out on the collinear and heavy quark fields so as to remove all the ultrasoft-collinear and ultrasoft-heavy-quark interactions at leading power, respectively.

We are now ready to appraise the leading contribution of $\mathcal{C}_{\alpha,\{h\}}^{[\kappa]}$ at each perturbative order. On the tree level, the leading terms of $\mathcal{C}_{\alpha,\{h\}}^{[\kappa]}$ are determined by the effective Hamiltonian constructed out of the SCET and pNRQCD fields above. To evaluate the amplitudes induced by this Hamiltonian, we match the QCD amplitudes evaluated at the threshold $M_{t\bar{t}} = 2m_t$ onto the effective field theories. During the calculation, we make use of the `Mathematica` packages `FeynArts` [273], `FeynCalc` [274–276], and `FeynHelpers` [277] to generate the amplitudes for the individual partonic channels and then employ `FeynOnium` [278] to recast the Dirac spinors of the heavy quarks in terms of Pauli spinors. It follows that,

$$\mathcal{C}_{\alpha,\{h\}}^{[\kappa]} \xrightarrow{\beta_{t\bar{t}} \rightarrow 0} \sum_{n=0}^{\infty} \left(\frac{\alpha_s}{4\pi} \right)^{n+1} \mathcal{C}_{\text{thr},\alpha,\{h\}}^{[\kappa],(n)} + \dots, \quad (2.23)$$

where $\mathcal{C}_{\text{thr},\alpha,\{h\}}^{[\kappa],(n)}$ characterises the leading contribution in the threshold domain $\beta_{t\bar{t}} \rightarrow 0$ at the n -th order. The LO results read,

$$\begin{aligned} \mathcal{C}_{\text{thr},\{h\}}^{[q_n \bar{q}_n],(0)} &= \left[0 \quad \frac{4i\sqrt{2}\pi^2}{m_t^2} \left(\xi_t^\dagger \vec{\sigma} \eta_{\bar{t}} \right) \cdot (\bar{v}_{\bar{n}} \vec{\gamma}_\perp u_n) \right]^{\mathbf{T}}, \\ \mathcal{C}_{\text{thr},\{h\}}^{[q_{\bar{n}} \bar{q}_n],(0)} &= \left[0 \quad \frac{4i\sqrt{2}\pi^2}{m_t^2} \left(\xi_t^\dagger \vec{\sigma} \eta_{\bar{t}} \right) \cdot (\bar{v}_n \vec{\gamma}_\perp u_{\bar{n}}) \right]^{\mathbf{T}}, \\ \mathcal{C}_{\text{thr},\{h\}}^{[g_n g_{\bar{n}}],(0)} &= \left[-\frac{8\pi^2}{m_t} \sqrt{\frac{2}{3}} \xi_t^\dagger \eta_{\bar{t}} \varepsilon_\perp^{\epsilon_n \epsilon_{\bar{n}}} \quad 0 \quad -\frac{8\pi^2}{m_t} \sqrt{\frac{5}{3}} \xi_t^\dagger \eta_{\bar{t}} \varepsilon_\perp^{\epsilon_n \epsilon_{\bar{n}}} \right]^{\mathbf{T}}. \end{aligned} \quad (2.24)$$

Here, ξ_t^\dagger and $\eta_{\bar{t}}$ denote the Pauli spinors for the top and antitop quarks, respectively, resulting from the quantum field operators ψ^\dagger and χ in Eq. (2.22) acting on the external states $\langle t\bar{t} |$, with $\vec{\sigma}$ being a spatial vector consisting of the Pauli matrices. Similarly, $u_n(\bar{n})$ and $v_n(\bar{n})$ denote the Dirac spinors of the incoming massless quark and antiquarks induced by the collinear field operator φ_n in Eq. (2.21), while $\vec{\gamma}_\perp$ is the transverse component of the Dirac matrices. The contraction of the totally antisymmetric tensor and the polarisation vectors is abbreviated to $\varepsilon_\perp^{\epsilon_n \epsilon_{\bar{n}}} \equiv \varepsilon^{\mu\nu\rho\sigma} n_\mu \bar{n}_\nu \varepsilon_{n,\rho} \varepsilon_{\bar{n},\sigma}$. In writing Eq. (2.24), the bases $c_{\{a_i\}}^{qq}$ and $c_{\{a_i\}}^{gg}$ in Eq. (C.1) are employed to project out the colour states of the hard amplitudes. As shown in Eq. (2.24), $\mathcal{C}_{\text{thr},\{h\}}^{[q_n \bar{q}_n],(0)}$ and $\mathcal{C}_{\text{thr},\{h\}}^{[q_{\bar{n}} \bar{q}_n],(0)}$ only include the colour-octet contributions as the LO partonic process $q\bar{q} \rightarrow t\bar{t}$ only contains colour-octet s -channel diagrams. This differs for $gg \rightarrow t\bar{t}$, where the s -channel and u -channel diagrams both contribute, leading to the presence of both colour-singlet and color-octet configurations in $\mathcal{C}_{\text{thr},\{h\}}^{[g_n g_{\bar{n}}],(0)}$.

The leading contribution of $\mathcal{C}_{\alpha,\{h\}}^{[\kappa]}$ on the one-loop level is calculated with the amplitudes induced by the time product of the Coulomb vertex in Eq. (2.22) and the tree-level Hamiltonian. To evaluate the ensuing loop integral, following the method in [224], the residue theorem is first applied to integrate out the temporal component of the loop momentum, and the integration of the remaining spatial components can be completed via Feynman parameterisation. After removing the IRC poles within the $\overline{\text{MS}}$ scheme [212], it yields,

$$\begin{aligned} \mathcal{C}_{\text{thr},\{h\}}^{[q_n \bar{q}_n],(1)} &= \left[0 \quad \frac{4i\sqrt{2}\pi^2}{m_t^2} \left(\xi_t^\dagger \vec{\sigma} \eta_{\bar{t}} \right) \cdot (\bar{v}_{\bar{n}} \vec{\gamma}_\perp u_n) \left(-\frac{\pi^2}{6\beta_{t\bar{t}}} + \frac{i\pi L_{t\bar{t}}}{3\beta_{t\bar{t}}} \right) \right]^{\mathbf{T}}, \\ \mathcal{C}_{\text{thr},\{h\}}^{[q_{\bar{n}} \bar{q}_n],(1)} &= \left[0 \quad \frac{4i\sqrt{2}\pi^2}{m_t^2} \left(\xi_t^\dagger \vec{\sigma} \eta_{\bar{t}} \right) \cdot (\bar{v}_n \vec{\gamma}_\perp u_{\bar{n}}) \left(-\frac{\pi^2}{6\beta_{t\bar{t}}} + \frac{i\pi L_{t\bar{t}}}{3\beta_{t\bar{t}}} \right) \right]^{\mathbf{T}}, \\ \mathcal{C}_{\text{thr},\{h\}}^{[g_n g_{\bar{n}}],(1)} &= \left[-\frac{8\pi^2}{m_t} \sqrt{\frac{2}{3}} \xi_t^\dagger \eta_{\bar{t}} \varepsilon_\perp^{\epsilon_n \epsilon_{\bar{n}}} \left(\frac{4\pi^2}{3\beta_{t\bar{t}}} - \frac{8i\pi L_{t\bar{t}}}{3\beta_{t\bar{t}}} \right) \quad 0 \quad -\frac{8\pi^2}{m_t} \sqrt{\frac{5}{3}} \xi_t^\dagger \eta_{\bar{t}} \varepsilon_\perp^{\epsilon_n \epsilon_{\bar{n}}} \left(-\frac{\pi^2}{6\beta_{t\bar{t}}} + \frac{i\pi L_{t\bar{t}}}{3\beta_{t\bar{t}}} \right) \right]^{\mathbf{T}}, \end{aligned} \quad (2.25)$$

where $L_{t\bar{t}} \equiv \ln \left(\frac{\mu}{2\beta_{t\bar{t}} m_t} \right)$, using an analogous notation to Eq. (2.24). We have verified that the logarithmic dependences in Eq. (2.25) indeed satisfy the RGE suggested in [212, 279] up to the power corrections of $\mathcal{O}(\beta_{t\bar{t}}^0)$ and also that the non-logarithmic terms of Eq. (2.25) reproduce the NLO correction of the imaginary part of the pNRQCD Green function [101, 163, 164, 170]. Comparing with the LO results of Eq. (2.24), we observe that the leading-power one-loop corrections of Eq. (2.25) contain the same colour configurations only. This echoes the colour conservation in the leading-power Coulomb-gluon exchanges but might be broken when adding ultrasoft radiation at subleading power.

At last, it is worth noting that aside from the Coulomb exchanges, it is also possible to consider the collinear and hard contribution to the one-loop amplitude $\mathcal{C}_{\alpha,\{h\}}^{[\kappa]}$. However, while the hard loop momenta can not generate any threshold enhanced contributions, according to Eq. (2.21), the internal collinear propagators can only result in scaleless and thus vanishing loop integrals for on-shell amplitudes. Therefore, in deriving Eq. (2.25), we are only concerned with the contributions induced by the Coulomb potential.

From Eq. (2.24) and Eq. (2.25), we can determine the asymptotic behaviour of $\mathcal{C}_{\alpha,\{h\}}^{[\kappa]}$ in the threshold regime,

$$\mathcal{C}_{\alpha,\{h\}}^{[\kappa]} \xrightarrow{\beta_{t\bar{t}} \rightarrow 0} \left(\frac{\alpha_s}{4\pi}\right) \left\{ \underbrace{\mathcal{C}_{\text{thr},\alpha,\{h\}}^{[\kappa],(0)}}_{\sim \mathcal{O}(\beta_{t\bar{t}}^0)} + \mathcal{O}(\beta_{t\bar{t}}) \right\} + \left(\frac{\alpha_s}{4\pi}\right)^2 \left\{ \underbrace{\mathcal{C}_{\text{thr},\alpha,\{h\}}^{[\kappa],(1)}}_{\sim \mathcal{O}(\beta_{t\bar{t}}^{-1})} + \mathcal{O}(\beta_{t\bar{t}}^0) \right\} \dots \quad (2.26)$$

Here we only present the results up to the one-loop level, which is sufficient for us to analyse the N²LL resummation in $\tilde{\Sigma}_{t\bar{t}}^{\text{res},[\kappa]}$. The asymptotic expansion of $\mathcal{C}_{\alpha,\{h\}}^{[\kappa]}$ at the two loop accuracy and beyond can be carried out in an analogous manner, even including higher power correction in $\beta_{t\bar{t}}$. Further discussion can be found in [99, 280].

Soft function

We now move onto the investigation of the behaviour of the soft function $\mathcal{S}_{[\kappa]}^{\alpha\beta}$ in the limit $\beta_{t\bar{t}} \rightarrow 0$. In principle, the threshold limit of the HQET-based soft function could be extracted by comparison with the soft function in pNRQCD. However, due to the fact that HQET and pNRQCD follow a different sequence in performing the UV renormalisation and the asymptotic expansion—the threshold expansion of the soft function in HQET prioritises the UV renormalisation, whilst the soft sector in pNRQCD is derived by the $\beta_{t\bar{t}}$ expansion in the first place—this kind of comparison has to be delivered on the differential cross section level, rather than mapping the soft sectors between the two directly. One example to demonstrate the non-commutativity can be found in the inclusive soft functions [281, 282] for the threshold resummation.

With this in mind, we will directly expand the analytic results for $\mathcal{S}_{[\kappa]}^{\alpha\beta}$ in the limit $\beta_{t\bar{t}} \rightarrow 0$. Remaining at the N²LL level in $\tilde{\Sigma}_{t\bar{t}}^{\text{res},[\kappa]}$, using Eqs. (2.7-2.8), we only require the soft contribution up to the one-loop level, for which the analytic expression have been derived in [110] with the help of a Mellin-Barnes transformation [283, 284]. Expanding those renormalised results in the small parameter $\beta_{t\bar{t}}$, it yields that

$$\mathcal{S}_{[\kappa]}^{\alpha\beta} \xrightarrow{\beta_{t\bar{t}} \rightarrow 0} \delta^{\alpha\beta} + \left(\frac{\alpha_s}{4\pi}\right) \left[\mathcal{S}_{\text{thr},[\kappa]}^{(1),\alpha\beta} + \mathcal{O}(\beta_{t\bar{t}}) \right] + \mathcal{O}(\alpha_s^2) \dots, \quad (2.27)$$

where

$$\mathcal{S}_{\text{thr},[q_n \bar{q}_n]}^{(1),\alpha\beta} = \mathcal{S}_{\text{thr},[q_n \bar{q}_n]}^{(1),\alpha\beta} = \begin{bmatrix} \frac{16L_\nu L_T}{3} - \frac{8L_T^2}{3} - \frac{4\pi^2}{9} & 0 \\ 0 & \frac{16L_\nu L_T}{3} - \frac{8L_T^2}{3} + 6L_T - \frac{4\pi^2}{9} \end{bmatrix}, \quad (2.28)$$

$$\mathcal{S}_{\text{thr},[gg]}^{(1),\alpha\beta} = \begin{bmatrix} 12L_\nu L_T - 6L_T^2 - \pi^2 & 0 & 0 \\ 0 & 12L_\nu L_T - 6L_T^2 + 6L_T - \pi^2 & 0 \\ 0 & 0 & 12L_\nu L_T - 6L_T^2 + 6L_T - \pi^2 \end{bmatrix}.$$

Herein, we use the notations $L_\nu = \ln[\mu^2/\nu^2]$, $L_T = \ln[b_T^2 \mu^2/b_0^2]$, and $b_0 = 2 \exp(-\gamma_E)$ with γ_E being again the Euler constant. From the results above, it is seen that no threshold enhanced behaviour emerges from the NLO soft function. We can therefore establish,

$$\mathcal{S}_{\text{thr},[\kappa]}^{(1),\alpha\beta} \sim \mathcal{O}(1). \quad (2.29)$$

Evolution kernel $\mathcal{V}_{\alpha\beta}^{[\kappa]}$

Finally, we investigate the behaviour of non-cusp resummation kernel $\mathcal{V}_{\alpha\beta}^{[\kappa]}$ in the vicinity of the threshold. According to the definitions in Eqs. (2.12) and (2.13), $\mathcal{V}_{\alpha\beta}^{[\kappa]}$ comprises the exponential of the $\mathbf{r}_h^{[\kappa],(0)}$ matrices up to NLL accuracy. Starting at N²LL, however, they are supplemented with additional perturbative correction matrices, $\mathbf{J}^{[\kappa]}$, to accommodate the two-loop non-cusp anomalous dimension [212, 213]. Hence, the analysis

of the threshold behaviour of $\mathcal{V}_{\alpha\beta}^{[\kappa]}$ reduces to the expansion of $\mathbf{r}_h^{[\kappa],(0)}$, $\mathbf{J}^{[\kappa]}$, and the transformation matrices $\mathbf{R}_{[\kappa]}$ in $\beta_{t\bar{t}}$.

The $\mathbf{r}_h^{[\kappa],(0)}$ matrices can be constructed from the eigenvalues of the one-loop non-cusp anomalous dimensions $\gamma_h^{[\kappa],(0)}$ [212,213], for which we solve the characteristic equations for the contributing partonic processes using **Mathematica**. Expanding in $\beta_{t\bar{t}}$, the leading and subleading power contributions read,

$$\mathbf{r}_h^{[\kappa],(0)} \xrightarrow{\beta_{t\bar{t}} \rightarrow 0} \mathbf{r}_{h,\text{thr}}^{[\kappa],(0)} + \mathcal{O}(\beta_{t\bar{t}}), \quad (2.30)$$

where

$$\begin{aligned} \mathbf{r}_{h,\text{thr}}^{[q_n \bar{q}_n, \bar{q}_n q_n],(0)} &= \begin{bmatrix} -8 - \frac{8i\pi}{3\beta_{t\bar{t}}} & 0 \\ 0 & \frac{i\pi}{3\beta_{t\bar{t}}} + 6i\pi - 14 \end{bmatrix}, \\ \mathbf{r}_{h,\text{thr}}^{[g_n g_{\bar{n}}],(0)} &= \begin{bmatrix} -\frac{46}{3} - \frac{8i\pi}{3\beta_{t\bar{t}}} & 0 & 0 \\ 0 & -\frac{64}{3} + \frac{i\pi}{3\beta_{t\bar{t}}} + 6i\pi & 0 \\ 0 & 0 & -\frac{64}{3} + \frac{i\pi}{3\beta_{t\bar{t}}} + 6i\pi \end{bmatrix}. \end{aligned} \quad (2.31)$$

Here, all terms suppressed by positive powers of $\beta_{t\bar{t}}$ are omitted as they are not related to the leading behaviour of the exponential function of Eq. (2.12) in the limit $\beta_{t\bar{t}} \rightarrow 0$. Of the remaining expression, the threshold-enhanced imaginary parts echo the $L_{t\bar{t}}$ -dependences in Eq. (2.25), driven by Coulomb vertex in Eq. (2.22).

To derive the diagonalisation matrix $\mathbf{R}_{[\kappa]}$, we solve for the eigenvectors of $\gamma_h^{[\kappa],(0)}$ with the diagonal entries of $\mathbf{r}_h^{[\kappa],(0)}$ and then fill the columns of $\mathbf{R}_{[\kappa]}$ with the resulting eigenvectors in line with the positions of their eigenvalues. There is, however, some arbitrariness involved in the solutions for the eigenvectors themselves. In this work, we require the eigenvectors constructing $\mathbf{R}_{[\kappa]}$ to, at most, be of $\mathcal{O}(\beta_{t\bar{t}}^0)$ in the threshold domain. Alternative choices of eigenvectors will lead to distinct expressions of $\mathbf{R}_{[\kappa]}$ as well as $\mathbf{J}^{[\kappa]}$, but do not alter the resulting $\mathcal{V}_{\alpha\beta}^{[\kappa]}$. To confirm this, we have compared the non-cusp kernel $\mathcal{V}_{\alpha\beta}^{[\kappa]}$ evaluated by our $\mathbf{R}_{[\kappa]}$ and its inverse matrix with those generated by the program **Diag** [285] and the built-in functions in **Mathematica**, finding numerical agreements in all three partonic channels at both NLL and N²LL accuracy. After carrying out the expansion in $\beta_{t\bar{t}}$, the leading terms from $\mathbf{R}_{[\kappa]}$ read,

$$\mathbf{R}_{[\kappa]} \xrightarrow{\beta_{t\bar{t}} \rightarrow 0} \mathbf{R}_{[\kappa]}^{\text{thr}} + \mathcal{O}(\beta_{t\bar{t}}), \quad (2.32)$$

where

$$\begin{aligned} \mathbf{R}_{[q_n \bar{q}_n, \bar{q}_n q_n]}^{\text{thr}} &= \begin{bmatrix} 1 & 0 \\ 0 & 1 \end{bmatrix}, \\ \mathbf{R}_{[g_n g_{\bar{n}}]}^{\text{thr}} &= \begin{bmatrix} 1 & 0 & 0 \\ 0 & 1 & \text{sign}[\cos(\theta_t)] \\ 0 & -\text{sign}[\cos(\theta_t)] & 1 \end{bmatrix}. \end{aligned} \quad (2.33)$$

Herein, the transformation matrices take diagonal form for the $\kappa = q_n \bar{q}_n$ and $\kappa = \bar{q}_n q_n$ channels in the threshold limit, while $\mathbf{R}_{[g_n g_{\bar{n}}]}^{\text{thr}}$ comprises additional off-diagonal entries $\pm \text{sign}[\cos(\theta_t)]$ in the colour-octet blocks. The reason for this phenomenon is that in the quark-antiquark initiated process, the eigenvalues for the one-loop anomalous dimensions differ from each other by $\mathcal{O}(\beta_{t\bar{t}}^{-1})$, but as for the $\kappa = g_n g_{\bar{n}}$ case, the eigenvalues accounting for colour-octet projections overlap with each other until $\mathcal{O}(\beta_{t\bar{t}})$, which, in solving for their eigenvectors, can bring in additional contributions from the colour-octet blocks and in turn result in the appearances of $\pm \text{sign}[\cos(\theta_t)]$ in $\mathbf{R}_{[g_n g_{\bar{n}}]}^{\text{thr}}$. When applying $\mathbf{R}_{[g_n g_{\bar{n}}]}^{\text{thr}}$ onto the diagonalisation, one encounters a change in sign when the scattering angle θ_t crosses $\pi/2$. This is caused by the small- $\beta_{t\bar{t}}$ expansion of the square root operation in the eigenvalues and is associated with the branch cuts therein.

Equipped with the above transformation matrices and the two-loop anomalous dimensions [212,213], we are now able to evaluate and expand the matrix $\mathbf{J}^{[\kappa]}$ via Eq. (2.14),

$$\mathbf{J}^{[\kappa]} \xrightarrow{\beta_{t\bar{t}} \rightarrow 0} \mathbf{J}_{\text{thr}}^{[\kappa]} + \mathcal{O}(\beta_{t\bar{t}}^0), \quad (2.34)$$

where

$$\mathbf{J}_{\text{thr}}^{[q_n \bar{q}_n, \bar{q}_n q_n]} = \begin{bmatrix} -\frac{220i\pi}{4761\beta_{t\bar{t}}} & 0 \\ 0 & \frac{55i\pi}{9522\beta_{t\bar{t}}} \end{bmatrix}, \quad (2.35)$$

$$\mathbf{J}_{\text{thr}}^{[g_n g_n]} = \begin{bmatrix} -\frac{220i\pi}{4761\beta_{t\bar{t}}} & 0 & 0 \\ 0 & \frac{55i\pi}{9522\beta_{t\bar{t}}} & 0 \\ 0 & 0 & \frac{55i\pi}{9522\beta_{t\bar{t}}} \end{bmatrix}.$$

Akin to Eq. (2.31), the expressions for $\mathbf{J}_{\text{thr}}^{[\kappa]}$ contain the power-like divergence in the imaginary parts. Here, we only need to retain the leading singular terms.

Substituting the expressions of Eq. (2.31) into Eqs. (2.12-2.13), we arrive at the leading behaviour of the evolution kernel $\mathbf{V}_h^{[\kappa]}$ in the threshold domain,

$$\mathbf{V}_h^{[\kappa]} \Big|_{\text{NLL}(\prime)} \xrightarrow{\beta_{t\bar{t}} \rightarrow 0} \mathbf{V}_{h,\text{thr}}^{[\kappa],(0)} + \mathcal{O}(\beta_{t\bar{t}}^0), \quad (2.36)$$

$$\mathbf{V}_h^{[\kappa]} \Big|_{\text{N}^2\text{LL}(\prime)} \xrightarrow{\beta_{t\bar{t}} \rightarrow 0} \mathbf{V}_{h,\text{thr}}^{[\kappa],(1)} + \mathcal{O}(\beta_{t\bar{t}}^{-1}), \quad (2.37)$$

where

$$\mathbf{V}_{h,\text{thr}}^{[q_n \bar{q}_n, \bar{q}_n q_n],(0)} = \begin{bmatrix} \left[\frac{\alpha_s(\mu_h)}{\alpha_s(\mu_s)} \right]^{-\frac{12}{23} - \frac{4i\pi}{23\beta_{t\bar{t}}}} & & 0 \\ & & \left[\frac{\alpha_s(\mu_h)}{\alpha_s(\mu_s)} \right]^{\frac{i\pi}{46\beta_{t\bar{t}}} + \frac{9i\pi}{23} - \frac{21}{23}} \\ 0 & & \left[\frac{\alpha_s(\mu_h)}{\alpha_s(\mu_s)} \right]^{\frac{i\pi}{46\beta_{t\bar{t}}} + \frac{9i\pi}{23} - \frac{21}{23}} \end{bmatrix}, \quad (2.38)$$

$$\mathbf{V}_{h,\text{thr}}^{[g_n g_n],(0)} = \begin{bmatrix} \left[\frac{\alpha_s(\mu_h)}{\alpha_s(\mu_s)} \right]^{-1 - \frac{4i\pi}{23\beta_{t\bar{t}}}} & & 0 & 0 \\ & & \left[\frac{\alpha_s(\mu_h)}{\alpha_s(\mu_s)} \right]^{\frac{i\pi}{46\beta_{t\bar{t}}} + \frac{9i\pi}{23} - \frac{32}{23}} & \\ 0 & & \left[\frac{\alpha_s(\mu_h)}{\alpha_s(\mu_s)} \right]^{\frac{i\pi}{46\beta_{t\bar{t}}} + \frac{9i\pi}{23} - \frac{32}{23}} & 0 \\ 0 & & 0 & \left[\frac{\alpha_s(\mu_h)}{\alpha_s(\mu_s)} \right]^{\frac{i\pi}{46\beta_{t\bar{t}}} + \frac{9i\pi}{23} - \frac{32}{23}} \end{bmatrix},$$

and

$$\mathbf{V}_{h,\text{thr}}^{[q_n \bar{q}_n, \bar{q}_n q_n],(1)} = \frac{\alpha_s(\mu_s)\alpha_s(\mu_h)}{\beta_{t\bar{t}}^2} \begin{bmatrix} \frac{3025}{22667121} \left[\frac{\alpha_s(\mu_h)}{\alpha_s(\mu_s)} \right]^{-\frac{12}{23} - \frac{4i\pi}{23\beta_{t\bar{t}}}} & & 0 \\ & & \frac{3025}{1450695744} \left[\frac{\alpha_s(\mu_h)}{\alpha_s(\mu_s)} \right]^{\frac{i\pi}{46\beta_{t\bar{t}}} + \frac{9i\pi}{23} - \frac{21}{23}} \\ 0 & & \left[\frac{\alpha_s(\mu_h)}{\alpha_s(\mu_s)} \right]^{\frac{i\pi}{46\beta_{t\bar{t}}} + \frac{9i\pi}{23} - \frac{21}{23}} \end{bmatrix}, \quad (2.39)$$

$$\mathbf{V}_{h,\text{thr}}^{[g_n g_n],(1)} = \frac{\alpha_s(\mu_s)\alpha_s(\mu_h)}{\beta_{t\bar{t}}^2} \begin{bmatrix} \frac{3025}{22667121} \left[\frac{\alpha_s(\mu_h)}{\alpha_s(\mu_s)} \right]^{-1 - \frac{4i\pi}{23\beta_{t\bar{t}}}} & & 0 & 0 \\ & & \frac{3025}{1450695744} \left[\frac{\alpha_s(\mu_h)}{\alpha_s(\mu_s)} \right]^{\frac{i\pi}{46\beta_{t\bar{t}}} + \frac{9i\pi}{23} - \frac{32}{23}} & \\ 0 & & \left[\frac{\alpha_s(\mu_h)}{\alpha_s(\mu_s)} \right]^{\frac{i\pi}{46\beta_{t\bar{t}}} + \frac{9i\pi}{23} - \frac{32}{23}} & 0 \\ 0 & & 0 & \frac{3025}{1450695744} \left[\frac{\alpha_s(\mu_h)}{\alpha_s(\mu_s)} \right]^{\frac{i\pi}{46\beta_{t\bar{t}}} + \frac{9i\pi}{23} - \frac{32}{23}} \end{bmatrix}.$$

Examining the above evolution kernels in detail, we observe an intensely oscillating behaviour in the diagonal entries at NLL as $\beta_{t\bar{t}} \rightarrow 0$, which is always bounded from above though and, thus, remains finite. The results at N²LL accuracy, however, exhibit quadratic divergences that factorise from the matrix structure of the

evolution kernel. These divergences are induced by the product of pairs of $\mathbf{J}_{\text{thr}}^{[\kappa]}$ matrices, detailed in Eq. (2.35), when assembled according to Eq. (2.13). Comparing this result to the exact evolution function of Eqs. (2.12-2.13), we find that the expressions in Eqs. (2.38-2.39) can indeed replicate the desired asymptotic behaviour in the vicinity of $\beta_{t\bar{t}} = 0$. More details on this numerical assessment can be found in App. B.

Combined resummation

Summarising the scaling laws in Eqs. (2.19-2.20), Eq. (2.26), Eq. (2.29), and Eqs. (2.38-2.39), we can determine the asymptotic behaviour of $\tilde{\Sigma}_{t\bar{t}}^{\text{res},[\kappa]}$ with the help of Eqs. (2.7-2.8),²

$$\begin{aligned} \tilde{\Sigma}_{t\bar{t}}^{\text{res},[\kappa]} \Big|_{\text{NLL}} &\xrightarrow{\beta_{t\bar{t}} \rightarrow 0} \underbrace{\tilde{\Sigma}_{t\bar{t},\text{thr}}^{\text{res},[\kappa]} \Big|_{\text{NLL}}}_{\mathcal{O}(\beta_{t\bar{t}}^0)} + \mathcal{O}(\beta_{t\bar{t}}), \\ \tilde{\Sigma}_{t\bar{t}}^{\text{res},[\kappa]} \Big|_{\text{N}^2\text{LL}} &\xrightarrow{\beta_{t\bar{t}} \rightarrow 0} \underbrace{\tilde{\Sigma}_{t\bar{t},\text{thr}}^{\text{res},[\kappa]} \Big|_{\text{N}^2\text{LL}}}_{\mathcal{O}(\beta_{t\bar{t}}^{-5})} + \mathcal{O}(\beta_{t\bar{t}}^{-4}), \end{aligned} \quad (2.40)$$

where

$$\begin{aligned} \tilde{\Sigma}_{t\bar{t},\text{thr}}^{\text{res},[q_n^i \bar{q}_{\bar{n}}^j]} \Big|_{\text{NLL}} &= \frac{64\pi^2 \alpha_s^2(\mu_h)}{9} \left[\frac{\alpha_s(\mu_h)}{\alpha_s(\mu_s)} \right]^{-\frac{42}{23}} \mathcal{D}_{\text{thr},[q_n^i \bar{q}_{\bar{n}}^j]}^{\text{res},(1)} f_{q_n^i/N}(\tilde{\eta}_n, \mu_b) f_{\bar{q}_{\bar{n}}^j/\bar{N}}(\tilde{\eta}_{\bar{n}}, \mu_b), \\ \tilde{\Sigma}_{t\bar{t},\text{thr}}^{\text{res},[g_n g_{\bar{n}}]} \Big|_{\text{NLL}} &= \left\{ \frac{2\pi^2 \alpha_s^2(\mu_h)}{3} \left[\frac{\alpha_s(\mu_h)}{\alpha_s(\mu_s)} \right]^{-2} + \frac{5\pi^2 \alpha_s^2(\mu_h)}{3} \left[\frac{\alpha_s(\mu_h)}{\alpha_s(\mu_s)} \right]^{-\frac{64}{23}} \right\} \\ &\quad \times \mathcal{D}_{\text{thr},[g_n g_{\bar{n}}]}^{\text{res},(1)} f_{g/N}(\tilde{\eta}_n, \mu_b) f_{g/\bar{N}}(\tilde{\eta}_{\bar{n}}, \mu_b), \end{aligned} \quad (2.41)$$

and

$$\begin{aligned} \tilde{\Sigma}_{t\bar{t},\text{thr}}^{\text{res},[q_n^i \bar{q}_{\bar{n}}^j]} \Big|_{\text{N}^2\text{LL}} &= - \frac{\alpha_s^5(\mu_h) \alpha_s^2(\mu_s)}{\beta_{t\bar{t}}^5} \frac{9150625 \pi^3}{3551374364050766592} \left[\frac{\alpha_s(\mu_h)}{\alpha_s(\mu_s)} \right]^{-\frac{42}{23}} \\ &\quad \times \mathcal{D}_{\text{thr},[q_n^i \bar{q}_{\bar{n}}^j]}^{\text{res},(2)} f_{q_i/N}(\tilde{\eta}_n, \mu_b) f_{\bar{q}_j/\bar{N}}(\tilde{\eta}_{\bar{n}}, \mu_b), \\ \tilde{\Sigma}_{t\bar{t},\text{thr}}^{\text{res},[g_n g_{\bar{n}}]} \Big|_{\text{N}^2\text{LL}} &= \frac{\alpha_s^5(\mu_h) \alpha_s^2(\mu_s)}{\beta_{t\bar{t}}^5} \left\{ \frac{36602500 \pi^3}{4624185369857769} \left[\frac{\alpha_s(\mu_h)}{\alpha_s(\mu_s)} \right]^{-2} - \frac{45753125 \pi^3}{75762653099749687296} \left[\frac{\alpha_s(\mu_h)}{\alpha_s(\mu_s)} \right]^{-\frac{64}{23}} \right\} \\ &\quad \times \mathcal{D}_{\text{thr},[g_n g_{\bar{n}}]}^{\text{res},(2)} f_{g/N}(\tilde{\eta}_n, \mu_b) f_{g/\bar{N}}(\tilde{\eta}_{\bar{n}}, \mu_b). \end{aligned} \quad (2.42)$$

Once again, we omit the expression for the $\kappa = \bar{q}_n^i q_{\bar{n}}^j$ case, for which the results at NLL and N²LL can be derived from the $\kappa = q_n^i \bar{q}_{\bar{n}}^j$ case by appropriately swapping the labels $n \leftrightarrow \bar{n}$. In Eqs. (2.41-2.42), we have introduced the resummation kernels $\mathcal{D}_{\text{thr},[\kappa]}^{\text{res},(1,2)}$ to encode the contribution of Eq. (2.9) evaluated at threshold, $M_{t\bar{t}} = 2m_t$, with the superscripts $\{1, 2\}$ denoting the logarithmic precision. For the NLL results in Eqs. (2.41), due to the lack of perturbative corrections to the fixed-order ingredients, the soft function is equal to a unit matrix and the beam functions are reduced to the PDFs with the momentum fractions $\tilde{\eta}_n = 2m_t e^{Y_{t\bar{t}}}/\sqrt{s}$ and $\tilde{\eta}_{\bar{n}} = 2m_t e^{-Y_{t\bar{t}}}/\sqrt{s}$. Conversely, evaluating the N²LL expressions of Eq. (2.42), we emphasise that the perturbative corrections, which comprise the hard contributions of Eq. (2.25) and its complex conjugate as well as their non-cusp evaluations in Eq. (2.39), account for the leading singular behaviour of $\tilde{\Sigma}_{t\bar{t}}^{\text{res},[\kappa]}$.

²Please note that the coefficient functions at the given orders will have to be expanded for the appropriate order counting of the resummed cross section. In particular, $(\mathcal{C}_{\alpha,\{h'\}}^{[\kappa],[0]} + \frac{\alpha_s}{4\pi} \mathcal{C}_{\alpha,\{h'\}}^{[\kappa],[1]})^\dagger (\mathcal{C}_{\beta,\{h\}}^{[\kappa],[0]} + \frac{\alpha_s}{4\pi} \mathcal{C}_{\beta,\{h\}}^{[\kappa],[1]}) = \mathcal{C}_{\alpha,\{h'\}}^{[\kappa],[0],\dagger} \mathcal{C}_{\beta,\{h\}}^{[\kappa],[0]} + \frac{\alpha_s}{4\pi} (\mathcal{C}_{\alpha,\{h'\}}^{[\kappa],[0],\dagger} \mathcal{C}_{\beta,\{h\}}^{[\kappa],[1]} + \mathcal{C}_{\alpha,\{h'\}}^{[\kappa],[1],\dagger} \mathcal{C}_{\beta,\{h\}}^{[\kappa],[0]}) + \mathcal{O}(\alpha_s^2)$, etc.

Using the results of Eqs. (2.41-2.42), we note that while the NLL resummation approaches a constant as $\beta_{t\bar{t}} \rightarrow 0$, the N²LL results display quintic divergences. To be precise, $\tilde{\Sigma}_{t\bar{t}}^{\text{res}, [q_n^i \bar{q}_n^j]}$ approaches negative infinity in the limit $\beta_{t\bar{t}} \rightarrow 0$, whereas the sign of the threshold limit of $\tilde{\Sigma}_{t\bar{t}}^{\text{res}, [g_n g_n]}$ is subject to the competition between colour-singlet and colour-octet contributions, as shown in the first and second term in the curly brackets of Eq. (2.42), respectively. Under regular LHC conditions and conventional scale definitions, the singlet term is by far dominant, though, inducing a positive overall sign.³

Combining the scalings of Eq. (2.40) with Eqs. (2.15), we are able to establish the asymptotic properties of the resummed q_T and $\Delta\phi_{t\bar{t}}$ spectra in the threshold domain. We note that the kinematic variables introduce an additional suppression in the limit $\beta_{t\bar{t}} \rightarrow 0$,

$$\begin{aligned} d^2 \tilde{P}_t^\perp &\sim \mathcal{O}(\beta_{t\bar{t}}^2), & |\tilde{P}_t^\perp| &\sim |\tilde{P}_t^z| \sim \mathcal{O}(\beta_{t\bar{t}}), \\ dM_{t\bar{t}}^2 &= 2M_{t\bar{t}}^2 \left(\frac{\beta_{t\bar{t}}}{1 - \beta_{t\bar{t}}^2} \right) d\beta_{t\bar{t}} = 8m_t^2 \beta_{t\bar{t}} d\beta_{t\bar{t}} + \dots \end{aligned} \quad (2.43)$$

This yields,

$$\begin{aligned} \frac{d^3 \sigma_{t\bar{t}}^{\text{res}}}{d\beta_{t\bar{t}} dY_{t\bar{t}} dq_T} &\xrightarrow{\beta_{t\bar{t}} \rightarrow 0} \underbrace{\beta_{t\bar{t}}^2}_{\text{kin}} \otimes \underbrace{\left\{ \mathcal{O}(\beta_{t\bar{t}}^0) + \mathcal{O}(\beta_{t\bar{t}}^{-1}) + \dots \right\}}_{\mathcal{C}_{\alpha, \{h\}}^{[\kappa]}} \otimes \underbrace{\left\{ \mathcal{O}(\beta_{t\bar{t}}^0) + \mathcal{O}(\beta_{t\bar{t}}^{-4}) + \dots \right\}}_{\mathbf{V}_h^{[\kappa]}} \otimes \dots \\ &\sim \underbrace{\mathcal{O}(\beta_{t\bar{t}}^2)}_{\text{NLL}} + \underbrace{\mathcal{O}(\beta_{t\bar{t}}^{-3})}_{\text{N}^2\text{LL}} + \dots, \\ \frac{d^3 \sigma_{t\bar{t}}^{\text{res}}}{d\beta_{t\bar{t}} dY_{t\bar{t}} d\Delta\phi_{t\bar{t}}} &\xrightarrow{\beta_{t\bar{t}} \rightarrow 0} \underbrace{\beta_{t\bar{t}}^3}_{\text{kin}} \otimes \underbrace{\left\{ \mathcal{O}(\beta_{t\bar{t}}^0) + \mathcal{O}(\beta_{t\bar{t}}^{-1}) + \dots \right\}}_{\mathcal{C}_{\alpha, \{h\}}^{[\kappa]}} \otimes \underbrace{\left\{ \mathcal{O}(\beta_{t\bar{t}}^0) + \mathcal{O}(\beta_{t\bar{t}}^{-4}) + \dots \right\}}_{\mathbf{V}_h^{[\kappa]}} \otimes \dots \\ &\sim \underbrace{\mathcal{O}(\beta_{t\bar{t}}^3)}_{\text{NLL}} + \underbrace{\mathcal{O}(\beta_{t\bar{t}}^{-2})}_{\text{N}^2\text{LL}} + \dots \end{aligned} \quad (2.44)$$

In the first line of each of the equations in Eq. (2.44), the scalings for the kinematic prefactor, the hard sector, and the non-cusp evolution kernel are spelt out, capturing the asymptotic behaviour of the differential spectra $d^3\sigma_{t\bar{t}}^{\text{res}}/(d\beta_{t\bar{t}}dY_{t\bar{t}}d\mathcal{Q})$ up to N²LL accuracy. For simplicity, we omit the scalings from the beam functions, the soft sector, and the diagonal resummation kernel, since (at least) up to N²LL all of them approach a constant in the vicinity of the threshold $\beta_{t\bar{t}} = 0$. The second lines then present the resulting asymptotic behaviour of the q_T and $\Delta\phi_{t\bar{t}}$ differential distributions at the logarithmic accuracies of our concern.

We observe that both the q_T and the $\Delta\phi_{t\bar{t}}$ differential spectra at NLL experience significant kinematic suppression near threshold, whereas at N²LL, thanks to the Coulomb enhancement from the hard sector and the non-cusp evolution kernel, see Eq. (2.25) and Eq. (2.39), the behaviour of $d^3\sigma_{t\bar{t}}^{\text{res}}/(d\beta_{t\bar{t}}dY_{t\bar{t}}dq_T)$ and $d^3\sigma_{t\bar{t}}^{\text{res}}/(d\beta_{t\bar{t}}dY_{t\bar{t}}d\Delta\phi_{t\bar{t}})$ reverses and they instead develop cubic and quadratic divergences, respectively. Although the existence of such a divergence has been implied in earlier calculations [88, 104, 105, 109, 206], where additional perturbative expansions were applied to the non-cusp kernel $\mathbf{V}_h^{[\kappa]}$ in place of the original solution derived in [210, 211], Eq. (2.44) for the first time presents their specific threshold behaviour. In turn, this finding will help to interpret the limitation of a HQET and SCET based analysis, thereby paving the way for the future combined resummation of Coulomb, soft and collinear corrections.

Further, we want to emphasise that for lack of a resummation of the Coulomb interactions, Eq. (2.44) should be interpreted as the threshold limit of a HQET and SCET based resummation, testing the integrability in Eq. (2.15) over the entire $t\bar{t}$ production phase space, rather than an implication on a full QCD calculation in this limit. An analysis of the threshold behaviour of a full QCD result invariably necessitates the use of pNRQCD or vNRQCD in its derivation. Finally, we conclude that the resummation formalism in Eq. (2.15) *cannot* be straightforwardly applied to evaluate the single differential observables $d\sigma_{t\bar{t}}^{\text{res}}/dq_T$ and $d\sigma_{t\bar{t}}^{\text{res}}/d\Delta\phi_{t\bar{t}}$ beyond NLL, unless a kinematic constraint on $\beta_{t\bar{t}}$, or equivalently $\Delta E_{t\bar{t}}$ or $M_{t\bar{t}}$, is put in place to remove the

³The difference in magnitude of the prefactors of the singlet and octet coefficients would have to be overcome by an extreme ratio of the strong couplings at the soft and hard scales, necessitating a soft scale choice extremely close to the Λ_{QCD} .

threshold regime from the $\beta_{t\bar{t}}$ integration. Instead, in the following, we will propose two *ad hoc* prescriptions to smoothly and consistently match the well-separated domain $\Delta E_{t\bar{t}} \sim \mathcal{O}(m_t)$ to the threshold region $\Delta E_{t\bar{t}} \ll M_{t\bar{t}}$ for a generic observable $d^3\sigma_{t\bar{t}}^{\text{res}}/(d\beta_{t\bar{t}}dY_{t\bar{t}}d\mathcal{Q})$.

2.3 Prescriptions to extend the resummation region

2.3.1 D-prescription: Resummation with a decomposed Sudakov factor

In order to sufficiently weaken the threshold divergences in the evolution kernel $\mathbf{V}_h^{[\kappa]}$, which, according to Eqs. (2.44), constitute the main singular contribution at N²LL, we introduce a first prescription, dubbed D-prescription in the following.

We start by analysing the elements of $\mathbf{V}_h^{[\kappa]}$ in the well-separated domain, i.e. $\Delta E_{t\bar{t}} \sim \mathcal{O}(m_t)$. As defined in Eq. (2.13), at N²LL accuracy, $\mathbf{V}_h^{[\kappa]}$ includes the NLL resummation kernel sandwiched between the perturbative corrections $(1 + \alpha_s(\mu_s)\mathbf{J}^{[\kappa]})/(4\pi)$ and $(1 - \alpha_s(\mu_h)\mathbf{J}^{[\kappa]})/(4\pi)$. In the region $\Delta E_{t\bar{t}} \sim \mathcal{O}(m_t)$, both correction terms are of a similar magnitude to the non-logarithmic contributions in the hard and soft functions. Therefore, the product of them is expected to be numerically comparable with the N³LL coefficients. In consequence, during our phenomenological investigation, we can truncate all terms proportional to $\alpha_s(\mu_s)\alpha_s(\mu_h)$ in Eq. (2.13), at the cost of additional non-logarithmic corrections in the well-separated domain, yielding

$$\mathbf{V}_h^{[\kappa]}(v_t, v_{\bar{t}}, \mu_s, \mu_h) \Big|_{\text{N}^2\text{LLD}} = \sum_{n_s, n_h=0}^{n_s+n_h=1} \left(\frac{\alpha_s(\mu_s)}{4\pi} \right)^{n_s} \left(\frac{\alpha_s(\mu_h)}{4\pi} \right)^{n_h} \mathbf{V}_h^{[\kappa],(n_s, n_h)}(v_t, v_{\bar{t}}, \mu_s, \mu_h) \Big|_{\text{N}^2\text{LLD}}, \quad (2.45)$$

where

$$\begin{aligned} \mathbf{V}_h^{[\kappa],(0,0)}(v_t, v_{\bar{t}}, \mu_s, \mu_h) \Big|_{\text{N}^2\text{LLD}} &= \mathbf{R}_{[\kappa]}^{-1} \exp \left\{ \frac{\mathbf{r}_h^{[\kappa],(0)}}{2\beta_0} \ln \left[\frac{\alpha_s(\mu_h)}{\alpha_s(\mu_s)} \right] \right\} \mathbf{R}_{[\kappa]} = \mathbf{V}_h^{[\kappa]}(v_t, v_{\bar{t}}, \mu_s, \mu_h) \Big|_{\text{NLL}}, \\ \mathbf{V}_h^{[\kappa],(1,0)}(v_t, v_{\bar{t}}, \mu_s, \mu_h) \Big|_{\text{N}^2\text{LLD}} &= \mathbf{R}_{[\kappa]}^{-1} \mathbf{J}^{[\kappa]} \exp \left\{ \frac{\mathbf{r}_h^{[\kappa],(0)}}{2\beta_0} \ln \left[\frac{\alpha_s(\mu_h)}{\alpha_s(\mu_s)} \right] \right\} \mathbf{R}_{[\kappa]}, \\ \mathbf{V}_h^{[\kappa],(0,1)}(v_t, v_{\bar{t}}, \mu_s, \mu_h) \Big|_{\text{N}^2\text{LLD}} &= - \mathbf{R}_{[\kappa]}^{-1} \exp \left\{ \frac{\mathbf{r}_h^{[\kappa],(0)}}{2\beta_0} \ln \left[\frac{\alpha_s(\mu_h)}{\alpha_s(\mu_s)} \right] \right\} \mathbf{J}^{[\kappa]} \mathbf{R}_{[\kappa]}. \end{aligned} \quad (2.46)$$

Herein, we have decomposed the original evolution kernel of Eq. (2.13) according to their $\alpha_s(\mu_s)$ and $\alpha_s(\mu_h)$ powers. The leading order contribution $\mathbf{V}_h^{[\kappa],(0,0)}$ contains no perturbative corrections and thus coincides with the NLL Sudakov factor in Eq. (2.12), while starting from $\mathbf{V}_h^{[\kappa],(1,0)}$ and $\mathbf{V}_h^{[\kappa],(0,1)}$ perturbative corrections encoded in the $\mathbf{J}^{[\kappa]}$ enter. To facilitate our discussion and comparison below, we will refer to the results in Eq. (2.45) as the non-cusp evolution kernel evaluated in the decomposed prescription (D-prescription), i.e. N²LLD.

It is worth noting that the non-cusp evolution evaluated in the D-prescription cannot precisely satisfy the hard RGE as its original form in Eq. (2.13) did at N²LL. This can be confirmed by taking the derivative of Eq. (2.45) with respect to $\ln \mu_s$. It follows that

$$\begin{aligned} \frac{\partial}{\partial \ln \mu_s} \mathbf{V}_h^{[\kappa]}(v_t, v_{\bar{t}}, \mu_s, \mu_h) \Big|_{\text{N}^2\text{LLD}} &= \beta(\alpha_s(\mu_s)) \frac{\partial}{\partial \alpha_s(\mu_s)} \mathbf{V}_h^{[\kappa]}(v_t, v_{\bar{t}}, \mu_s, \mu_h) \Big|_{\text{N}^2\text{LLD}} \\ &= \beta(\alpha_s(\mu_s)) \mathbf{R}_{[\kappa]}^{-1} \left[- \frac{1}{\alpha_s(\mu_s)} \frac{\mathbf{r}_h^{[\kappa],(0)}}{2\beta_0} + \frac{\mathbf{J}^{[\kappa]}}{4\pi} - \frac{\mathbf{J}^{[\kappa]} \mathbf{r}_h^{[\kappa],(0)}}{4\pi 2\beta_0} \right] \exp \left\{ \frac{\mathbf{r}_h^{[\kappa],(0)}}{2\beta_0} \ln \left[\frac{\alpha_s(\mu_h)}{\alpha_s(\mu_s)} \right] \right\} \mathbf{R}_{[\kappa]} \\ &\quad + \beta(\alpha_s(\mu_s)) \mathbf{R}_{[\kappa]}^{-1} \left[\frac{1}{\alpha_s(\mu_s)} \frac{\mathbf{r}_h^{[\kappa],(0)}}{2\beta_0} \right] \exp \left\{ \frac{\mathbf{r}_h^{[\kappa],(0)}}{2\beta_0} \ln \left[\frac{\alpha_s(\mu_h)}{\alpha_s(\mu_s)} \right] \right\} \frac{\alpha_s(\mu_h)}{4\pi} \mathbf{J}^{[\kappa]} \mathbf{R}_{[\kappa]}. \end{aligned} \quad (2.47)$$

According to the definition in Eq. (2.14), $\mathbf{J}^{[\kappa]}$ fulfills the identity,

$$\mathbf{J}^{[\kappa]} \left(\mathbf{I} - \frac{\mathbf{r}_h^{[\kappa],(0)}}{2\beta_0} \right) = \frac{\beta_1}{2\beta_0^2} \mathbf{r}_h^{[\kappa],(0)} - \frac{\mathbf{r}_h^{[\kappa],(1)}}{2\beta_0} - \frac{\mathbf{r}_h^{[\kappa],(0)}}{2\beta_0} \mathbf{J}^{[\kappa]}. \quad (2.48)$$

Reinserting this relation back to Eq. (2.47) gives

$$\begin{aligned}
& \left. \frac{\partial}{\partial \ln \mu_s} \mathbf{V}_h^{[\kappa]}(v_t, v_{\bar{t}}, \mu_s, \mu_h) \right|_{\text{N}^2\text{LLD}} \\
&= \mathbf{R}_{[\kappa]}^{-1} \left\{ \left[\frac{\alpha_s(\mu_s)}{4\pi} \mathbf{r}_h^{[\kappa],(0)} + \left(\frac{\alpha_s(\mu_s)}{4\pi} \right)^2 \mathbf{r}_h^{[\kappa],(1)} + \mathcal{O}(\alpha_s^3) \right] \left[\mathbf{I} + \frac{\alpha_s(\mu_s)}{4\pi} \mathbf{J}^{[\kappa]} \right] \right\} \exp \left\{ \frac{\mathbf{r}_h^{[\kappa],(0)}}{2\beta_0} \ln \left[\frac{\alpha_s(\mu_h)}{\alpha_s(\mu_s)} \right] \right\} \mathbf{R}_{[\kappa]} \\
&\quad - \mathbf{R}_{[\kappa]}^{-1} \left\{ \frac{\alpha_s(\mu_s)}{4\pi} \mathbf{r}_h^{[\kappa],(0)} + \mathcal{O}(\alpha_s^2) \right\} \exp \left\{ \frac{\mathbf{r}_h^{[\kappa],(0)}}{2\beta_0} \ln \left[\frac{\alpha_s(\mu_h)}{\alpha_s(\mu_s)} \right] \right\} \frac{\alpha_s(\mu_h)}{4\pi} \mathbf{J}^{[\kappa]} \mathbf{R}_{[\kappa]}, \tag{2.49}
\end{aligned}$$

where we have expanded the QCD beta function in $\alpha_s(\mu_s)$. In this result we observe that while the expression in the second line meets the N²LL RGE of the hard sector, up to perturbative corrections of $\sim \mathcal{O}(\alpha_s^3)$, which is given by differentiating Eq. (2.13) with respect to $\ln \mu_s$, yielding

$$\frac{\partial}{\partial \ln \mu_s} \mathbf{V}_h^{[\kappa]} = \mathbf{R}_{[\kappa]}^{-1} \left[\frac{\alpha_s(\mu_s)}{4\pi} \mathbf{r}_h^{[\kappa],(0)} + \left(\frac{\alpha_s(\mu_s)}{4\pi} \right)^2 \mathbf{r}_h^{[\kappa],(1)} + \mathcal{O}(\alpha_s^3) \right] \mathbf{R}_{[\kappa]} \mathbf{V}_h^{[\kappa]}, \tag{2.50}$$

an additional contribution enters in the third line. This additional term takes a form similar to the NLL evolution equation, spoiling the N²LL accuracy of $\mathbf{V}_h^{[\kappa]}|_{\text{N}^2\text{LLD}}$. In view of this difference, the decomposition of Eq. (2.45) should be interpreted as an *ad hoc* prescription to diminish the divergence in the threshold limit rather than an exact solution of the hard RGE.

An analogous decomposition should also be applied to the other partonic functions in Eqs. (2.7) and (2.8)

to remove the combined contributions from different fixed-order ingredients, giving

$$\begin{aligned}
& \widetilde{\Sigma}_{t\bar{t}}^{\text{res}, [q_n^i \bar{q}_n^j]}(\vec{b}_T, Y_{t\bar{t}}, M_{t\bar{t}}, \Omega_t) \Big|_{\text{N}^2\text{LLD}} \\
&= \left(\frac{1}{2N_c} \right)^2 \mathcal{D}_{[q_n^i \bar{q}_n^j]}^{\text{res}}(b_T, M_{t\bar{t}}, \mu_h, \mu_b, \mu_s, \nu_b, \nu_s) \\
&\times \sum_{\{n_i, n'_i, n''_i, n'''_i\}} \left(\frac{\alpha_s(\mu_s)}{4\pi} \right)^{n_s + n'_s + n''_s} \left(\frac{\alpha_s(\mu_b)}{4\pi} \right)^{n_b + n'_b} \left(\frac{\alpha_s(\mu_h)}{4\pi} \right)^{n_h + n'_h + n''_h + n'''_h} \\
&\quad \times \mathcal{B}_n^{[q_n^i], (n_b)}(\eta_n, b_T, \mu_b, \nu_b) \mathcal{B}_{\bar{n}}^{[\bar{q}_n^j], (n'_b)}(\eta_{\bar{n}}, b_T, \mu_b, \nu_b) \\
&\quad \times \sum_{\{\alpha, \beta, h\}} \left\{ \mathcal{S}_{[q_n \bar{q}_n], (n_s)}^{\alpha_1 \beta_1}(\vec{b}_T, v_t, v_{\bar{t}}, \mu_s, \nu_s) \left[\mathcal{V}_{\alpha_1 \alpha_2}^{[q_n \bar{q}_n], (n'_s, n'_h)}(v_t, v_{\bar{t}}, \mu_s, \mu_h) \mathcal{C}_{\alpha_2; h_n h_{\bar{n}} h_t h_{\bar{t}}}^{[q_n^i \bar{q}_n^j], (n_h)} \right]^* \right. \\
&\quad \quad \quad \left. \times \left[\mathcal{V}_{\beta_1 \beta_2}^{[q_n \bar{q}_n], (n''_s, n''_h)}(v_t, v_{\bar{t}}, \mu_s, \mu_h) \mathcal{C}_{\beta_2; h_n h_{\bar{n}} h_t h_{\bar{t}}}^{[q_n^i \bar{q}_n^j], (n'''_h)} \right] \right\} \\
&\quad \times \theta \left[1 - (n_h + n'_h + n''_h + n'''_h) - (n_s + n'_s + n''_s) - (n_b + n'_b) \right],
\end{aligned} \tag{2.51}$$

$$\begin{aligned}
& \widetilde{\Sigma}_{t\bar{t}}^{\text{res}, [g_n g_{\bar{n}}]}(\vec{b}_T, Y_{t\bar{t}}, M_{t\bar{t}}, \Omega_t) \Big|_{\text{N}^2\text{LLD}} \\
&= \left(\frac{1}{N_c^2 - 1} \right)^2 \mathcal{D}_{[g_n g_{\bar{n}}]}^{\text{res}}(b_T, M_{t\bar{t}}, \mu_h, \mu_b, \mu_s, \nu_b, \nu_s) \\
&\times \sum_{\{n_i, n'_i, n''_i, n'''_i\}} \left(\frac{\alpha_s(\mu_s)}{4\pi} \right)^{n_s + n'_s + n''_s} \left(\frac{\alpha_s(\mu_b)}{4\pi} \right)^{n_b + n'_b} \left(\frac{\alpha_s(\mu_h)}{4\pi} \right)^{n_h + n'_h + n''_h + n'''_h} \\
&\quad \times \sum_{\{\alpha, \beta, h, h'\}} \left\{ \mathcal{S}_{[g_n g_{\bar{n}}], (n_s)}^{\alpha_1 \beta_1}(\vec{b}_T, v_t, v_{\bar{t}}, \mu_s, \nu_s) \mathcal{B}_{n, h'_n h_n}^{[g_n], (n_b)}(\eta_n, \vec{b}_T, \mu_b, \nu_b) \mathcal{B}_{\bar{n}, h'_n h_{\bar{n}}}^{[g_{\bar{n}}], (n'_b)}(\eta_{\bar{n}}, \vec{b}_T, \mu_b, \nu_b) \right. \\
&\quad \quad \quad \times \left[\mathcal{V}_{\alpha_1 \alpha_2}^{[g_n g_{\bar{n}}], (n'_s, n'_h)}(v_t, v_{\bar{t}}, \mu_s, \mu_h) \mathcal{C}_{\alpha_2; h'_n h'_n h_t h_{\bar{t}}}^{[g_n g_{\bar{n}}], (n_h)} \right]^* \\
&\quad \quad \quad \left. \times \left[\mathcal{V}_{\beta_1 \beta_2}^{[g_n g_{\bar{n}}], (n''_s, n''_h)}(v_t, v_{\bar{t}}, \mu_s, \mu_h) \mathcal{C}_{\beta_2; h_n h_{\bar{n}} h_t h_{\bar{t}}}^{[g_n g_{\bar{n}}], (n'''_h)} \right] \right\} \\
&\quad \times \theta \left[1 - (n_h + n'_h + n''_h + n'''_h) - (n_s + n'_s + n''_s) - (n_b + n'_b) \right],
\end{aligned}$$

where the Heaviside function $\theta(x)$ is introduced with $\theta(x) = 1$ for $x \geq 0$ and $\theta(x) = 0$ otherwise. The $\mathcal{V}_{\alpha\beta}^{[\kappa], (n_s, n_h)}$ refers to the element in the non-cusp resummation kernel of Eq. (2.45) at index $\{\alpha, \beta\}$. The perturbative expansion of the fixed-order coefficient functions is defined as,

$$\begin{aligned}
\mathcal{S}_{[\kappa]}^{\alpha\beta} &= \sum_{n_s=0}^{\infty} \left(\frac{\alpha_s(\mu_s)}{4\pi} \right)^{n_s} \mathcal{S}_{[\kappa], (n_s)}^{\alpha\beta}, \\
\mathcal{C}_{\alpha, \{h\}}^{[\kappa]} &= \sum_{n_h=0}^{\infty} \left(\frac{\alpha_s(\mu_h)}{4\pi} \right)^{n_h+1} \mathcal{C}_{\alpha, \{h\}}^{[\kappa], (n_h)}, \\
\mathcal{B}_{n(\bar{n})}^{[\kappa]} &= \sum_{n_b=0}^{\infty} \left(\frac{\alpha_s(\mu_b)}{4\pi} \right)^{n_b} \mathcal{B}_{n(\bar{n})}^{[\kappa], (n_b)}.
\end{aligned} \tag{2.52}$$

The asymptotic behaviour of Eqs. (2.51) in the threshold limit $\beta_{t\bar{t}} \rightarrow 0$ can be obtained by repeating the expansion procedure of Sec. 2.2. Analysing the fixed order constituents, as demonstrated in Eq. (2.19), (2.26), and (2.29), the soft and beam-collinear functions approach a constant in the limit $\beta_{t\bar{t}} \rightarrow 0$ up to NLO, while a power like divergence of $\mathcal{O}(\beta_{t\bar{t}}^{-1})$ still emerges from the NLO hard sector as a result of the Coulomb interaction. As for the evolution kernels, the diagonal entries $\mathcal{D}_{[\kappa]}^{\text{res}}$ continue to be regular in the threshold domain, see Eq. (2.20), while the singular behaviour of the non-cusp kernel \mathbf{V}_h is now reduced by

one power of $\beta_{t\bar{t}}$ after the decomposition in Eq. (2.45), according to the scaling rules of Eq. (2.30-2.35), i.e.

$$\mathbf{V}_h^{[\kappa]} \Big|_{\text{N}^2\text{LLD}} \sim \mathcal{O}(\beta_{t\bar{t}}^{-1}). \quad (2.53)$$

In summary, we arrive at,

$$\lim_{\beta_{t\bar{t}} \rightarrow 0} \widetilde{\Sigma}_{t\bar{t}}^{\text{res},[\kappa]} \Big|_{\text{N}^2\text{LLD}} \sim \mathcal{O}(\beta_{t\bar{t}}^{-1}). \quad (2.54)$$

In comparison with Eq. (2.40), the thus defined D-prescription reduces the degree of the divergence to $\mathcal{O}(\beta_{t\bar{t}}^{-1})$, pushing all terms of higher divergence to $\text{N}^2\text{LL}'$ and beyond. Although our resummed cross section still diverges as $\beta_{t\bar{t}} \rightarrow 0$, this singularity can be well contained by the kinematical suppression introduced through the phase space element and the observable definition, see Eq. (2.43). Therefore, we can now safely lift the kinematic constraint in Eq. (2.15) and take into account the full $M_{t\bar{t}}$ range in the phase space integral for the single differential observables $d\sigma_{t\bar{t}}^{\text{res}}/dq_T$ and $d\sigma_{t\bar{t}}^{\text{res}}/d\Delta\phi_{t\bar{t}}$.

At last, we would like to stress that in the previous calculations on the soft [206] and zero-jettiness [109] resummations, the expansion of the product of the fixed-order contributions and the hard evolution kernels in the strong coupling α_s was already used to remove the Coulomb divergence and thereby accomplish N^2LL accurate results. Eqs. (2.51) in our formulation is in fact equivalent to their solution, with the only exception that the soft and beam-collinear sectors were adapted as appropriate to the observables of interest. An analogous prescription was also implemented in the q_T [104,105] and threshold [88] resummation, where, in place of α_s , the expansion therein proceeded in the scaling $\lambda_N \sim \alpha_s \sim 1/\ln(\mu_h/\mu_s)$. This method is equivalent to Eqs. (2.51) of our formulation as well, since, up to N^2LL , the result of the λ_N expansion can be absorbed into the running of α_s .

2.3.2 R-prescription: Resummation with a re-exponentiated anomalous dimension

Alternatively, we can also mitigate the threshold singularity of $\mathbf{V}_h^{[\kappa]}$ at N^2LL by re-exponentiating the divergent contributions in the anomalous dimension $\gamma_h^{[\kappa]}$. We will call this the R-prescription in the following. To accomplish this it is worth noting that, to accommodate the Coulomb enhancement in the threshold domain, it is convenient to organise the perturbative contributions using the parameter $\lambda_{t\bar{t}} \sim \beta_{t\bar{t}} \sim \alpha_s$ [101, 163, 164, 170]. Even though a systematic resummation of Coulomb, soft, and beam-collinear singularities is not the focus of this paper, in the following we will show that this scaling rule can facilitate the regularisation of the threshold divergence of Eq. (2.39).

Expanding the anomalous dimension $\gamma_h^{[\kappa]}$ up to two-loop level [212, 213] in the parameter $\lambda_{t\bar{t}}$, we arrive at the following power series,

$$\gamma_h^{[\kappa]} \xrightarrow{\beta_{t\bar{t}} \rightarrow 0} \left(\frac{\alpha_s(\mu)}{4\pi} \right) \gamma_{h,\text{thr}}^{[\kappa],(0)} + \left(\frac{\alpha_s(\mu)}{4\pi} \right)^2 \gamma_{h,\text{thr}}^{[\kappa],(1)} + \mathcal{O}(\lambda_{t\bar{t}}^2), \quad (2.55)$$

where

$$\begin{aligned} \gamma_{h,\text{thr}}^{[q_n \bar{q}_n],(0)} &= \gamma_{h,\text{thr}}^{[\bar{q}_n q_n],(0)} = \begin{bmatrix} -\frac{8i\pi}{3\beta_{t\bar{t}}} - 8 & 0 \\ 0 & \frac{i\pi}{3\beta_{t\bar{t}}} + 6i\pi - 14 \end{bmatrix}, \\ \gamma_{h,\text{thr}}^{[g_n g_n],(0)} &= \begin{bmatrix} -\frac{46}{3} - \frac{8i\pi}{3\beta_{t\bar{t}}} & 0 & 0 \\ 0 & \frac{i\pi}{3\beta_{t\bar{t}}} + 6i\pi - \frac{64}{3} & 0 \\ 0 & 0 & \frac{i\pi}{3\beta_{t\bar{t}}} + 6i\pi - \frac{64}{3} \end{bmatrix}, \\ \gamma_{h,\text{thr}}^{[q_n \bar{q}_n],(1)} &= \gamma_{h,\text{thr}}^{[\bar{q}_n q_n],(1)} = \begin{bmatrix} -\frac{344i\pi}{27\beta_{t\bar{t}}} & 0 \\ 0 & \frac{43i\pi}{27\beta_{t\bar{t}}} \end{bmatrix}, \\ \gamma_{h,\text{thr}}^{[g_n g_n],(1)} &= \begin{bmatrix} -\frac{344i\pi}{27\beta_{t\bar{t}}} & 0 & 0 \\ 0 & \frac{43i\pi}{27\beta_{t\bar{t}}} & 0 \\ 0 & 0 & \frac{43i\pi}{27\beta_{t\bar{t}}} \end{bmatrix}. \end{aligned} \quad (2.56)$$

Here, while we retain the leading and subleading singular contributions in the one-loop anomalous dimension, only the leading terms are needed in the two loop results, in accordance with our scaling rule. At this point, it is important to note that in the threshold limit all $\gamma_h^{[\kappa]}$ are diagonal up to two-loop order. This allows us to solve the hard RGE for the evolution kernel in the low $\beta_{t\bar{t}}$ region exactly,

$$\frac{d}{d \ln \mu} \ln \tilde{\mathbf{V}}_{h,\text{thr}}^{[\kappa]} = \gamma_{h,\text{thr}}^{[\kappa]}, \quad (2.57)$$

which leads to the results at NLL and N²LL accuracy,

$$\begin{aligned} \tilde{\mathbf{V}}_{h,\text{thr}}^{[\kappa],(0)} &= \exp \left\{ \frac{\gamma_{\text{thr},h}^{[\kappa],(0)}}{2\beta_0} \ln \left[\frac{\alpha_s(\mu_h)}{\alpha_s(\mu_s)} \right] \right\}, \\ \tilde{\mathbf{V}}_{h,\text{thr}}^{[\kappa],(1)} &= \exp \left\{ \frac{\gamma_{\text{thr},h}^{[\kappa],(0)}}{2\beta_0} \ln \left[\frac{\alpha_s(\mu_h)}{\alpha_s(\mu_s)} \right] - \frac{\alpha_s(\mu_h) - \alpha_s(\mu_s)}{4\pi} \underbrace{\left(\gamma_{h,\text{thr}}^{[\kappa],(0)} \frac{\beta_1}{2\beta_0^2} - \frac{\gamma_{h,\text{thr}}^{[\kappa],(1)}}{2\beta_0} \right)}_{\rightarrow \mathbf{J}_{\text{thr}}^{[\kappa]} + \mathcal{O}(\beta_{t\bar{t}}^0)} \right\}, \end{aligned} \quad (2.58)$$

where β_i stands for the QCD beta function [286, 287]. With this result we find that the NLL evolutions here can exactly reproduce the leading contributions in Eq. (2.38) which are derived by expanding the analytic expression of Eq. (2.12) in the limit $\beta_{t\bar{t}} \rightarrow 0$.

In particular, at finite $\beta_{t\bar{t}}$, where the $\gamma_h^{[\kappa]}$ are in general not diagonal at N²LL, no closed solutions are available. Hence, approximate solutions are used, for example in Eq. (2.13), where only the one-loop anomalous dimensions are exponentiated and the logarithmic corrections relevant at N²LL are applied by multiplying $(\mathbf{I} + \frac{\alpha_s(\mu_s)}{4\pi} \mathbf{J}^{[\kappa]})$ and $(\mathbf{I} - \frac{\alpha_s(\mu_h)}{4\pi} \mathbf{J}^{[\kappa]})$, respectively. This structural difference can lead to differences in the asymptotic behaviour between the solutions in Eq. (2.58) and Eq. (2.39), respectively, in the threshold limit. For instance, the $\mathbf{V}_{h,\text{thr}}^{[\kappa],(1)}$ of Eq. (2.39) are directly proportional to the product $\alpha_s(\mu_h)\alpha_s(\mu_s)(\mathbf{J}_{\text{thr}}^{[\kappa]})^2$ which, according to Eq. (2.35), develops divergences of $\mathcal{O}(\beta_{t\bar{t}}^{-2})$ as $\beta_{t\bar{t}} \rightarrow 0$. However, as we have now moved all anomalous dimensions into the exponent and owing to the fact that their singular terms reside in the imaginary part only, see Eq. (2.56), the $\tilde{\mathbf{V}}_{h,\text{thr}}^{[\kappa],(1)}$ exhibits oscillatory but finite behaviour in the limit $\beta_{t\bar{t}} \rightarrow 0$. We can exploit this improved behaviour to remove the threshold divergences of Eq. (2.13).

Noting that the RGE of Eq. (2.57) is subject to the counting rule $\lambda_{t\bar{t}} \sim \beta_{t\bar{t}} \sim \alpha_s$, which is appropriate in the threshold domain but can receive significant power corrections in the well-separated region at large $\beta_{t\bar{t}}$, we introduce the following matching procedure,

$$\mathbf{V}_h^{[\kappa]} \Big|_{\text{N}^2\text{LL}_R} = f_{\text{tran}}(\beta_{t\bar{t}}, c_{\text{thr}}, r_{\text{thr}}) \tilde{\mathbf{V}}_{h,\text{thr}}^{[\kappa],(1)} \left[\tilde{\mathbf{V}}_{h,\text{exp}}^{[\kappa],(1)} \right]^{-1} \mathbf{V}_h^{[\kappa]} \Big|_{\text{N}^2\text{LL}} + \left[1 - f_{\text{tran}}(\beta_{t\bar{t}}, c_{\text{thr}}, r_{\text{thr}}) \right] \mathbf{V}_h^{[\kappa]} \Big|_{\text{N}^2\text{LL}}, \quad (2.59)$$

where in the first term the matrix $\tilde{\mathbf{V}}_{h,\text{exp}}^{[\kappa],(1)}$ is used to remove the overlap between $\tilde{\mathbf{V}}_{h,\text{thr}}^{[\kappa],(1)}$ and $\mathbf{V}_h^{[\kappa]}$. It can be extracted by expanding $\tilde{\mathbf{V}}_{h,\text{thr}}^{[\kappa],(1)}$ in $\alpha_s(\mu_s)$ and $\alpha_s(\mu_h)$ and retaining all contributions up to NLO, yielding

$$\begin{aligned} \tilde{\mathbf{V}}_{h,\text{exp}}^{[\kappa],(1)} &= \left[1 + \frac{\alpha_s(\mu_s)}{4\pi} \left(\gamma_{h,\text{thr}}^{[\kappa],(0)} \frac{\beta_1}{2\beta_0^2} - \frac{\gamma_{h,\text{thr}}^{[\kappa],(1)}}{2\beta_0} \right) \right] \\ &\quad \times \exp \left\{ \frac{\gamma_{\text{thr},h}^{[\kappa],(0)}}{2\beta_0} \ln \left[\frac{\alpha_s(\mu_h)}{\alpha_s(\mu_s)} \right] \right\} \left[1 - \frac{\alpha_s(\mu_h)}{4\pi} \left(\gamma_{h,\text{thr}}^{[\kappa],(0)} \frac{\beta_1}{2\beta_0^2} - \frac{\gamma_{h,\text{thr}}^{[\kappa],(1)}}{2\beta_0} \right) \right]. \end{aligned} \quad (2.60)$$

Multiplying $\tilde{\mathbf{V}}_{h,\text{thr}}^{[\kappa],(1)}$ by $[\tilde{\mathbf{V}}_{h,\text{exp}}^{[\kappa],(1)}]^{-1}$ removes terms of the same perturbative order as those already present in $\mathbf{V}_h^{[\kappa]}$ in Eq. (2.13), thereby eliminating any double-counting in the matched result. In the limit $\beta_{t\bar{t}} \rightarrow 0$, both $\tilde{\mathbf{V}}_{h,\text{exp}}^{[\kappa],(1)}$ and $\mathbf{V}_h^{[\kappa]}$ approach $\mathbf{V}_{h,\text{thr}}^{[\kappa],(1)}$ of Eq. (2.39), such that the first term of Eq. (2.59) is actually dictated by $\tilde{\mathbf{V}}_{h,\text{thr}}^{[\kappa],(1)}$. Away from the threshold regime, power corrections to Eq. (2.57) become relevant and its solution $\tilde{\mathbf{V}}_{h,\text{thr}}^{[\kappa],(1)}$ gradually loses its accuracy. Here, we introduce the transition function f_{tran} to switch

off their contribution in the well-separated regime, i.e.,

$$f_{\text{tran}}(\beta_{t\bar{t}}, c_{\text{thr}}, r_{\text{thr}}) = \begin{cases} 1, & \beta_{t\bar{t}} \leq c_{\text{thr}} - r_{\text{thr}}; \\ 1 - \frac{(\beta_{t\bar{t}} - c_{\text{thr}} + r_{\text{thr}})^2}{2r_{\text{thr}}^2}, & c_{\text{thr}} - r_{\text{thr}} < \beta_{t\bar{t}} \leq c_{\text{thr}}; \\ \frac{(\beta_{t\bar{t}} - c_{\text{thr}} - r_{\text{thr}})^2}{2r_{\text{thr}}^2}, & c_{\text{thr}} < \beta_{t\bar{t}} \leq c_{\text{thr}} + r_{\text{thr}}; \\ 0, & c_{\text{thr}} + r_{\text{thr}} \leq \beta_{t\bar{t}}, \end{cases} \quad (2.61)$$

where the parameters c_{thr} and r_{thr} are introduced to characterize the focal point and the transition radius, respectively. To determine their central values and ranges for the uncertainty estimation for our numerical evaluation in Sec. 3, we compare the numeric values of $\tilde{\mathbf{V}}_{h,\text{exp}}^{[\kappa],(1)}$ and $\mathbf{V}_h^{[\kappa]}$ to determine the range of validity for the RGE in Eq. (2.57), for details see App. B. In consequence, we choose

$$c_{\text{thr}}^{\text{def}} = 0.4, \quad r_{\text{thr}}^{\text{def}} = 0.1, \quad (2.62)$$

as our default choices and use the sets

$$\{c_{\text{thr}}, r_{\text{thr}}\} = \{0.35, 0.05\}, \{0.45, 0.15\} \quad (2.63)$$

to estimate the theoretical uncertainty associated with our matching procedure.

At variance with the D-prescription of Eq. (2.45), where the Coulomb singular terms are pushed to a higher logarithmic order, Eq. (2.59) reduces the threshold divergence by re-exponentiating the N²LL corrections that have been abandoned in the formalism of Eq. (2.13). To this end, we will call the hereby defined prescription the R-prescription in the following and label the evolution kernel evaluated via Eq. (2.59) with N²LL_R. Incorporating Eq. (2.59) into Eqs. (2.7) and (2.8), we derive the resummed partonic cross section

in the R-prescription,

$$\begin{aligned}
& \widetilde{\Sigma}_{t\bar{t}}^{\text{res}, [q_n^i \bar{q}_n^j]}(\vec{b}_T, Y_{t\bar{t}}, M_{t\bar{t}}, \Omega_t) \Big|_{\text{N}^2\text{LLR}} \\
&= \left(\frac{1}{2N_c} \right)^2 \mathcal{D}_{[q_n^i \bar{q}_n^j]}^{\text{res}}(b_T, M_{t\bar{t}}, \mu_h, \mu_b, \mu_s, \nu_b, \nu_s) \\
&\quad \times \sum_{\{n_i, n'_i\}} \left(\frac{\alpha_s(\mu_s)}{4\pi} \right)^{n_s} \left(\frac{\alpha_s(\mu_b)}{4\pi} \right)^{n_b+n'_b} \left(\frac{\alpha_s(\mu_h)}{4\pi} \right)^{n_h+n'_h} \\
&\quad \times \mathcal{B}_n^{[q_n^i], (n_b)}(\eta_n, b_T, \mu_b, \nu_b) \mathcal{B}_{\bar{n}}^{[\bar{q}_n^j], (n'_b)}(\eta_{\bar{n}}, b_T, \mu_b, \nu_b) \\
&\quad \times \sum_{\{\alpha, \beta, h\}} \left\{ \mathcal{S}_{[q_n \bar{q}_n], (n_s)}^{\alpha_1 \beta_1}(\vec{b}_T, v_t, v_{\bar{t}}, \mu_s, \nu_s) \left[\mathcal{V}_{\alpha_1 \alpha_2}^{[q_n \bar{q}_n]}(v_t, v_{\bar{t}}, \mu_s, \mu_h) \mathcal{C}_{\alpha_2; h_n h_{\bar{n}} h_t h_{\bar{t}}}^{[q_n^i \bar{q}_n^j], (n_h)} \right]^* \right. \\
&\quad \quad \quad \left. \times \left[\mathcal{V}_{\beta_1 \beta_2}^{[q_n \bar{q}_n]}(v_t, v_{\bar{t}}, \mu_s, \mu_h) \mathcal{C}_{\beta_2; h_n h_{\bar{n}} h_t h_{\bar{t}}}^{[q_n^i \bar{q}_n^j], (n'_h)} \right] \right\} \\
&\quad \times \theta(1-n_h) \theta(1-n'_h) \theta(1-n_s) \theta(1-n_b) \theta(1-n'_b), \tag{2.64}
\end{aligned}$$

$$\begin{aligned}
& \widetilde{\Sigma}_{t\bar{t}}^{\text{res}, [g_n g_{\bar{n}}]}(\vec{b}_T, Y_{t\bar{t}}, M_{t\bar{t}}, \Omega_t) \Big|_{\text{N}^2\text{LLR}} \\
&= \left(\frac{1}{N_c^2 - 1} \right)^2 \mathcal{D}_{[g_n g_{\bar{n}}]}^{\text{res}}(b_T, M_{t\bar{t}}, \mu_h, \mu_b, \mu_s, \nu_b, \nu_s) \\
&\quad \times \sum_{\{n_i, n'_i\}} \left(\frac{\alpha_s(\mu_s)}{4\pi} \right)^{n_s} \left(\frac{\alpha_s(\mu_b)}{4\pi} \right)^{n_b+n'_b} \left(\frac{\alpha_s(\mu_h)}{4\pi} \right)^{n_h+n'_h} \\
&\quad \times \sum_{\{\alpha, \beta, h, h'\}} \left\{ \mathcal{S}_{[g_n g_{\bar{n}}], (n_s)}^{\alpha_1 \beta_1}(\vec{b}_T, v_t, v_{\bar{t}}, \mu_s, \nu_s) \mathcal{B}_{n, h'_n h_n}^{[g_n], (n_b)}(\eta_n, \vec{b}_T, \mu_b, \nu_b) \mathcal{B}_{\bar{n}, h'_{\bar{n}} h_{\bar{n}}}^{[g_{\bar{n}}], (n'_b)}(\eta_{\bar{n}}, \vec{b}_T, \mu_b, \nu_b) \right. \\
&\quad \quad \quad \left. \times \left[\mathcal{V}_{\alpha_1 \alpha_2}^{[g_n g_{\bar{n}}]}(v_t, v_{\bar{t}}, \mu_s, \mu_h) \mathcal{C}_{\alpha_2; h'_n h'_n h_t h_{\bar{t}}}^{[g_n g_{\bar{n}}], (n_h)} \right]^* \left[\mathcal{V}_{\beta_1 \beta_2}^{[g_n g_{\bar{n}}]}(v_t, v_{\bar{t}}, \mu_s, \mu_h) \mathcal{C}_{\beta_2; h_n h_{\bar{n}} h_t h_{\bar{t}}}^{[g_n g_{\bar{n}}], (n'_h)} \right] \right\} \\
&\quad \times \theta(1-n_h) \theta(1-n'_h) \theta(1-n_s) \theta(1-n_b) \theta(1-n'_b).
\end{aligned}$$

Here the perturbative correction in each contribution has been included independently up to NLO, for which the product of the Heaviside step functions $\theta(1-n_i)$ is introduced to impose the boundary condition of the N²LL-level resummation. Again, $\mathcal{V}_{\alpha\beta}^{[\kappa]}$ denotes the element in the non-cusp resummation kernel of Eq. (2.59) at the α -th row and β -th column. Differing from the D-prescription in Eqs. (2.51), where the product of the NLO fixed-order contributions are pushed to terms of higher logarithmic order, all of those contributions are taken into account in the R-prescription of Eq. (2.64). In principle, if there were no threshold divergences emerging from the NLO non-logarithmic terms, these products could be categorised into the higher logarithmic corrections and should play a numerically minor role in the resummation. However, in light of the Coulomb singularity in Eq. (2.26) and the threshold enhancement in Eq. (2.38), the differences in organising the fixed-order correction between the D- and R-prescriptions can impact the q_T and $\Delta\phi_{t\bar{t}}$ spectra in the vicinity of $\beta_{t\bar{t}} = 0$ non-trivially. In Sec. 3.3, we will make use of this property to test the sensitivity of $d\sigma_{t\bar{t}}/d\Delta\phi_{t\bar{t}}$ and $d\sigma_{t\bar{t}}/dq_T$ to the treatment of the Coulomb interactions.

Taking the threshold limit $\beta_{t\bar{t}} \rightarrow 0$, the only singular contribution in Eq. (2.64) comes from the perturbative correction to the hard function, Eq. (2.26), giving rise to a quadratic divergence in the partonic function,

$$\widetilde{\Sigma}_{t\bar{t}}^{\text{res}, [\kappa]} \Big|_{\text{N}^2\text{LLR}} \xrightarrow{\beta_{t\bar{t}} \rightarrow 0} \mathcal{O}(\beta_{t\bar{t}}^{-2}). \tag{2.65}$$

In comparison with the corresponding expression in the D-prescription, Eq. (2.53), the result in Eq. (2.65) exhibits a stronger divergence in the threshold limit. Nevertheless, this divergence can still be accommodated by the kinematic suppression factors of Eq. (2.43), allowing us to remove the phase space restriction $M_{t\bar{t}}^{\text{min}}$ in Eq. (2.15) when evaluating the single differential observables $d\sigma_{t\bar{t}}^{\text{res}}/dq_T$ and $d\sigma_{t\bar{t}}^{\text{res}}/d\Delta\phi_{t\bar{t}}$.

2.4 Matching to fixed-order QCD

In the past subsections, we have taken the soft-collinear resummation for the q_T and $\Delta\phi_{t\bar{t}}$ spectra within the well-separated domain $\Delta E_{t\bar{t}} \sim \mathcal{O}(m_t)$ and then extended its coverage over the full $M_{t\bar{t}}$ range via two ad hoc prescriptions. During this analysis, we worked at leading-power accuracy, embedding the most singular behaviour as $q_T \rightarrow 0$ or $\Delta\phi_{t\bar{t}} \rightarrow 0$, but systematically neglected higher-power corrections. In the followings, we will restore them in part by matching resummation to a dedicated fixed-order QCD calculation. To this end, we introduce a matching procedure between the resummation and the fixed-order QCD calculation, defined through [124, 288, 289]

$$\begin{aligned} \frac{d\sigma_{t\bar{t}}^{\text{mat}}}{d\mathcal{Q}} &\equiv \left\{ \left[\frac{d\sigma_{t\bar{t}}^{\text{res}}}{d\mathcal{Q}} - \frac{d\sigma_{t\bar{t}}^{\text{s}}(\mu_{\text{f.o.}})}{d\mathcal{Q}} \right] f_{\text{tran}}(\mathcal{Q}, c_m, r_m) + \frac{d\sigma_{t\bar{t}}^{\text{s}}(\mu_{\text{f.o.}})}{d\mathcal{Q}} \right\} \mathcal{R}_{\text{fs}}(\mu_{\text{f.o.}}) \\ &= f_{\text{tran}}(\mathcal{Q}, c_m, r_m) \left(\frac{d\sigma_{t\bar{t}}^{\text{res}}}{d\mathcal{Q}} \right) \Bigg|_{\text{exp}} + \left\{ 1 - f_{\text{tran}}(\mathcal{Q}, c_m, r_m) \right\} \frac{d\sigma_{t\bar{t}}^{\text{f.o.}}(\mu_{\text{f.o.}})}{d\mathcal{Q}} + \dots, \end{aligned} \quad (2.66)$$

where $\mathcal{Q} \in \{q_T, \Delta\phi_{t\bar{t}}\}$ stands for the observables of our concern. $d\sigma_{t\bar{t}}^{\text{res}}/d\mathcal{Q}$ and $d\sigma_{t\bar{t}}^{\text{s}}/d\mathcal{Q}$ represent the resummed differential cross section and its perturbative expansion evaluated at the fixed-order scale $\mu_{\text{f.o.}}$. The modification factor \mathcal{R}_{fs} is introduced here to supply the power suppressed contributions that have been discarded in deriving the resummation in Eqs. (2.7) and (2.8). It is defined as,

$$\mathcal{R}_{\text{fs}}(\mu_{\text{f.o.}}) = \frac{d\sigma_{t\bar{t}}^{\text{f.o.}}(\mu_{\text{f.o.}})/d\mathcal{Q}}{d\sigma_{t\bar{t}}^{\text{s}}(\mu_{\text{f.o.}})/d\mathcal{Q}}. \quad (2.67)$$

Herein, $d\sigma_{t\bar{t}}^{\text{f.o.}}/d\mathcal{Q}$ denotes the fixed-order QCD results at the fixed-order scale $\mu_{\text{f.o.}}$, which will be appraised by means of the program SHERPA [290–293]. In calculating \mathcal{R}_{fs} , it is worth noting that starting from N²LO, the denominator is not positive definite and exhibits zeros. In this case, we expand \mathcal{R}_{fs} in $\alpha_s(\mu_{\text{f.o.}})$ in the second step of Eq. (2.66) following the methodology in [124]. Throughout our calculation, we will utilise

$$\mu_{\text{f.o.}}^{\text{def}} = M_{t\bar{t}} \quad (2.68)$$

as our default choice but employ the interval $\mu_{\text{f.o.}} \in [1/2, 2]M_{t\bar{t}}$ to estimate the theoretical uncertainty.

Again, the transition function f_{tran} is employed here to progressively fade out the resummation away from the singular region. f_{tran} in Eq. (2.66) formally takes the identical form as in Eq. (2.61), only being governed by different arguments \mathcal{Q} , c_m , and r_m here. The latter two parameters are subject to the range of validity of the leading power approximation, which we determine in Sec. 3.2 by comparing $d\sigma_{t\bar{t}}^{\text{s}}/d\mathcal{Q}$ and $d\sigma_{t\bar{t}}^{\text{f.o.}}/d\mathcal{Q}$.

3 Numerical Results

3.1 Input parameters

In order to validate and evaluate the expressions for the resummed cross sections of the q_T and $\Delta\phi_{t\bar{t}}$ spectra derived in the last section, we need to specify the following input parameters, the top quark mass m_t , strong coupling constant α_s , and the PDFs. We define the top quark mass in the pole mass scheme, using a value of $m_t = 173.4$ GeV. This is in line with our adopted UV renormalisation scheme for the hard sector. The strong coupling and the PDFs are evaluated by the LHAPDF package [294, 295], using the NNPDF31_nnlo_as_0118 [296] PDF set with $\alpha_s(m_Z) = 0.118$ in the $n_f = 5$ light flavour scheme.

The colour- and helicity-dependent amplitudes inherent in the partonic functions of Eqs. (2.7–2.8), Eq. (2.51), and Eq. (2.64), are evaluated using RECOLA [248, 249], up to NLO accuracy. After their combination with the soft and beam-collinear functions as well as the scale evolution kernels, the resulting resummed cross sections $\widehat{\Sigma}_{t\bar{t}}^{\text{res}, [\kappa]}$ are integrated over the relevant momentum and impact-parameter spaces using Cuba [297, 298] to give our resummed differential spectra $d\sigma_{t\bar{t}}^{\text{res}}/dq_T$ and $d\sigma_{t\bar{t}}^{\text{res}}/d\Delta\phi_{t\bar{t}}$.

Eventually, we match the resummation onto the fixed-order QCD calculations via Eq. (2.66). At NLO, the fixed order contributions comprise only the tree-level amplitudes in the domain $q_T > 0$ and $\Delta\phi_{t\bar{t}} > 0$, which can be automatically generated by SHERPA's [290–293] built-in matrix element generator AMEGIC [299]. We process its output using RIVET [300–302] to extract the observables $d\sigma_{t\bar{t}}^{\text{f.o.}}/dq_T$ and $d\sigma_{t\bar{t}}^{\text{f.o.}}/d\Delta\phi_{t\bar{t}}$. To calculate

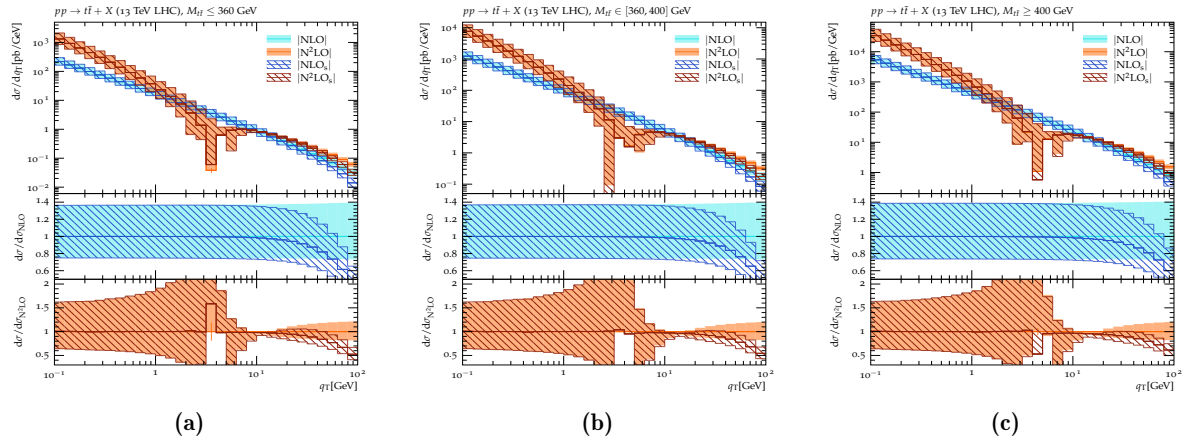


Figure 1: The transverse momentum spectrum of the $t\bar{t}$ -pair at fixed-order QCD at NLO and N^2 LO accuracy in the process $pp \rightarrow t\bar{t} + X$ at $\sqrt{s} = 13$ TeV within the intervals $M_{t\bar{t}} \leq 360$ GeV (left), $M_{t\bar{t}} \in [360, 400]$ GeV (centre), and $M_{t\bar{t}} \geq 400$ GeV (right). The NLO_s and N^2 LO_s results encode the leading singular behaviour derived from SCET+HQET.

the N^2 LO contributions, OPENLOOPS [303–306] is interfaced with SHERPA to calculate the renormalised one-loop corrections, which is then combined with the real-emission contribution generated again by AMEGIC within the dipole subtraction framework for single-parton divergences [307–310].

3.2 Validation

In the following, we confront the fixed-order expansion of the resummation in Eq. (2.15) with those evaluated in full QCD in order to establish the ability of our approximate calculation to reproduce the exact result in the relevant soft-collinear limits. Before analysing our numerical results in detail, it is worth noting that the expressions in Eq. (2.15) are applicable in the domain where the top and antitop quarks are well separated from their threshold production region. In this domain we are able to apply SCET+HQET to extract the soft and beam-collinear approximation in the low q_T and $\Delta\phi_{t\bar{t}}$ regime and thereby exploit the decoupling transformation [100, 147] to accomplish the factorisation in Eqs. (2.7-2.8). However, the situation is different in the threshold region where $\beta_{t\bar{t}}$ and $\Delta E_{t\bar{t}} \rightarrow 0$. Here, the (Coulomb) potential mode [223] comes into play via virtual gluon exchanges between the heavy partons and therefore Eq. (2.15) is not directly applicable. To this end, in the analysis below, we divide the phase space into three intervals, the threshold region $M_{t\bar{t}} \leq 360$ GeV, the transitional region $M_{t\bar{t}} \in [360, 400]$ GeV, and the well-separated region $M_{t\bar{t}} \geq 400$ GeV. We will use these three regions to examine the quality of the approximate result in the q_T and $\Delta\phi_{t\bar{t}}$ spectra, probing into the applicability and limitations of Eq. (2.15).

We begin our analysis with an examination of the transverse momentum spectra of the $t\bar{t}$ -pair in Fig. 1, where the differential distributions $d\sigma_{t\bar{t}}/dq_T$ of the SCET+HQET approximation are compared to those derived in full QCD. Therein, using cyan and apricot, we show the exact fixed-order full QCD results at NLO and N^2 LO, respectively, while the approximations are illustrated in the blue and red, labeled NLO_s and N^2 LO_s likewise. During their evaluation, we set the renormalisation and factorisation scales to $\mu_R = \mu_F = M_{t\bar{t}}$ as our central scale choice and use the interval $\mu_R = \mu_F \in [2, 0.5] M_{t\bar{t}}$ to estimate the theoretical uncertainties. We represent the scale uncertainties using corresponding coloured solid and hatched bands. In computing N^2 LO results, we invariably encounter zeros in both the full QCD and approximate calculations around $q_T \approx 3$ to 5 GeV, inducing significant Monte-Carlo statistical uncertainties shown via vertical error bars. Please note, that the distributions to the left of the respective zero-crossings are negative and we are therefore showing the absolute values.

From the main plots in Fig. 1, we observe that, up to N^2 LO, the asymptotic behaviour of the full QCD calculation is well captured by the leading singular contributions derived using SCET+HQET in the low q_T domain for all three $M_{t\bar{t}}$ slices, including the scale variations. As q_T increases, power corrections progressively corrupt the leading singular approximation and enlarge the discrepancies between NLO and NLO_s, and N^2 LO and N^2 LO_s, respectively, with the deviations becoming appreciable only around $q_T \geq 20$ GeV. This phenomenon suggests that, up to N^2 LO, the (Coulomb) potential region [223] near the $t\bar{t}$ production

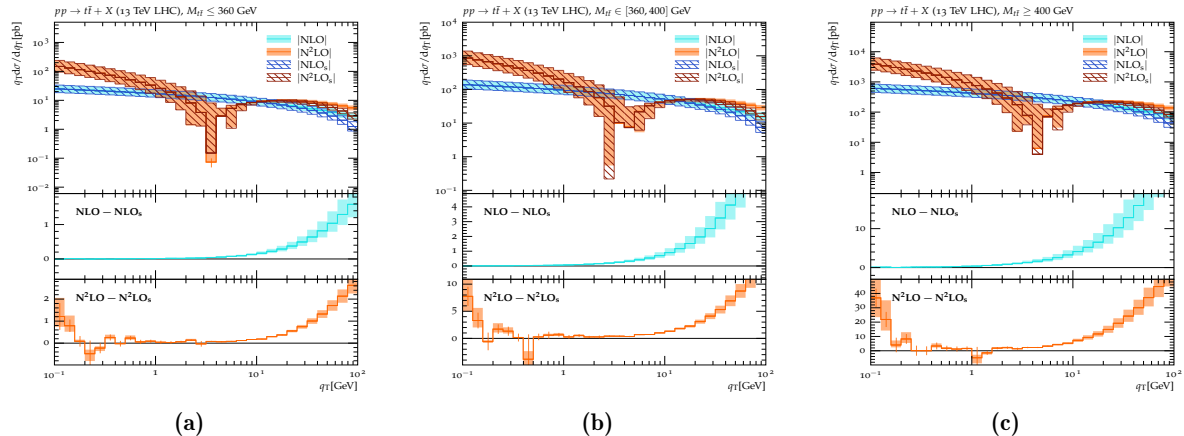


Figure 2: The weighted transverse momentum spectrum of the $t\bar{t}$ -pair at fixed-order QCD at NLO and N^2 LO accuracy in the process $pp \rightarrow t\bar{t} + X$ at $\sqrt{s} = 13$ TeV within the intervals $M_{t\bar{t}} \leq 360$ GeV (left), $M_{t\bar{t}} \in [360, 400]$ GeV (centre), and $M_{t\bar{t}} \geq 400$ GeV (right). The NLO_s and N^2LO_s results encode the leading singular behaviour derived from SCET+HQET.

threshold does not incur additional leading singular terms as $q_T \rightarrow 0$.

To make a more quantitative assessment of the leading power approximation, the first (second) subplots of Fig. 1 are devoted to the ratio between NLO_s (N^2LO_s) and NLO (N^2LO). We observe that with only percent level deviations up to $q_T = 20$ GeV, the q_T spectra derived through SCET+HQET manage to describe the asymptotic behaviour of the full QCD results at both NLO and N^2 LO precisions. Further increase in q_T increases the deviations between both approaches as higher-power corrections become increasingly important. Nevertheless, for $q_T \approx 50$ GeV, the leading power approximation can still account for 80% contribution of the exact differential distributions $d\sigma_{t\bar{t}}/dq_T$.

In pursuit of further ascertaining the SCET+HQET prediction, we investigate the weighted differential distributions $d\sigma_{t\bar{t}}/d \ln q_T$ in the low $q_T \rightarrow 0$ regime, which are expected to observe the power series,

$$\frac{d\sigma_{t\bar{t}}}{d \ln q_T} = q_T \frac{d\sigma_{t\bar{t}}}{dq_T} \sim \sigma_{t\bar{t}}^{\text{LO}} \sum_{m,n} \left(\frac{\alpha_s}{4\pi}\right)^m \left[\underbrace{c_{m,n}^{(0)} \ln^n(q_T)}_{\text{LP}} + \underbrace{c_{m,n}^{(1)} q_T \ln^n(q_T)}_{\text{NLP}} + \underbrace{c_{m,n}^{(2)} q_T^2 \ln^n(q_T)}_{\text{N}^2\text{LP}} + \dots \right], \quad (3.1)$$

where $\sigma_{t\bar{t}}^{\text{LO}}$ is the LO cross section and the $c_{m,n}^{(i)}$ are the coefficients at the respective order of the expansion. The numerical results for $d\sigma_{t\bar{t}}/d \ln q_T$ are presented in Fig. 2. Differing from the findings of Fig. 1, where acute enhancements are showcased in the low q_T region, the asymptotic behaviour in $d\sigma_{t\bar{t}}/d \ln q_T$ is alleviated as compared to that of $d\sigma_{t\bar{t}}/dq_T$ by the application of the weighting factor q_T . To examine whether the leading power behaviour can be entirely replicated by Eq. (2.15), we exhibit the difference between the full QCD results and the EFT ones in the first and second subgraphs of Fig. 2. At NLO, their difference declines monotonously as q_T decreases in all three $M_{t\bar{t}}$ intervals, demonstrating that the leading power contributions are indeed subtracted by the fixed-order expansion of Eq. (2.15). Regarding the interval $q_T \in [0.3, 100]$ GeV, analogous scenarios can also be found at N^2 LO from the bottom subgraphs in Fig. 2, thereby justifying the EFT results from Eq. (2.15). However, further decreasing q_T incurs non-negligible Monte-Carlo statistical uncertainties, giving rise to deviations between the exact and approximate calculations of up to ~ 3 times the variance estimated there, but still within (sub)percent level relative accuracy w.r.t. the magnitude of $d\sigma_{t\bar{t}}/d \ln q_T$.

Finally, we exhibit the q_T and weighted q_T distributions in Fig. 3, evaluated over the full phase space. Unsurprisingly, the behaviours observed in Fig. 3a and Fig. 3b closely resemble those found in Fig. 1c and Fig. 2c, respectively, as the slice $M_{t\bar{t}} \geq 400$ GeV accounts for the bulk of contributions in the phase space integrals. With these findings, we are now in a position to determine the coefficients c_m and r_m comprised in the arguments of the transition function f_{tran} of Eq. (2.66) governing our matching procedure. From the analysis above, we find that for all three invariant-mass slices, the leading power approximation of Eq. (2.15) is capable of reproducing the asymptotic behaviour of the exact QCD calculation up to $q_T \sim 10$ GeV within percent level accuracy. At a level of $\sim 80\%$ of the full theory, this holds until $q_T \sim 50$ GeV. In light of this,

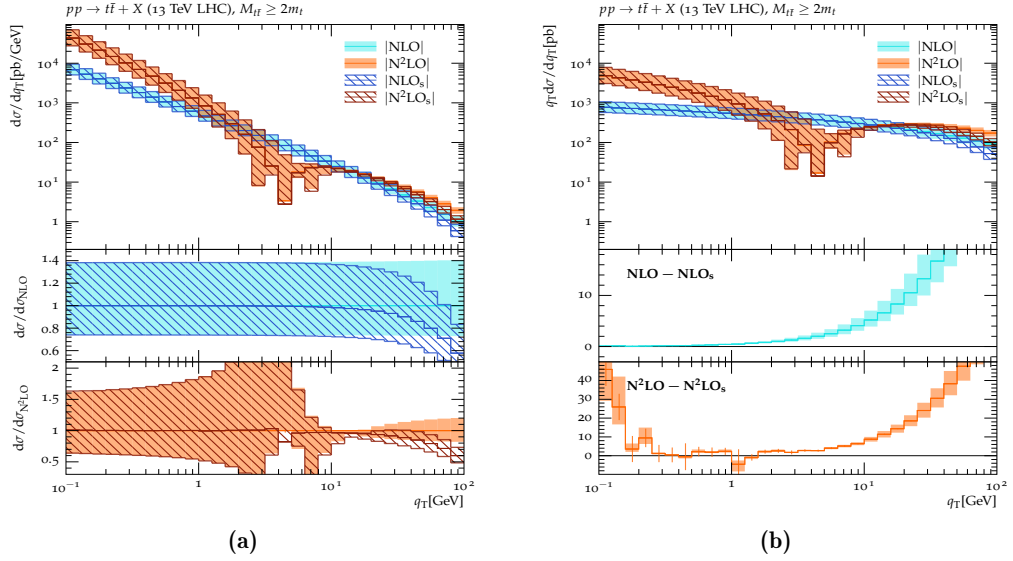


Figure 3: The transverse momentum (left) and weighted transverse momentum (right) spectra of the $t\bar{t}$ -pair at fixed-order QCD at NLO and N²LO accuracy in the process $pp \rightarrow t\bar{t} + X$ at $\sqrt{s} = 13$ TeV in the full phase space. The NLO_s and N²LO_s results encode the leading singular behaviour derived from SCET+HQET.

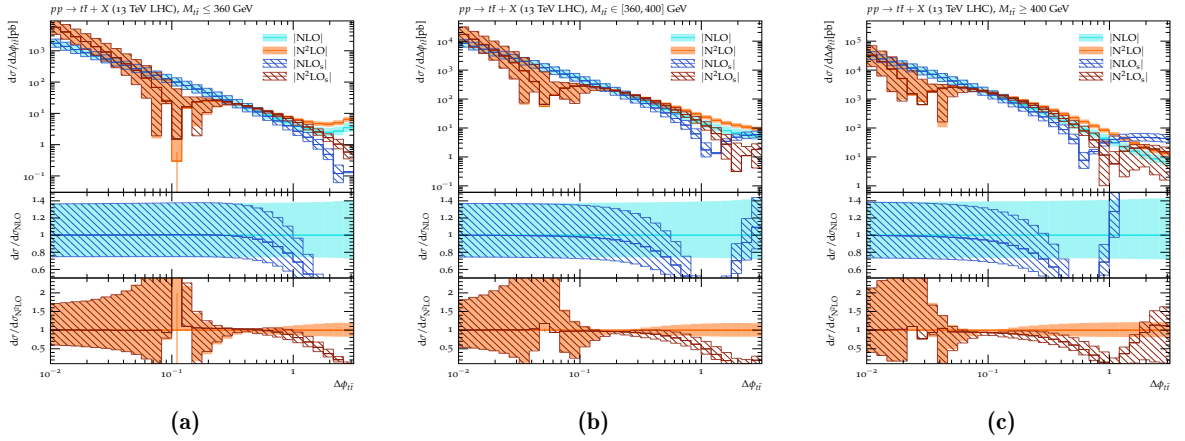


Figure 4: The spectrum of the azimuthal separation of the $t\bar{t}$ -pair at fixed-order QCD at NLO and N²LO accuracy in the process $pp \rightarrow t\bar{t} + X$ at $\sqrt{s} = 13$ TeV within the intervals $M_{t\bar{t}} \leq 360$ GeV (left), $M_{t\bar{t}} \in [360, 400]$ GeV (centre), and $M_{t\bar{t}} \geq 400$ GeV (right). The NLO_s and N²LO_s results encode the leading singular behaviour derived from SCET+HQET.

we will make use of

$$\{c_m, r_m\} = \{50 \text{ GeV}, 35 \text{ GeV}\} \quad (3.2)$$

as our default choice during the implementation of the matching procedure. With these parameters, the resummation in Eq. (2.15) is fully retained until $q_T = 15$ GeV, after which the transition function f_{tran} phases out the resummation gradually, reducing it to half its size at $q_T = 50$ GeV and completely terminating it at $q_T = 85$ GeV. In order to estimate the theoretical uncertainties associated with our matching procedure, we adopt the following alternative matching parameters

$$\{c_m, r_m\} = \{45 \text{ GeV}, 30 \text{ GeV}\}, \{55 \text{ GeV}, 40 \text{ GeV}\} \quad (3.3)$$

and construct an envelope of the calculated spectra.

We now move on to the fixed-order results for the spectra of the azimuthal separation of the top and anti-top,

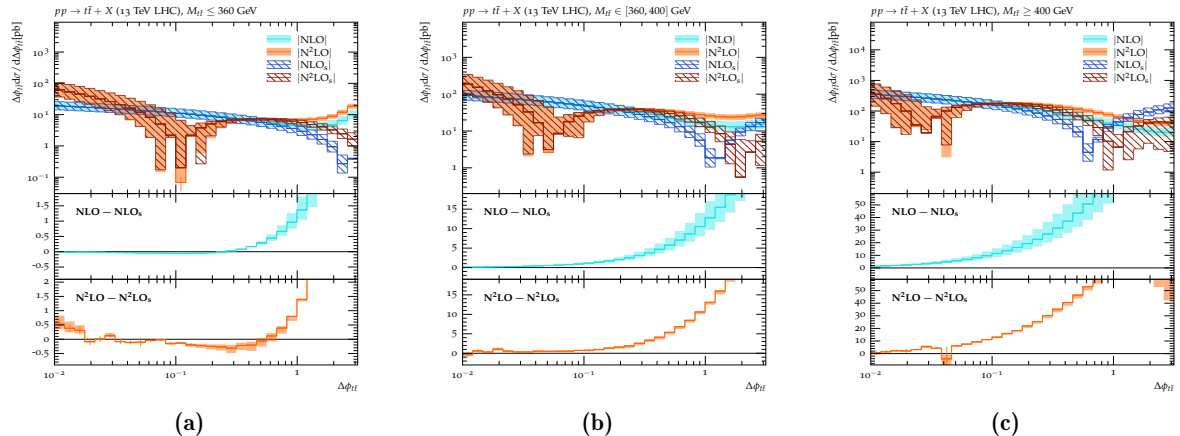


Figure 5: The weighted spectrum of the azimuthal separation of the $t\bar{t}$ -pair at fixed-order QCD at NLO and N^2 LO accuracy in the process $pp \rightarrow t\bar{t} + X$ at $\sqrt{s} = 13$ TeV within the intervals $M_{t\bar{t}} \leq 360$ GeV (left), $M_{t\bar{t}} \in [360, 400]$ GeV (centre), and $M_{t\bar{t}} \geq 400$ GeV (right). The NLO_s and N^2LO_s results encode the leading singular behaviour derived from SCET+HQET.

$\Delta\phi_{t\bar{t}}$, displayed in Fig. 4.⁴

Akin to the q_T spectra in Fig. 1, the $d\sigma_{t\bar{t}}/d\Delta\phi_{t\bar{t}}$ in the main plots of Fig. 4 exhibit a similarly singular behaviour in the low $\Delta\phi_{t\bar{t}}$ domain, at both NLO and N^2 LO. However, comparing the exact and approximate results, even though the SCET+HQET calculations are able to reproduce the correct asymptotic behaviour in the region $\Delta\phi_{t\bar{t}} \rightarrow 0$ in all three $M_{t\bar{t}}$ slices, the size of the missing power corrections are markedly larger than in the q_T case. To be precise, at NLO, while the SCET+HQET approximation agrees with the full QCD result within percent level accuracy below $q_T = 10$ GeV in the q_T spectra in all three $M_{t\bar{t}}$ regions of Fig. 1, the $\Delta\phi_{t\bar{t}}$ distributions of Fig. 4 show a deviation of the EFT-based approximation from the full theory of a few permille around $\Delta\phi_{t\bar{t}} \sim 0.2$ in the $M_{t\bar{t}} \leq 360$ GeV slice, increasing to approximately 5% in $M_{t\bar{t}} \in [360, 400]$ GeV, and reaching more than 10% in the interval $M_{t\bar{t}} \geq 400$ GeV. An analogous behaviour can be found in the N^2 LO results, although the region where the approximate results deviate from the exact one is shifted to slightly higher $\Delta\phi_{t\bar{t}}$, around $\Delta\phi_{t\bar{t}} \sim 1$. To interpret this phenomenon, it merits reminding that the derivation of Eq. (2.15) is subject to an asymptotic expansion of the differential cross section in a given kinematic parameter, for instance, $\lambda_T = q_T/Q_h$ in the q_T spectra and $\lambda_\tau = \Delta\phi_{t\bar{t}}\tilde{P}_t^\perp/Q_h$ in the $\Delta\phi_{t\bar{t}}$ ones, where Q_h represents a hard scale of the similar magnitude to $M_{t\bar{t}}$ and m_t . In Fig. 1, focusing on a constant value of q_T , λ_T varies gently as $M_{t\bar{t}}$ changes when progressing through our three slices since the PDFs effectively suppress contributions from, individually, highly boosted top and antitop quarks. However, the situation for $\Delta\phi_{t\bar{t}}$ in Fig. 4 is different as λ_τ is sensitive to the variable \tilde{P}_t^\perp , the transverse momentum of the top quark measured in the rest frame of the $t\bar{t}$ system, and is therefore proportional to $\beta_{t\bar{t}}$ in the threshold domain. In turn, $\beta_{t\bar{t}}$ scales with $M_{t\bar{t}}$ in the left panel, and thus takes the typical values of around 0.2 for $M_{t\bar{t}} < 360$ GeV, rising to values of about 0.5 for $M_{t\bar{t}} \in [360, 400]$ GeV, and ultimately reaching $\beta_{t\bar{t}} \sim \mathcal{O}(1)$ for $M_{t\bar{t}} > 400$ GeV. As a consequence of this additional kinematic suppression upon the expansion parameter λ_τ , weaker power corrections are observed in Fig. 4a than in Fig. 4b, with the largest power corrections found in Fig. 4c, for constant $\Delta\phi_{t\bar{t}}$.

As before, we further assess the quality of the leading power approximation by studying the weighted differential distributions $d\sigma_{t\bar{t}}/d\ln\Delta\phi_{t\bar{t}}$. They are expected to observe the following power series in the asymptotic domain,

$$\begin{aligned} \frac{d\sigma_{t\bar{t}}}{d\ln\Delta\phi_{t\bar{t}}} &= \Delta\phi_{t\bar{t}} \frac{d\sigma_{t\bar{t}}}{d\Delta\phi_{t\bar{t}}} \\ &\sim \sigma_{t\bar{t}}^{LO} \sum_{m,n} \left(\frac{\alpha_s}{4\pi}\right)^m \left[\underbrace{\tilde{c}_{m,n}^{(0)} \ln^n(\Delta\phi_{t\bar{t}})}_{LP} + \underbrace{\tilde{c}_{m,n}^{(1)} \Delta\phi_{t\bar{t}} \ln^n(\Delta\phi_{t\bar{t}})}_{NLP} + \underbrace{\tilde{c}_{m,n}^{(2)} \Delta\phi_{t\bar{t}}^2 \ln^n(\Delta\phi_{t\bar{t}})}_{N^2LP} + \dots \right], \end{aligned} \quad (3.4)$$

⁴It should be noted that the results in Figs. 4c and 5c, illustrating the region $M_{t\bar{t}} \geq 400$ GeV have already been evaluated in [110]. To facilitate the comparison and later discussion, however, we exhibit them here once again.

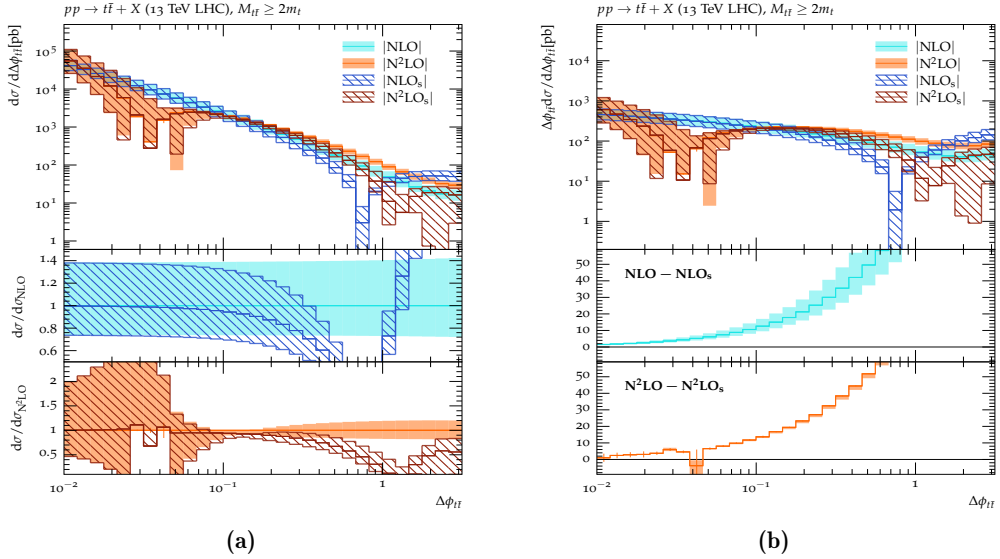


Figure 6: The spectrum (left) and weighted spectrum (right) of the $t\bar{t}$ -pair at fixed-order QCD at NLO and $N^2\text{LO}$ accuracy in the process $pp \rightarrow t\bar{t} + X$ at $\sqrt{s} = 13$ TeV in the full phase space. The $N\text{LO}_s$ and $N^2\text{LO}_s$ results encode the leading singular behaviour derived from SCET+HQET.

wherein again $\sigma_{t\bar{t}}^{\text{LO}}$ is the LO cross section and the $\tilde{c}_{m,n}^{(i)}$ are the coefficients at the respective order of the expansion. Numerical results for $d\sigma_{t\bar{t}}/d\ln\Delta\phi_{t\bar{t}}$ in our three $M_{t\bar{t}}$ slices are displayed in Fig. 5. From the main plots therein, we find in all three regions that the approximate SCET+HQET calculation can reproduce the desired singular behaviour also of the weighted $\Delta\phi_{t\bar{t}}$ spectra of the full QCD calculations at both NLO and $N^2\text{LO}$. Similarly, as illustrated in the middle and bottom subplots of Fig. 5, their difference progressively decreases as $\Delta\phi_{t\bar{t}}$ decreases from $\Delta\phi_{t\bar{t}} \sim \mathcal{O}(1)$, until in the $\Delta\phi_{t\bar{t}} \sim \mathcal{O}(10^{-2})$ non-negligible integration uncertainties are encountered. These observations demonstrate that at least up to $N^2\text{LO}$, the fixed-order expansion of Eq. (2.15) is able to describe the leading singular contributions of the full theory.

Again, in a parallel to our appraisal of the approximate q_T spectra, we examine the inclusive $\Delta\phi_{t\bar{t}}$ and weighted $\Delta\phi_{t\bar{t}}$ spectra in Fig. 6. Once again, they effectively reproduce the results for $M_{t\bar{t}} > 400$ GeV as this region carries the bulk of the cross section. With its help we can now determine the coefficients \tilde{c}_m and \tilde{r}_m for the transition function f_{tran} of Eq. (2.66), employed to match the resummed $\Delta\phi_{t\bar{t}}$ spectrum to its fixed-order counter-part. Considering that the size of the power corrections in the $\Delta\phi_{t\bar{t}}$ distribution is $M_{t\bar{t}}$ -dependent, the values of \tilde{c}_m and \tilde{r}_m are chosen differently for each region, i.e.,

$$\begin{aligned} \{\tilde{c}_m, \tilde{r}_m\} &= \{0.5, 0.3\}, & M_{t\bar{t}} \leq 360 \text{ GeV}, \\ \{\tilde{c}_m, \tilde{r}_m\} &= \{0.3, 0.2\}, & M_{t\bar{t}} \geq 360 \text{ GeV}. \end{aligned} \quad (3.5)$$

Therein, in view of the excellent agreement between the approximate and exact results in Fig. 4a, we extend the active range of the soft and collinear resummation in the region $M_{t\bar{t}} < 360$ GeV. In consequence, here, the resummation is fully active for $\Delta\phi_{t\bar{t}} < 0.2$ and then will be gradually turned off, being reduced to half its strength at $\Delta\phi_{t\bar{t}} = 0.5$ and eliminated at $\Delta\phi_{t\bar{t}} = 0.8$. Otherwise, a tightened choice of \tilde{c}_m and \tilde{r}_m is made for both other invariant mass domains. Here, the resummation is restricted to the region $\Delta\phi_{t\bar{t}} < 0.1$, reduced to half-value at $\Delta\phi_{t\bar{t}} = 0.3$, and terminated for $\Delta\phi_{t\bar{t}} > 0.5$. To investigate the sensitivity of the final matched $\Delta\phi_{t\bar{t}}$ results to the choice of f_{tran} , we also embed the following alternatives as matching parameters,

$$\begin{aligned} \{\tilde{c}_m, \tilde{r}_m\} &= \{0.45, 0.25\}, \{0.55, 0.35\}, & M_{t\bar{t}} \leq 360 \text{ GeV}, \\ \{\tilde{c}_m, \tilde{r}_m\} &= \{0.25, 0.15\}, \{0.35, 0.25\}, & M_{t\bar{t}} \geq 360 \text{ GeV}. \end{aligned} \quad (3.6)$$

3.3 Resummation-improved q_T and $\Delta\phi_{t\bar{t}}$ distributions

In the following, we introduce the resummation-improved q_T and $\Delta\phi_{t\bar{t}}$ spectra based on Eq. (2.15), including the threshold region $\beta_{t\bar{t}} \rightarrow 0$ by employing two *ad hoc* prescriptions, i.e. the D-prescription of Eq. (2.51) and

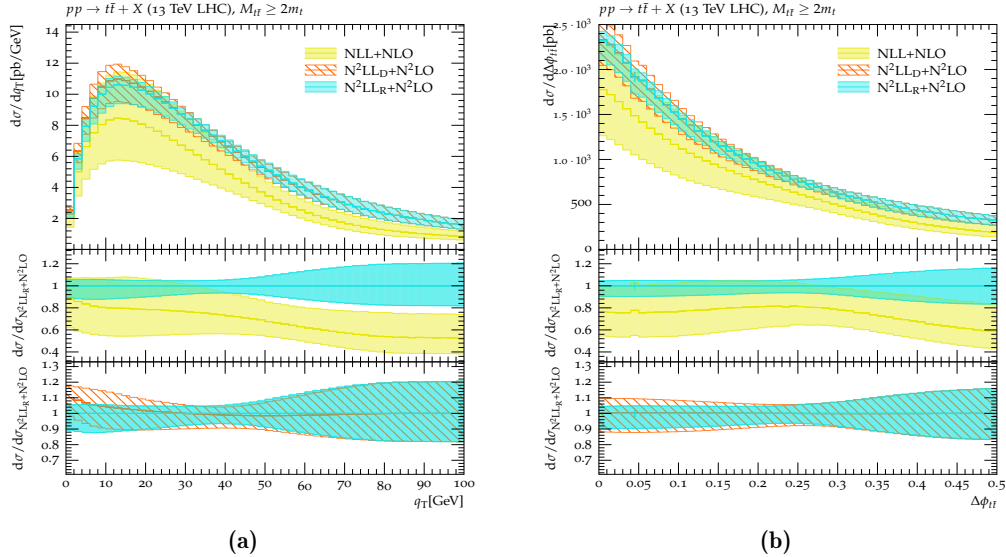


Figure 7: The resummation-improved q_T (left) and $\Delta\phi_{t\bar{t}}$ (right) spectra of the process $pp \rightarrow t\bar{t} + X$ at $\sqrt{s} = 13$ TeV.

the R-prescription of Eq. (2.64). Therein, as illustrated in Eqs. (2.7-2.8), our R(a)GE-based resummation is subject to two sets of auxiliary scales, $\{\mu_h, \mu_b, \mu_s\}$ and $\{\nu_b, \nu_s\}$, characterising the typical scales in the virtuality and rapidity renormalisation, respectively. In addition, the matching procedure of Eq. (2.66), introduces the fixed-order scale $\mu_{f.o.}$. Their default choices are presented in Eq. (2.17) and Eq. (2.68). To estimate the corresponding theoretical uncertainties, we vary all such scales within the intervals $\mu \in [\frac{1}{2}, 2] \mu^{\text{def}}$ ($\mu = \mu_h, \mu_s, \mu_b, \mu_{f.o.}$) and $\nu \in [\frac{1}{2}, 2] \nu^{\text{def}}$ ($\nu = \nu_s, \nu_b$). We denote the resulting variation as δ_{scale} . Furthermore, our matching procedure of Eq. (2.66) also introduces the coefficients $\{c_m, r_m\}$ (for q_T) and $\{\tilde{c}_m, \tilde{r}_m\}$ (for $\Delta\phi_{t\bar{t}}$) governing the active range of the soft and beam-collinear resummation. Similarly, while the D-prescription does not introduce further parameters, the R-prescription involves a second matching, see Eq. (2.59), as it embeds terms to mitigate the threshold singularity in the resummation kernel. Its associated parameters are $\{c_{\text{thr}}, r_{\text{thr}}\}$. Their default choice has been presented in Eqs. (3.2), (3.5), and (2.62), respectively. We estimate the uncertainty of the corresponding matching procedure using alternative matching parameter as defined in Eqs. (3.3), (3.6), and (2.63), giving the combined matching uncertainty estimate δ_{mat} . Finally, both sources of uncertainties, δ_{scale} and δ_{mat} , are combined in quadrature, giving the total uncertainty,⁵

$$\delta_{\text{tot}} = \sqrt{\delta_{\text{mat}}^2 + \delta_{\text{scale}}^2}. \quad (3.7)$$

With this definition, we present in Fig. 7 the single differential distributions $d\sigma_{t\bar{t}}/dq_T$ and $d\sigma_{t\bar{t}}/d\Delta\phi_{t\bar{t}}$ over the whole phase space, integrated over all $M_{t\bar{t}}$ values. Therein, the results at NLL+NLO are calculated from a literal implementation of Eq. (2.15) since neither the NLL non-cusp evolution kernel $\mathbf{V}_h^{[\kappa]}$ nor the tree-level hard functions $\mathcal{C}_{\alpha, \{h\}}^{[\kappa]}$ induce any singular behaviour in the limit $\beta_{t\bar{t}} \rightarrow 0$, and thus no modification of the resummation is required in the threshold regime. These NLL+NLO results are depicted in the yellow bands in Fig. 7a (q_T) and 7b ($\Delta\phi_{t\bar{t}}$). Comparing the shapes of both distributions, however, we observe that while a classical Sudakov peak is formed in the low q_T regime, the $\Delta\phi_{t\bar{t}}$ spectrum grows monotonically as $\Delta\phi_{t\bar{t}} \rightarrow 0$. To understand this structural difference, it is worth reminding that although both the q_T and $\Delta\phi_{t\bar{t}}$ resummations comprise the same partonic kernels in Eqs. (2.7-2.8), which approach constants as q_T and $\Delta\phi_{t\bar{t}}$ vanish, the calculation of the q_T spectrum invokes an additional factor $\propto q_T$ which is absent in the $\Delta\phi_{t\bar{t}}$ case, see Eq. (2.15). In consequence, the resummed q_T spectrum experiences kinematical suppression as $q_T \rightarrow 0$ and in turn develops a Sudakov peak, whereas the $\Delta\phi_{t\bar{t}}$ spectrum does not.

⁵We note here that we have introduced a numerical cutoff into the impact-parameter space integrals of Eq. (2.15) to evade the QCD Landau divergence [140], $b_T^{\text{cut}} = 2 \text{ GeV}^{-1}$. To estimate the uncertainties associated with this choice, we also evaluate q_T and $\Delta\phi_{t\bar{t}}$ spectra with the alternatives $b_T^{\text{cut}} = 3 \text{ GeV}^{-1}$ and $b_T^{\text{cut}} = 4 \text{ GeV}^{-1}$. We find the variation generally to be on the permille level, comparable to the statistical error from the Monte-Carlo integration. Therefore, we do not take them into account when calculating δ_{tot} here.

At the core of this paper, however, are the $N^2LL_D+N^2LO$ and $N^2LL_R+N^2LO$ calculations shown in the red and cyan in Fig. 7. They are derived via the *ad hoc* D- and R-prescriptions of Eq. (2.51) and Eq. (2.64), respectively. It merits recalling that in these prescriptions two fundamentally distinct methods are adopted to address the Coulomb-gluon-induced threshold singularities of Eq. (2.44). While the D-prescription simply shifts them to terms of higher logarithmic order, N^3LL and beyond, see Eq. (2.51), the R-prescription re-exponentiates the leading Coulomb singularities from the non-cusp kernel $V_h^{[\kappa]}$ via solving the respective renormalisation group evolution equation in the $\beta_{t\bar{t}} \rightarrow 0$ limit, see Eq. (2.57), and leaves the singularities of the hard scattering amplitudes $C_{\alpha;\{h\}}^{[\kappa]}$ and their complex conjugate to be cancelled by the respective phase space suppression factors through Eq. (2.64). Therefore, comparing the results using the D- and R-prescriptions allows us to assess the sensitivity of the q_T and $\Delta\phi_{t\bar{t}}$ spectra to the details of how the Coulomb-singular contributions, that are not systematically accommodated by the SCET+HQET based resummation in Eq. (2.15) and can neither be fully accessed by scale variations, are addressed.

Examining our results in detail, we find that the central value at $N^2LL_R+N^2LO$ mostly coincides with that of $N^2LL_D+N^2LO$ for the $\Delta\phi_{t\bar{t}}$ spectrum of Fig. 7b, with the uncertainty band of the former being fully contained in that of the latter. Our findings are somewhat different for the q_T spectrum of Fig. 7a, however. We observe a difference of around 10% between the $N^2LL_D+N^2LO$ and $N^2LL_R+N^2LO$ as $q_T \rightarrow 0$, while both calculations again agree very well for the rest of the spectrum. This difference can be understood from the kinematics in Eqs. (2.15), where $d\sigma_{t\bar{t}}/d\Delta\phi_{t\bar{t}}$ comprises an additional factor of $|\vec{P}_{t\bar{t}}^\perp|$ compared to $d\sigma_{t\bar{t}}/dq_T$. As $\beta_{t\bar{t}} \rightarrow 0$, this factor becomes of $\mathcal{O}(\beta_{t\bar{t}})$ and effectively removes the threshold contribution that are the main driver of the difference between the D- and R-prescriptions in the phase space integration in the $\Delta\phi_{t\bar{t}}$ spectrum. Consequently, the well-separated domain, $\Delta E_{t\bar{t}} \sim \mathcal{O}(m_t)$ or $\beta_{t\bar{t}} \sim \mathcal{O}(1)$, dominates the single differential $\Delta\phi_{t\bar{t}}$ spectrum, which leads to the converging uncertainty bands of $N^2LL_R+N^2LO$ and $N^2LL_D+N^2LO$ and also the proximity of their central values. Nevertheless, the absence of such a dampening factor in q_T spectrum emphasises the impact of threshold-enhanced terms in the Coulomb limit, leading to a sizeable dependence on the details of their treatment even after integrating over the entire $M_{t\bar{t}}$ or $\beta_{t\bar{t}}$ range.

Given this observation, in order to further improve the description of the q_T spectrum, an HQET+SCET-only-based analysis will be insufficient to describe the entire phase space for lack of an adequate description of higher-order Coulomb-enhanced terms. To remove any ambiguity caused by the choice of *ad hoc* prescriptions, it will become necessary to develop a combined resummation of the Coulomb, soft, and collinear corrections via SCET+pNRQCD (or vNRQCD), at least in the threshold regime. Conversely, the negligible difference between $N^2LL_R+N^2LO$ and $N^2LL_D+N^2LO$ in the $\Delta\phi_{t\bar{t}}$ spectrum indicates a weaker sensitivity to these Coulomb interactions. Nonetheless, it is worth noting that the inclusion of the threshold regime in Eq. (2.15) is still subject to *ad hoc* prescriptions to regularise the threshold divergences. We expect that, in this case as well, the introduction of the aforementioned combined resummation will make the application of such prescriptions unnecessary.

4 Conclusions

In this paper we presented the resummation-improved transverse momentum and, for the first time, azimuthal separation spectra of the $t\bar{t}$ -pair at N^2LL+N^2LO accuracy, and studied their predictions for top-antitop pair production at the 13 TeV at the LHC. We based our calculation on the observation that as for such high colliding energies the domain where the top and antitop quarks are kinematically well separated, $\Delta E_{t\bar{t}} \sim \mathcal{O}(m_t)$, dominates the process $pp \rightarrow t\bar{t} + X$ and, therefore, the asymptotic behaviour in the limits $q_T \rightarrow 0$ and $\Delta\phi_{t\bar{t}} \rightarrow 0$ can be mostly captured by the soft and beam-collinear resummation via HQET+SCET. We then endeavored to extend this description over the entire phase space, including the threshold regime, $\Delta E_{t\bar{t}} \rightarrow 0$ or $\beta_{t\bar{t}} \rightarrow 0$, where the exchange of Coulomb gluons adds new potentially divergent corrections to our process. Implementing this method at NLL, however, proved to be straightforward, as the involved functions of the HQET+SCET resummation at this accuracy were found to be regular in the threshold limit. Nevertheless, starting from N^2LL , we demonstrated that Coulomb divergences manifest themselves in both the hard function and its non-cusp evolution kernels. This, in turn prohibited a direct application of the soft and collinear resummation result to the entire phase space.

In order to address these Coulomb divergences emerging in our soft and collinear resummation, we introduced two *ad hoc* prescriptions, referenced as D- and R-prescriptions, respectively. While the threshold enhanced terms in D-prescription are simply shifted to a higher logarithmic order, they are in part re-

summed in R-prescription. Here, the leading singular terms induced by the two-loop non-cusp anomalous are re-exponentiated via solving the hard renormalisation group equation as $\beta_{t\bar{t}} \rightarrow 0$. Comparing their respective predictions allowed us to quantitatively assess the inherent uncertainty of our calculation and the sensitivity of both the q_T and $\Delta\phi_{t\bar{t}}$ spectra to Coulomb interactions.

Finally, we implemented both prescriptions to calculate $d\sigma_{t\bar{t}}/d\Delta\phi_{t\bar{t}}$ and $d\sigma_{t\bar{t}}/dq_T$, labelling their predictions $N^2LL_D+N^2LO$ and $N^2LL_R+N^2LO$. We observed that the central values from D- and R-prescriptions mostly coincide in $d\sigma_{t\bar{t}}/d\Delta\phi_{t\bar{t}}$, with the uncertainty band of the latter being fully contained by that of the former. Conversely, we found a deviation of around 10% between both prescriptions as $q_T \rightarrow 0$ in $d\sigma_{t\bar{t}}/dq_T$. This indicates that applying our soft-collinear resummation onto the q_T spectrum introduces a non-negligible ambiguity at N^2LL in the absence of necessary higher-order contributions from the threshold domain. Therefore, to further improve the theoretical accuracy of the q_T spectrum, a combined resummation of Coulomb, soft, and collinear corrections via SCET and pNRQCD (or alternatively vNRQCD) in the threshold regime seems warranted. Similarly, while the negligible deviation between the D- and R-prescriptions in the $\Delta\phi_{t\bar{t}}$ spectrum indicates a weaker sensitivity to Coulomb interactions, it is worth noting that extending the soft and collinear resummation coverage to the whole $M_{t\bar{t}}$ phase space still necessitates *ad hoc* prescriptions to regularise the arising Coulomb divergences as $\Delta E_{t\bar{t}} \rightarrow 0$. We expect that a combined resummation will be beneficial in this case as well, removing the need for either prescription.

Acknowledgements

WJ would like to thank Li Lin Yang for sharing valuable details in computing the hard evolution kernel in [88, 104, 105, 311]. WJ is also grateful to Guoxing Wang for the helpful discussion on the threshold soft function in [282]. WJ and MS would also like to express our gratitude to Ben Pecjak for taking the time to respond to our numerous queries. MS is funded by the Royal Society through a University Research Fellowship (URF\R1\180549, URF\R\231031) and an Enhancement Award (RGF\EA\181033, CEC19\100349, and RF\ERE\210397) as well as the STFC (ST/X003167/1 and ST/X000745/1).

A Comparison of D- and R-prescriptions in the double differential distributions

It is interesting to analyse our results double-differentially, i.e. examining both the q_T and $\Delta\phi_{t\bar{t}}$ spectra in three different regions of the $t\bar{t}$ invariant mass $M_{t\bar{t}}$, $M_{t\bar{t}} \leq 360$ GeV, $M_{t\bar{t}} \in [360, 400]$ GeV, and $M_{t\bar{t}} \geq 400$ GeV. We can use these three regions, containing the $t\bar{t}$ production threshold and the Coulomb divergences, a transition region, and the well-separated region where $\Delta E_{t\bar{t}} \sim \mathcal{O}(m_t)$, respectively, to investigate the development of the differences between the D- and R-prescriptions as $M_{t\bar{t}}$ varies. The q_T and $\Delta\phi_{t\bar{t}}$ differential distributions within these intervals are presented in Fig. 8, including the NLL+NLO, $N^2LL_D+N^2LO$, and $N^2LL_R+N^2LO$ calculations depicted in the yellow, red, and cyan bands, respectively. As to the last two slices, due to the absence of Coulomb divergences, we also add the results evaluated with the original evolution kernels of Eq. (2.13), labelled N^2LL+N^2LO and shown as a dark-grey hatched band.⁶

Fig. 8c and Fig. 8f illustrate $d\sigma_{t\bar{t}}/dq_T$ and $d\sigma_{t\bar{t}}/d\Delta\phi_{t\bar{t}}$, respectively, for $M_{t\bar{t}} \geq 400$ GeV, where the top and antitop quarks are kinematically well separated and our soft-collinear resummation possesses the best predictivity. It is observed that the central values from N^2LL , N^2LL_D , and N^2LL_R coincide within a few percent of each other and their uncertainty bands marginally overlap with that calculated at NLL. This phenomenon confirms our derivation in Sec. 2.3 in that the difference amongst D-prescription, R-prescription and the original evolution kernels in Eq. (2.13) is numerically of N^2LL' and beyond for the separated domain and therefore the deviations between them can be well captured by the scale variation in this domain.

However, lowering $M_{t\bar{t}}$ leads to distinct scenarios. As exhibited in Fig. 8b and Fig. 8e, although the unmodified N^2LL result is still in good agreement with N^2LL_D , 50% (20%) deviations are observed in the N^2LL_R calculation in the low q_T ($\Delta\phi_{t\bar{t}}$) domains. To interpret this, it merits recalling that N^2LL_D shifts threshold enhanced terms in part from $\mathbf{V}_h^{[\kappa]}$ of N^2LL to higher logarithmic orders, while N^2LL_R re-exponentiates the leading Coulomb singularities from $\mathbf{V}_h^{[\kappa]}$ on top of N^2LL and also embeds the NLO corrections from both

⁶It should be noted that the NLL+NLO and N^2LL+N^2LO results in Fig. 8f have been published in [110] and are shown here for comparison.

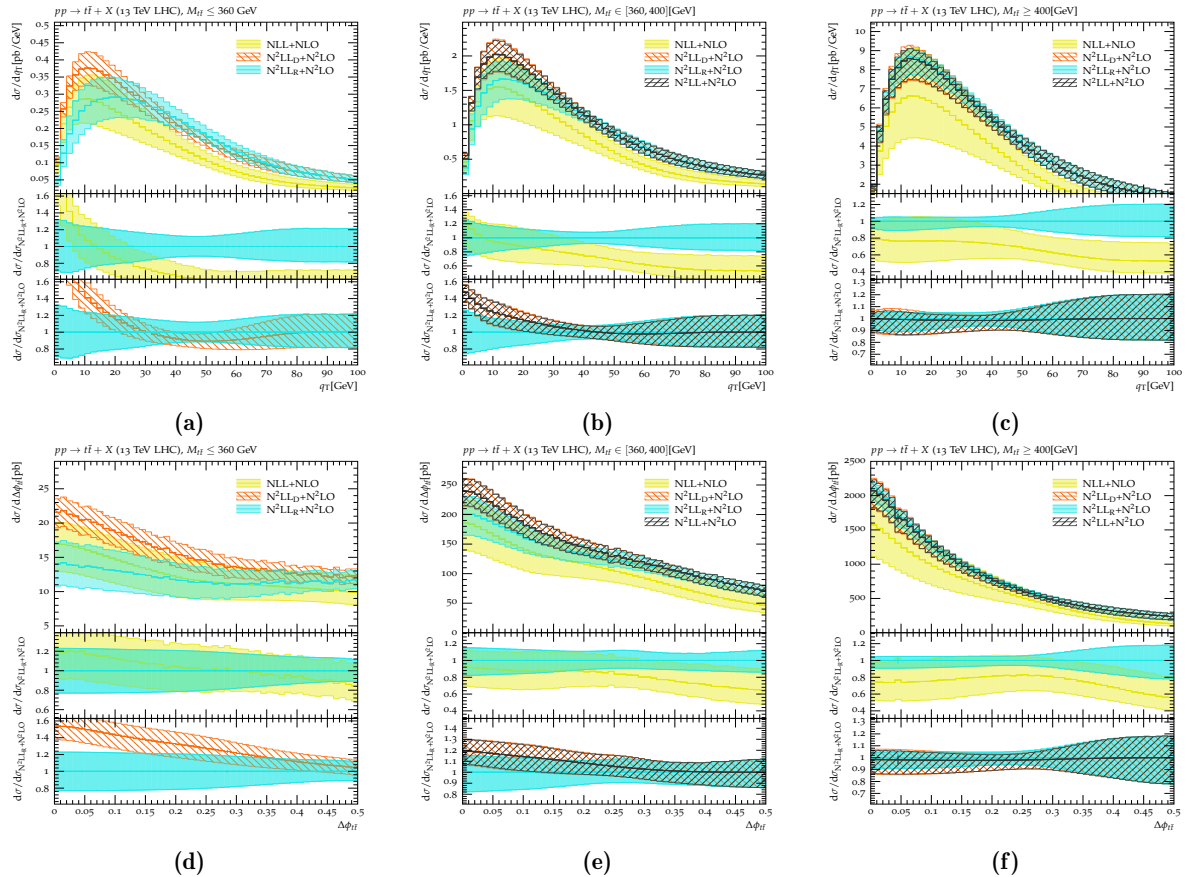


Figure 8: Comparison of the D- and R-prescriptions within the intervals $M_{t\bar{t}} \leq 360$ GeV (left), $M_{t\bar{t}} \in [360, 400]$ GeV (centre), and $M_{t\bar{t}} \geq 400$ GeV (right).

$\mathcal{C}_{\alpha; \{h\}}^{[\kappa]}$ and its complex conjugate. Nevertheless, the threshold enhancements generated by $\mathbf{V}_h^{[\kappa]}$ are generally weaker than those from the hard sector in the region $M_{t\bar{t}} \in [360, 400]$ GeV. For instance, according to Eq. (2.25) and Eq. (2.39), $\mathbf{V}_h^{[\kappa]}$ entails the leading Coulomb divergence $\sim \frac{\alpha_s^2}{\beta_{t\bar{t}}^2} \left\{ \left(\frac{55}{4761} \right)^2, \left(\frac{55}{38088} \right)^2 \right\}$ at N²LO, whereas the product of $\mathcal{C}_{\alpha; \{h\}}^{[\kappa]}$ and its complex conjugate is $\sim \frac{\alpha_s^2}{\beta_{t\bar{t}}^2} \left\{ \left(\frac{\pi}{3} \right)^2, \left(\frac{\pi}{24} \right)^2 \right\}$. Here the first (second) entry refers to the color-singlet (color octet) contributions of the top-antitop quark pair. Given this numerical hierarchy, the interval $M_{t\bar{t}} \in [360, 400]$ GeV is dominated by enhancements in the hard section and therefore gives rise to non-negligible deviation between N²LL_R and N²LL_D as well as the unmodified N²LL.

Further decreasing $M_{t\bar{t}}$ focusses on the threshold regime, as shown in Fig. 8a and Fig. 8d, where the discrepancies between N²LL_D and N²LL_R are observed to be up to $\sim 100\%$ in the low q_T realm and $\sim 60\%$ in the low $\Delta\phi_{t\bar{t}}$ domain, owing to the growth of threshold enhanced contributions. This phenomenon, together with those in Fig. 8b and Fig. 8e, demonstrates the origin of the difference between D- and R-prescriptions observed in Fig. 7.

B Numerical results of hard-scale evolution kernel

In this appendix we deliver a numerical comparison amongst the original non-cusp evolution kernel in Eqs. (2.12-2.13) as proposed in [210, 211], the leading singular approximation from Eqs. (2.38-2.39), and the expansion of the re-exponentiated kernel in Eq. (2.60). During our computation, we fix $\mu_h = M_{t\bar{t}}$ and $\mu_s = 1$ GeV as well as the scattering angle of the top quark $\theta_t = \pi/3$.

Fig. 9 exhibits the NLL results of \mathbf{V}_h in Eq. (2.12) and $\mathbf{V}_{h, \text{thr}}$ in Eq. (2.38) in solid and dashed lines, respectively. Therein, the dependence of all the entries of \mathbf{V}_h is displayed with respect to $\beta_{t\bar{t}}$. For $\mathbf{V}_{h, \text{thr}}$, we show the non-zero components only. Due to the facts that the leading threshold enhanced terms in

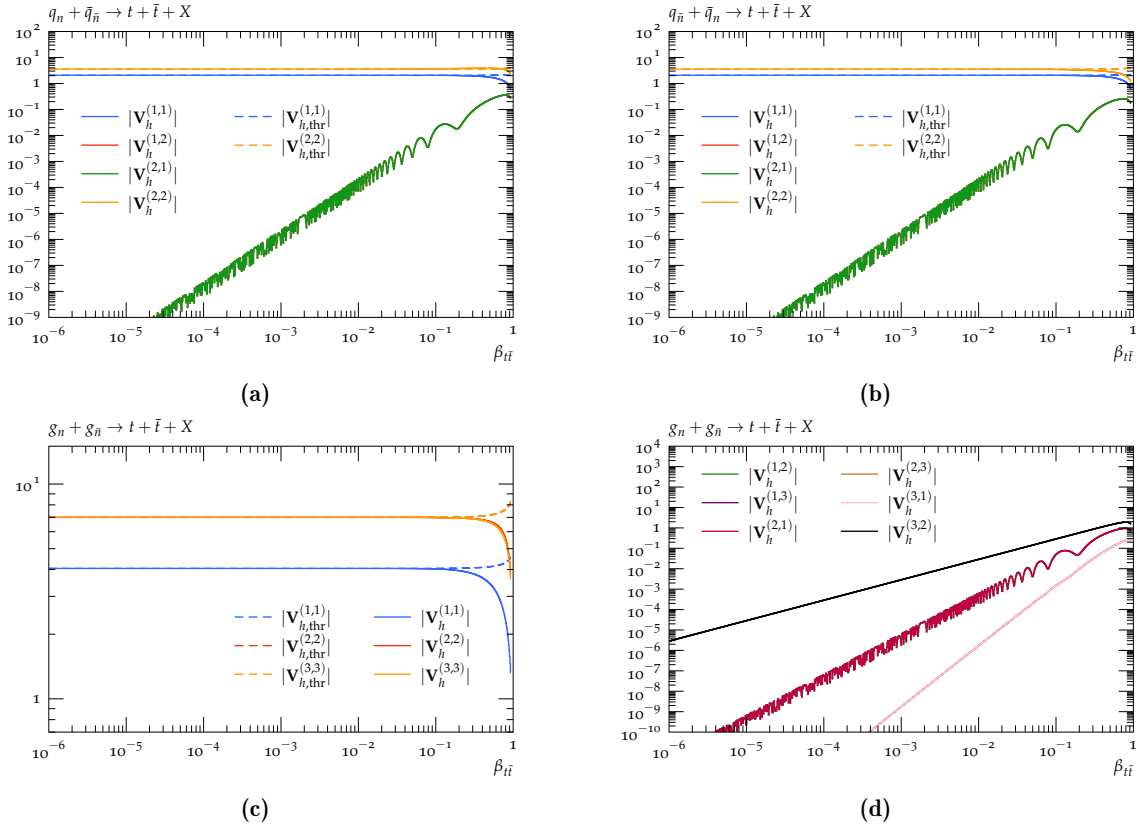


Figure 9: Comparison of the non-cusp evolution kernel \mathbf{V}_h in Eq. (2.12) and its leading terms $\mathbf{V}_{h,\text{thr}}$ in Eq. (2.38) in the threshold regime at NLL. Therein, $|\mathbf{V}_{h,(\text{thr})}^{(m,n)}|$ denotes the absolute value of the entry of $\mathbf{V}_{h,(\text{thr})}$ in the m -th row and n -th column from respective partonic process.

the NLO anomalous dimension only manifest themselves in the imaginary parts and that the complete Coulomb singular behaviour has been exponentiated at NLL in both Eq. (2.12) and Eq. (2.38), the NLL kernel illustrated in Fig. 9 invokes no divergence as $\beta_{t\bar{t}} \rightarrow 0$. Comparing \mathbf{V}_h with $\mathbf{V}_{h,\text{thr}}$, we find that the leading approximation is capable of replicating the correct asymptotic behaviour of all the diagonal entries of \mathbf{V}_h , while the non-diagonal elements of \mathbf{V}_h become progressive smaller in the low $\beta_{t\bar{t}}$ region. This indicates the non-diagonal entries of \mathbf{V}_h are all power suppressed in magnitude and it is thus in agreement with the absence of the off-diagonal contributions in $\mathbf{V}_{h,\text{thr}}$ in Eq. (2.38).

In a bid to scrutinise our leading approximation in Eq. (2.38) further, we plot the result of the product $(\mathbf{V}_{h,\text{thr}}^{-1} \mathbf{V}_h)$ in Fig. 10. We observe that $(\mathbf{V}_{h,\text{thr}}^{-1} \mathbf{V}_h)$ approaches the unity matrix for all three partonic processes of interest. This phenomenon shows that $\mathbf{V}_{h,\text{thr}}^{-1}$ is able to serve as a qualified inverse matrix of \mathbf{V}_h in the vicinity of $\beta_{t\bar{t}} = 0$. Further, it details that the approximation in Eq. (2.38) indeed manages to reproduce the leading asymptotic behaviour of Eq. (2.12).

In Figs. 11 we confront \mathbf{V}_h of Eq. (2.13) with $\mathbf{V}_{h,\text{thr}}$ of Eq. (2.39) at N^2LL . At variance with the findings of Figs. 9 and 10, the diagonal entries of \mathbf{V}_h develop divergent behaviour in the threshold domain, as a result of the Coulomb singularity residing in Eq. (2.35), which $\mathbf{V}_{h,\text{thr}}$ is able to replicate at N^2LL . Further, differing from \mathbf{V}_h at NLL, where all the non-diagonal entries in Fig. 9 generally decline in magnitude as $\beta_{t\bar{t}}$ reduces, the non-diagonal constituents in Fig. 11 can experience enhancements in the threshold domain, such as $|\mathbf{V}_h^{(3,2)}|$ in Fig. 11d. The reason for this phenomenon is that in the expression of Eq. (2.39), only the leading singular terms of Eq. (2.39), which are of $\mathcal{O}(\beta_{t\bar{t}}^{-2})$, have been taken into account. Divergence of $\mathcal{O}(\beta_{t\bar{t}}^{-1})$ are, however, still possible. To verify that there is no stronger divergent behaviour in non-diagonal elements other than that of Eq. (2.39), we present the results of $(\mathbf{V}_{h,\text{thr}}^{-1} \mathbf{V}_h)$ in Fig. 12. It is found that all but the diagonal elements are reduced substantially as $\beta_{t\bar{t}} \rightarrow 0$, while all the diagonal elements of the product $(\mathbf{V}_{h,\text{thr}}^{-1} \mathbf{V}_h)$ approach unity. This unambiguously shows that our leading approximation in Eq. (2.39) can describe the asymptotic behaviour of Eq. (2.13) at N^2LL as well.

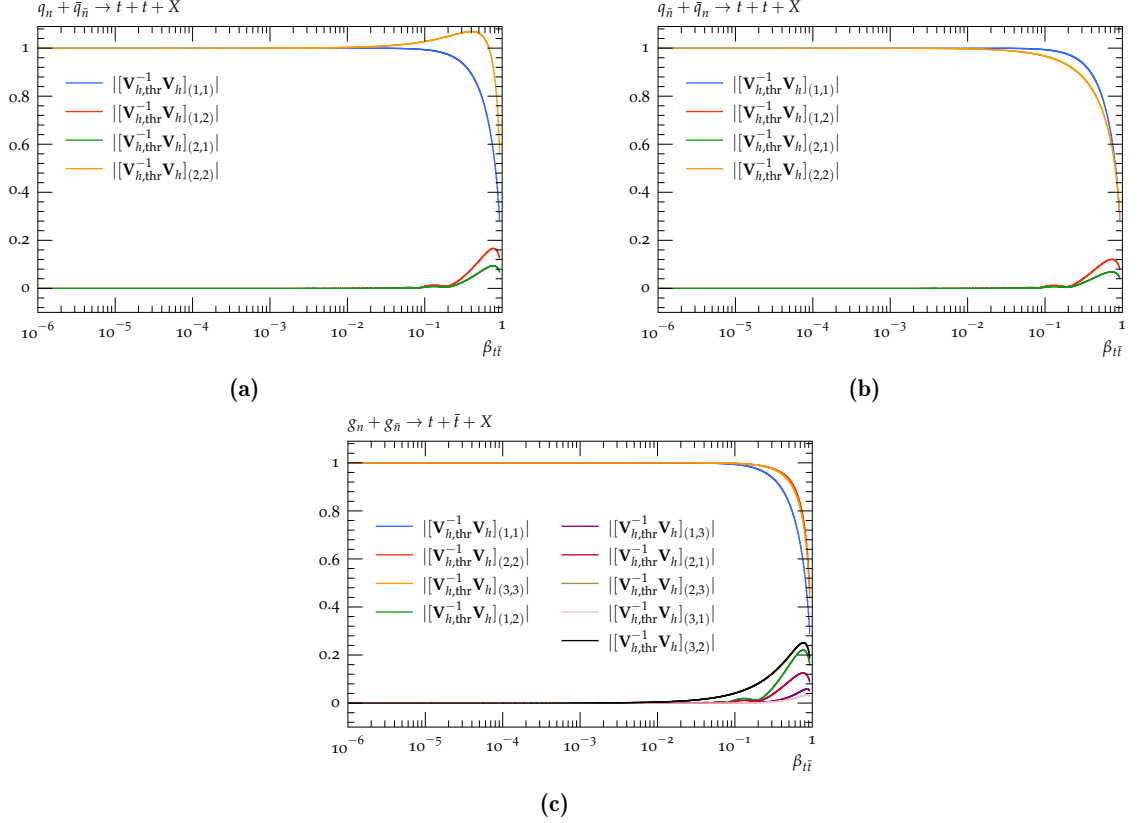


Figure 10: Product of the non-cusp evolution \mathbf{V}_h in Eq. (2.12) and the inverse matrix $\mathbf{V}_{h,\text{thr}}^{-1}$ in Eq. (2.38) at NLL. Therein, $|\mathbf{V}_{h,\text{thr}}^{-1} \mathbf{V}_h|_{m,n}$ denotes the absolute value of the entry of $(\mathbf{V}_{h,\text{thr}}^{-1} \mathbf{V}_h)$ in the m -th row and n -th column from respective partonic process.

Eventually, Figs. 13 and 14 depict the results of \mathbf{V}_h of Eq. (2.13) and $\tilde{\mathbf{V}}_{h,\text{exp}}$ in Eq. (2.60) at N^2LL , the expansion of the re-exponentiated Sudakov factor. Owing to the fact that in comparison with the leading singular result of $\mathbf{V}_{h,\text{thr}}$ in Eq. (2.39), $\tilde{\mathbf{V}}_{h,\text{exp}}$ is embedded with more power corrections, the agreement between \mathbf{V}_h and $\tilde{\mathbf{V}}_{h,\text{exp}}$ is considerably improved compared to Figs. 11 and 12. For instance, focussing on the quark-induced process, while in Fig. 12a, the deviation between the leading approximation $\mathbf{V}_{h,\text{thr}}$ in Eq. (2.39) and \mathbf{V}_h in Eq. (2.13) rapidly surges above $\beta_{t\bar{t}} \sim 10^{-3}$, in Fig. 14a, numerical agreement of \mathbf{V}_h and $\tilde{\mathbf{V}}_{h,\text{exp}}$ holds up to $\beta_{t\bar{t}} \sim 10^{-1}$ within around 10%. In light of this excellent agreement, in matching the re-exponentiated Sudakov factor onto \mathbf{V}_h in Eq. (2.59), we choose the matching parameters $c_{\text{thr}}^{\text{def}} = 0.4$ and $r_{\text{thr}}^{\text{def}} = 0.1$ as defined in Eq. (2.62). In this way, the re-exponentiation impact is fully switched on in the domain $\beta_{t\bar{t}} \leq 0.3$ but then gets gradually faded out until the total shutdown at $\beta_{t\bar{t}} = 0.5$. This choice of this active range brings the difference between \mathbf{V}_h and $\tilde{\mathbf{V}}_{h,\text{exp}}$ under control, i.e. generally below 40% for all three partonic channels, and also steers clear of the tail region in Fig. 14 where the power correction to the small $\beta_{t\bar{t}}$ expansion escalates dramatically.

C Definitions of the color and helicity bases

Here we present the colour bases [247] used in calculating $\mathcal{C}_{\alpha;\{h\}}^{[\kappa]}$ and $\mathcal{S}_{[\kappa]}^{\alpha\beta}$ in Eqs. (2.7-2.8),

$$\begin{aligned}
c_{a_1 a_2 a_3 a_4}^{qq,(1)} &= \frac{1}{3} \delta_{a_1 a_2} \delta_{a_3 a_4}, & c_{a_1 a_2 a_3 a_4}^{qq,(2)} &= \frac{1}{\sqrt{2}} \sum_c T_{a_1 a_2}^c T_{a_3 a_4}^c, \\
c_{a_1 a_2 a_3 a_4}^{gg,(1)} &= \frac{1}{2\sqrt{6}} \delta_{a_1 a_2} \delta_{a_3 a_4}, & c_{a_1 a_2 a_3 a_4}^{gg,(2)} &= \frac{i}{2\sqrt{3}} \sum_c f^{a_1 c a_2} T_{a_3 a_4}^c, & c_{a_1 a_2 a_3 a_4}^{gg,(3)} &= \frac{1}{2} \sqrt{\frac{3}{5}} \sum_c d^{a_1 c a_2} T_{a_3 a_4}^c,
\end{aligned} \tag{C.1}$$

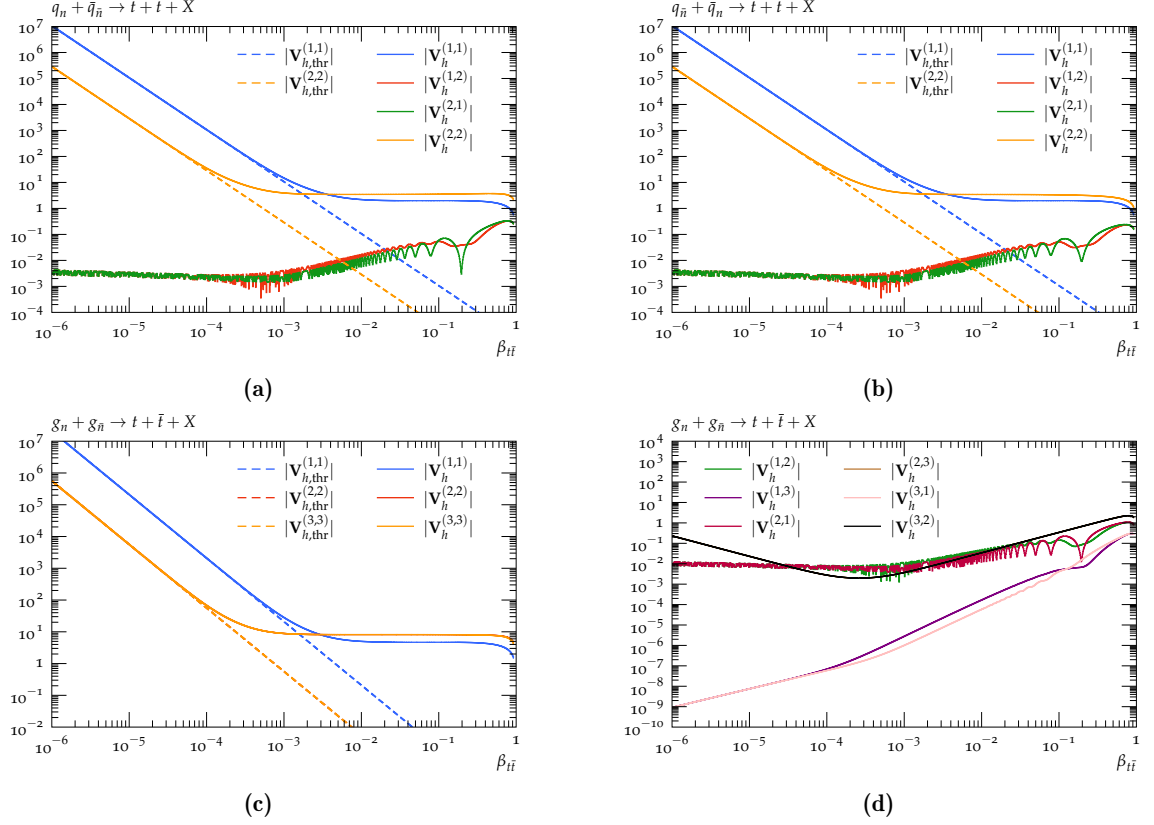


Figure 11: Comparison of the non-cusp evolution \mathbf{V}_h in Eq. (2.13) and its leading terms $\mathbf{V}_{h,\text{thr}}$ in Eq. (2.39) in the threshold regime at N²LL. Therein, $|\mathbf{V}_{h,(thr)}^{(m,n)}|$ denotes the absolute value of the entry of $\mathbf{V}_{h,(thr)}$ in the m -th row and n -th column from respective partonic process.

where T_{ab}^c stands for the generator in the fundamental representation of the SU(3) group. f_{abc} and d_{abc} mark the antisymmetric and symmetric structure constants for the SU(3) group, respectively.

We also specify the helicity bases concerned by the gluon-initialised channel [248, 249],

$$\epsilon_{n,\pm}^\mu \equiv \left\{ 0, \frac{\mp 1}{\sqrt{2}}, \frac{-i}{\sqrt{2}}, 0 \right\}, \quad \epsilon_{\bar{n},\pm}^\mu \equiv \left\{ 0, \frac{\pm 1}{\sqrt{2}}, \frac{-i}{\sqrt{2}}, 0 \right\}. \quad (\text{C.2})$$

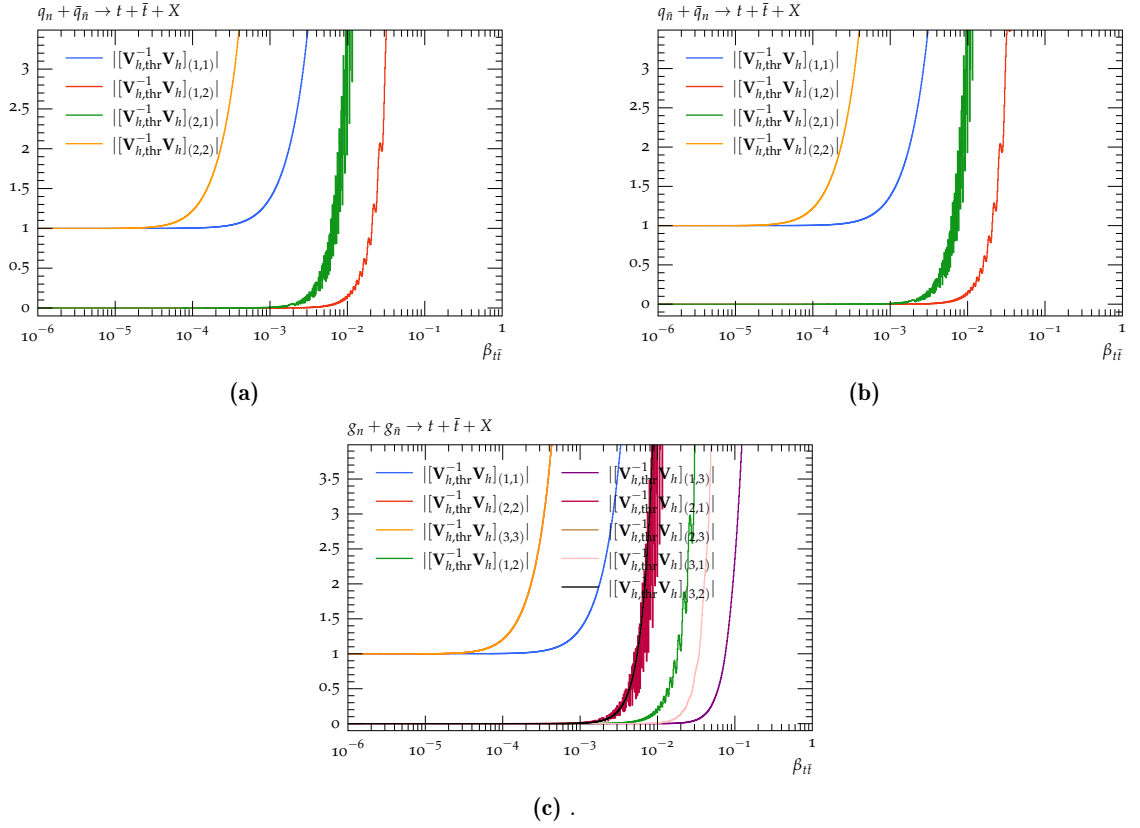


Figure 12: Product of the non-cusp evolution \mathbf{V}_h in Eq. (2.13) and the inverse matrix $\mathbf{V}_{h,\text{thr}}^{-1}$ in Eq. (2.39) at N²LL. Therein, $|\mathbf{V}_{h,\text{thr}}^{-1} \mathbf{V}_h|_{m,n}$ denotes the absolute value of the entry of $(\mathbf{V}_{h,\text{thr}}^{-1} \mathbf{V}_h)$ in the m -th row and n -th column from respective partonic process.

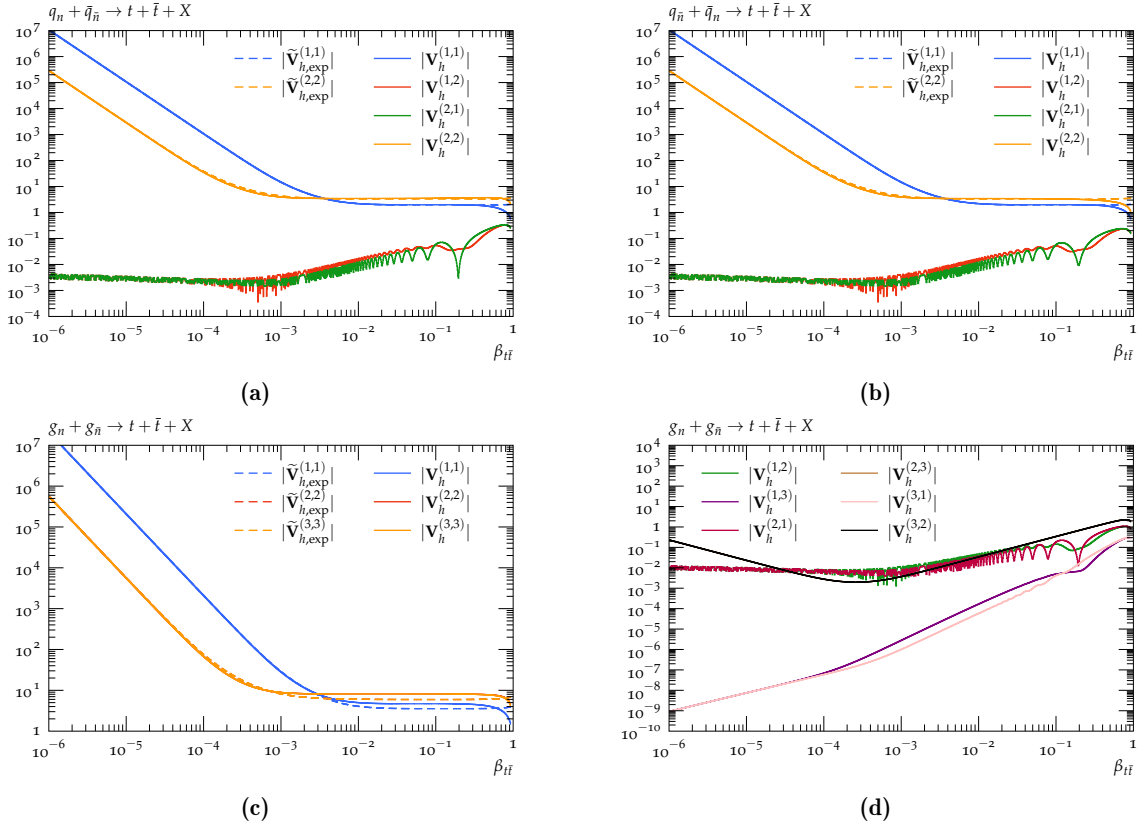


Figure 13: Comparison of the non-cusp evolution \mathbf{V}_h in Eq. (2.13) and $\tilde{\mathbf{V}}_{h,\text{exp}}$ in Eq. (2.60) at $N^2\text{LL}$. Therein, $|\mathbf{V}_h^{(m,n)}|$ and $|\tilde{\mathbf{V}}_{h,\text{exp}}^{(m,n)}|$ denote the absolute values of the entries of \mathbf{V}_h and $\tilde{\mathbf{V}}_{h,\text{exp}}$ in the m -th row and n -th column, respectively.

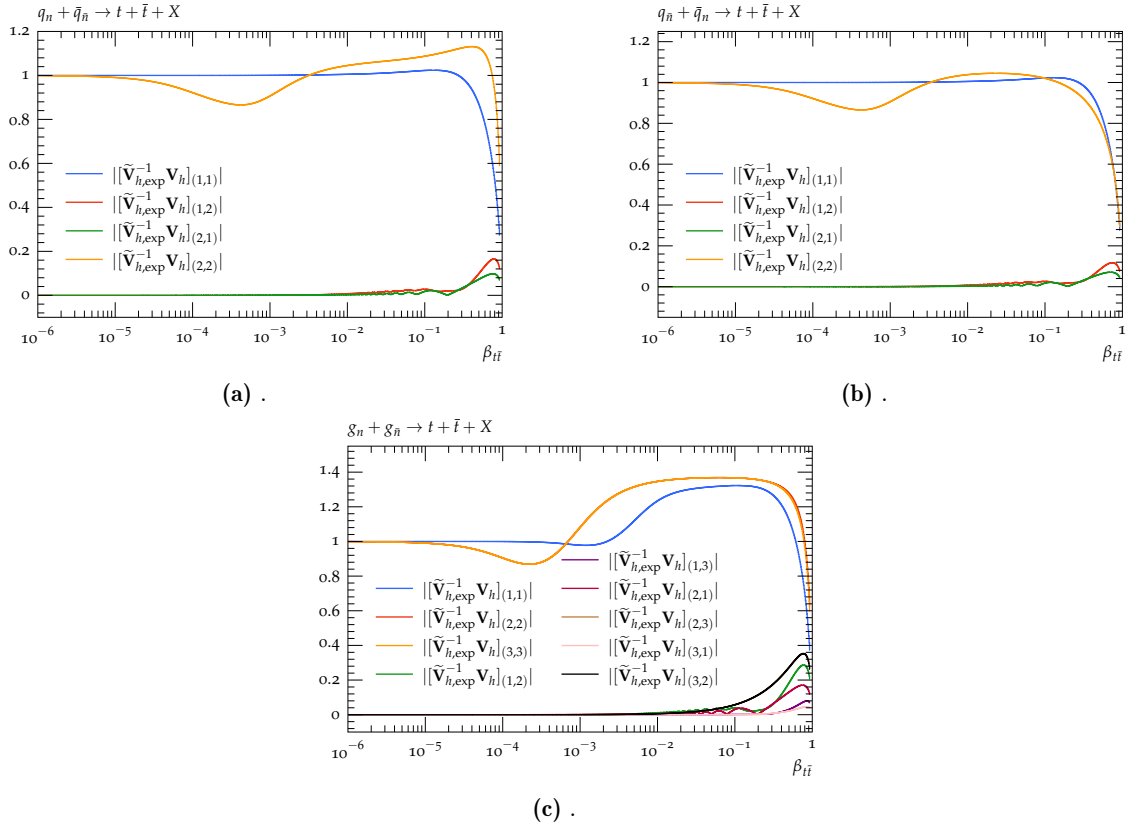


Figure 14: Product of the non-cusp evolution \mathbf{V}_h in Eq. (2.13) and the inverse matrix $\tilde{\mathbf{V}}_{h,\text{exp}}^{-1}$ in Eq. (2.60) at N²LL. Therein, $|\tilde{\mathbf{V}}_{h,\text{exp}}^{-1} \mathbf{V}_h|_{m,n}$ denotes the absolute value of the entry of $(\tilde{\mathbf{V}}_{h,\text{exp}}^{-1} \mathbf{V}_h)$ in the m -th row and n -th column from respective partonic process.

References

- [1] G. Aad et al., ATLAS collaboration, *Measurement of the $t\bar{t}$ production cross-section in pp collisions at $\sqrt{s} = 5.02$ TeV with the ATLAS detector*, JHEP **06** (2023), 138, [[arXiv:2207.01354](#) [hep-ex]].
- [2] A. M. Sirunyan et al., CMS collaboration, *Measurement of the inclusive $t\bar{t}$ cross section in pp collisions at $\sqrt{s} = 5.02$ TeV using final states with at least one charged lepton*, JHEP **03** (2018), 115, [[arXiv:1711.03143](#) [hep-ex]].
- [3] ATLAS collaboration, *Measurement of the $t\bar{t}$ production cross-section using dilepton events in pp collisions at $\sqrt{s} = 5.02$ TeV with the ATLAS detector*.
- [4] A. Tumasyan et al., CMS collaboration, *Measurement of the inclusive $t\bar{t}$ production cross section in proton-proton collisions at $\sqrt{s} = 5.02$ TeV*, JHEP **04** (2022), 144, [[arXiv:2112.09114](#) [hep-ex]].
- [5] S. Chatrchyan et al., CMS collaboration, *Measurement of the $t\bar{t}$ Production Cross Section in the All-Jet Final State in pp Collisions at $\sqrt{s} = 7$ TeV*, JHEP **05** (2013), 065, [[arXiv:1302.0508](#) [hep-ex]].
- [6] G. Aad et al., ATLAS collaboration, *Measurement of the $t\bar{t}$ production cross-section using $e\mu$ events with b-tagged jets in pp collisions at $\sqrt{s} = 7$ and 8 TeV with the ATLAS detector*, Eur. Phys. J. C **74** (2014), no. 10, 3109, [[arXiv:1406.5375](#) [hep-ex]], [Addendum: Eur.Phys.J.C 76, 642 (2016)].
- [7] G. Aad et al., ATLAS collaboration, *Measurement of the top quark pair production cross-section with ATLAS in the single lepton channel*, Phys. Lett. B **711** (2012), 244–263, [[arXiv:1201.1889](#) [hep-ex]].
- [8] V. Khachatryan et al., CMS collaboration, *Measurement of the t-tbar production cross section in the e-mu channel in proton-proton collisions at $\sqrt{s} = 7$ and 8 TeV*, JHEP **08** (2016), 029, [[arXiv:1603.02303](#) [hep-ex]].
- [9] V. Khachatryan et al., CMS collaboration, *Measurements of the $t\bar{t}$ production cross section in lepton+jets final states in pp collisions at 8 TeV and ratio of 8 to 7 TeV cross sections*, Eur. Phys. J. C **77** (2017), no. 1, 15, [[arXiv:1602.09024](#) [hep-ex]].
- [10] S. Chatrchyan et al., CMS collaboration, *Measurement of the $t\bar{t}$ Production Cross Section in pp Collisions at $\sqrt{s} = 7$ TeV with Lepton + Jets Final States*, Phys. Lett. B **720** (2013), 83–104, [[arXiv:1212.6682](#) [hep-ex]].
- [11] R. Aaij et al., LHCb collaboration, *First observation of top quark production in the forward region*, Phys. Rev. Lett. **115** (2015), no. 11, 112001, [[arXiv:1506.00903](#) [hep-ex]].
- [12] G. Aad et al., ATLAS, CMS collaboration, *Combination of inclusive top-quark pair production cross-section measurements using ATLAS and CMS data at $\sqrt{s} = 7$ and 8 TeV*, JHEP **07** (2023), 213, [[arXiv:2205.13830](#) [hep-ex]].
- [13] G. Aad et al., ATLAS collaboration, *Measurement of the top-quark mass in $t\bar{t} + 1$ -jet events collected with the ATLAS detector in pp collisions at $\sqrt{s} = 8$ TeV*, JHEP **11** (2019), 150, [[arXiv:1905.02302](#) [hep-ex]].
- [14] M. Aaboud et al., ATLAS collaboration, *Measurement of top quark pair differential cross-sections in the dilepton channel in pp collisions at $\sqrt{s} = 7$ and 8 TeV with ATLAS*, Phys. Rev. D **94** (2016), no. 9, 092003, [[arXiv:1607.07281](#) [hep-ex]], [Addendum: Phys.Rev.D 101, 119901 (2020)].
- [15] V. Khachatryan et al., CMS collaboration, *Measurement of the integrated and differential $t\bar{t}$ production cross sections for high- p_t top quarks in pp collisions at $\sqrt{s} = 8$ TeV*, Phys. Rev. D **94** (2016), no. 7, 072002, [[arXiv:1605.00116](#) [hep-ex]].
- [16] V. Khachatryan et al., CMS collaboration, *Measurement of the $t\bar{t}$ production cross section in the all-jets final state in pp collisions at $\sqrt{s} = 8$ TeV*, Eur. Phys. J. C **76** (2016), no. 3, 128, [[arXiv:1509.06076](#) [hep-ex]].
- [17] G. Aad et al., ATLAS collaboration, *Inclusive and differential cross-sections for dilepton $t\bar{t}$ production measured in $\sqrt{s} = 13$ TeV pp collisions with the ATLAS detector*, JHEP **07** (2023), 141, [[arXiv:2303.15340](#) [hep-ex]].

- [18] V. Khachatryan et al., CMS collaboration, *Measurement of the top quark pair production cross section in proton-proton collisions at $\sqrt{s} = 13$ TeV*, Phys. Rev. Lett. **116** (2016), no. 5, 052002, [arXiv:1510.05302 [hep-ex]].
- [19] R. Aaij et al., LHCb collaboration, *Measurement of forward top pair production in the dilepton channel in pp collisions at $\sqrt{s} = 13$ TeV*, JHEP **08** (2018), 174, [arXiv:1803.05188 [hep-ex]].
- [20] M. Aaboud et al., ATLAS collaboration, *Measurement of jet activity produced in top-quark events with an electron, a muon and two b-tagged jets in the final state in pp collisions at $\sqrt{s} = 13$ TeV with the ATLAS detector*, Eur. Phys. J. C **77** (2017), no. 4, 220, [arXiv:1610.09978 [hep-ex]].
- [21] G. Aad et al., ATLAS collaboration, *Measurement of the $t\bar{t}$ production cross-section and lepton differential distributions in $e\mu$ dilepton events from pp collisions at $\sqrt{s} = 13$ TeV with the ATLAS detector*, Eur. Phys. J. C **80** (2020), no. 6, 528, [arXiv:1910.08819 [hep-ex]].
- [22] G. Aad et al., ATLAS collaboration, *Measurement of the $t\bar{t}$ production cross-section in the lepton+jets channel at $\sqrt{s} = 13$ TeV with the ATLAS experiment*, Phys. Lett. B **810** (2020), 135797, [arXiv:2006.13076 [hep-ex]].
- [23] A. M. Sirunyan et al., CMS collaboration, *Measurement of the top quark pair production cross section in dilepton final states containing one τ lepton in pp collisions at $\sqrt{s} = 13$ TeV*, JHEP **02** (2020), 191, [arXiv:1911.13204 [hep-ex]].
- [24] CMS collaboration, *Measurement of the $t\bar{t}$ production cross section at 13 TeV in the all-jets final state*.
- [25] A. M. Sirunyan et al., CMS collaboration, *Measurement of the $t\bar{t}$ production cross section, the top quark mass, and the strong coupling constant using dilepton events in pp collisions at $\sqrt{s} = 13$ TeV*, Eur. Phys. J. C **79** (2019), no. 5, 368, [arXiv:1812.10505 [hep-ex]].
- [26] CMS collaboration, *First measurement of the top quark pair production cross section in proton-proton collisions at $\sqrt{s} = 13.6$ TeV*.
- [27] G. Aad et al., ATLAS collaboration, *Measurement of the $t\bar{t}$ cross section and its ratio to the Z production cross section using pp collisions at $s=13.6$ TeV with the ATLAS detector*, Phys. Lett. B **848** (2024), 138376, [arXiv:2308.09529 [hep-ex]].
- [28] G. Aad et al., ATLAS collaboration, *Measurements of top quark pair relative differential cross-sections with ATLAS in pp collisions at $\sqrt{s} = 7$ TeV*, Eur. Phys. J. C **73** (2013), no. 1, 2261, [arXiv:1207.5644 [hep-ex]].
- [29] S. Chatrchyan et al., CMS collaboration, *Measurement of Differential Top-Quark Pair Production Cross Sections in pp collisions at $\sqrt{s} = 7$ TeV*, Eur. Phys. J. C **73** (2013), no. 3, 2339, [arXiv:1211.2220 [hep-ex]].
- [30] G. Aad et al., ATLAS collaboration, *Measurements of normalized differential cross sections for $t\bar{t}$ production in pp collisions at $\sqrt{s} = 7$ TeV using the ATLAS detector*, Phys. Rev. D **90** (2014), no. 7, 072004, [arXiv:1407.0371 [hep-ex]].
- [31] G. Aad et al., ATLAS collaboration, *Differential top-antitop cross-section measurements as a function of observables constructed from final-state particles using pp collisions at $\sqrt{s} = 7$ TeV in the ATLAS detector*, JHEP **06** (2015), 100, [arXiv:1502.05923 [hep-ex]].
- [32] A. M. Sirunyan et al., CMS collaboration, *Measurement of double-differential cross sections for top quark pair production in pp collisions at $\sqrt{s} = 8$ TeV and impact on parton distribution functions*, Eur. Phys. J. C **77** (2017), no. 7, 459, [arXiv:1703.01630 [hep-ex]].
- [33] V. Khachatryan et al., CMS collaboration, *Measurement of the differential cross section for top quark pair production in pp collisions at $\sqrt{s} = 8$ TeV*, Eur. Phys. J. C **75** (2015), no. 11, 542, [arXiv:1505.04480 [hep-ex]].
- [34] G. Aad et al., ATLAS collaboration, *Measurements of top-quark pair differential cross-sections in the lepton+jets channel in pp collisions at $\sqrt{s} = 8$ TeV using the ATLAS detector*, Eur. Phys. J. C **76** (2016), no. 10, 538, [arXiv:1511.04716 [hep-ex]].

- [35] G. Aad et al., ATLAS collaboration, *Measurement of the differential cross-section of highly boosted top quarks as a function of their transverse momentum in $\sqrt{s} = 8$ TeV proton-proton collisions using the ATLAS detector*, Phys. Rev. D **93** (2016), no. 3, 032009, [arXiv:1510.03818 [hep-ex]].
- [36] A. Tumasyan et al., CMS collaboration, *Differential cross section measurements for the production of top quark pairs and of additional jets using dilepton events from pp collisions at $\sqrt{s} = 13$ TeV*, arXiv:2402.08486 [hep-ex].
- [37] CMS collaboration, *Measurement of differential cross sections for the production of top quark pairs and of additional jets in pp collisions at $\sqrt{s} = 13$ TeV*.
- [38] V. Khachatryan et al., CMS collaboration, *Measurement of differential cross sections for top quark pair production using the lepton+jets final state in proton-proton collisions at 13 TeV*, Phys. Rev. D **95** (2017), no. 9, 092001, [arXiv:1610.04191 [hep-ex]].
- [39] M. Aaboud et al., ATLAS collaboration, *Measurements of top-quark pair differential cross-sections in the $e\mu$ channel in pp collisions at $\sqrt{s} = 13$ TeV using the ATLAS detector*, Eur. Phys. J. C **77** (2017), no. 5, 292, [arXiv:1612.05220 [hep-ex]].
- [40] A. M. Sirunyan et al., CMS collaboration, *Measurement of normalized differential $t\bar{t}$ cross sections in the dilepton channel from pp collisions at $\sqrt{s} = 13$ TeV*, JHEP **04** (2018), 060, [arXiv:1708.07638 [hep-ex]].
- [41] A. M. Sirunyan et al., CMS collaboration, *Measurement of $t\bar{t}$ normalised multi-differential cross sections in pp collisions at $\sqrt{s} = 13$ TeV, and simultaneous determination of the strong coupling strength, top quark pole mass, and parton distribution functions*, Eur. Phys. J. C **80** (2020), no. 7, 658, [arXiv:1904.05237 [hep-ex]].
- [42] A. M. Sirunyan et al., CMS collaboration, *Measurement of differential $t\bar{t}$ production cross sections using top quarks at large transverse momenta in pp collisions at $\sqrt{s} = 13$ TeV*, Phys. Rev. D **103** (2021), no. 5, 052008, [arXiv:2008.07860 [hep-ex]].
- [43] G. Aad et al., ATLAS collaboration, *Measurements of top-quark pair single- and double-differential cross-sections in the all-hadronic channel in pp collisions at $\sqrt{s} = 13$ TeV using the ATLAS detector*, JHEP **01** (2021), 033, [arXiv:2006.09274 [hep-ex]].
- [44] G. Aad et al., ATLAS collaboration, *Measurements of differential cross-sections in top-quark pair events with a high transverse momentum top quark and limits on beyond the Standard Model contributions to top-quark pair production with the ATLAS detector at $\sqrt{s} = 13$ TeV*, JHEP **06** (2022), 063, [arXiv:2202.12134 [hep-ex]].
- [45] G. Aad et al., ATLAS collaboration, *Differential $t\bar{t}$ cross-section measurements using boosted top quarks in the all-hadronic final state with 139 fb^{-1} of ATLAS data*, JHEP **04** (2023), 080, [arXiv:2205.02817 [hep-ex]].
- [46] A. Tumasyan et al., CMS collaboration, *Measurement of differential $t\bar{t}$ production cross sections in the full kinematic range using lepton+jets events from proton-proton collisions at $\sqrt{s} = 13$ TeV*, Phys. Rev. D **104** (2021), no. 9, 092013, [arXiv:2108.02803 [hep-ex]].
- [47] A. M. Sirunyan et al., CMS collaboration, *Measurement of differential cross sections for the production of top quark pairs and of additional jets in lepton+jets events from pp collisions at $\sqrt{s} = 13$ TeV*, Phys. Rev. D **97** (2018), no. 11, 112003, [arXiv:1803.08856 [hep-ex]].
- [48] A. M. Sirunyan et al., CMS collaboration, *Measurements of $t\bar{t}$ differential cross sections in proton-proton collisions at $\sqrt{s} = 13$ TeV using events containing two leptons*, JHEP **02** (2019), 149, [arXiv:1811.06625 [hep-ex]].
- [49] G. Aad et al., ATLAS collaboration, *Measurements of top-quark pair differential and double-differential cross-sections in the ℓ +jets channel with pp collisions at $\sqrt{s} = 13$ TeV using the ATLAS detector*, Eur. Phys. J. C **79** (2019), no. 12, 1028, [arXiv:1908.07305 [hep-ex]], [Erratum: Eur.Phys.J.C 80, 1092 (2020)].

- [50] P. Nason, S. Dawson and R. K. Ellis, *The Total Cross-Section for the Production of Heavy Quarks in Hadronic Collisions*, Nucl. Phys. B **303** (1988), 607–633.
- [51] W. Beenakker, H. Kuijf, W. L. van Neerven and J. Smith, *QCD Corrections to Heavy Quark Production in p anti- p Collisions*, Phys. Rev. D **40** (1989), 54–82.
- [52] W. Beenakker, W. L. van Neerven, R. Meng, G. A. Schuler and J. Smith, *QCD corrections to heavy quark production in hadron hadron collisions*, Nucl. Phys. B **351** (1991), 507–560.
- [53] M. L. Mangano, P. Nason and G. Ridolfi, *Heavy quark correlations in hadron collisions at next-to-leading order*, Nucl. Phys. B **373** (1992), 295–345.
- [54] M. Czakon, P. Fiedler and A. Mitov, *Total Top-Quark Pair-Production Cross Section at Hadron Colliders Through $O(\alpha_s^4)$* , Phys. Rev. Lett. **110** (2013), 252004, [arXiv:1303.6254 [hep-ph]].
- [55] M. Czakon, D. Heymes and A. Mitov, *High-precision differential predictions for top-quark pairs at the LHC*, Phys. Rev. Lett. **116** (2016), no. 8, 082003, [arXiv:1511.00549 [hep-ph]].
- [56] M. Czakon, P. Fiedler, D. Heymes and A. Mitov, *NNLO QCD predictions for fully-differential top-quark pair production at the Tevatron*, JHEP **05** (2016), 034, [arXiv:1601.05375 [hep-ph]].
- [57] M. Czakon, D. Heymes and A. Mitov, *fastNNLO tables for NNLO top-quark pair differential distributions*, arXiv:1704.08551 [hep-ph].
- [58] M. Czakon, D. Heymes, A. Mitov, D. Pagani, I. Tsinikos and M. Zaro, *Top-pair production at the LHC through NNLO QCD and NLO EW*, JHEP **10** (2017), 186, [arXiv:1705.04105 [hep-ph]].
- [59] S. Catani, S. Devoto, M. Grazzini, S. Kallweit, J. Mazzitelli and H. Sargsyan, *Top-quark pair hadroproduction at next-to-next-to-leading order in QCD*, Phys. Rev. D **99** (2019), no. 5, 051501, [arXiv:1901.04005 [hep-ph]].
- [60] S. Catani, S. Devoto, M. Grazzini, S. Kallweit and J. Mazzitelli, *Top-quark pair hadroproduction at NNLO: differential predictions with the \overline{MS} mass*, JHEP **08** (2020), no. 08, 027, [arXiv:2005.00557 [hep-ph]].
- [61] M. Czakon, A. Mitov, M. Pellen and R. Poncelet, *NNLO QCD predictions for $W+c$ -jet production at the LHC*, JHEP **06** (2021), 100, [arXiv:2011.01011 [hep-ph]].
- [62] M. L. Czakon, T. Generet, A. Mitov and R. Poncelet, *B -hadron production in NNLO QCD: application to LHC $t\bar{t}$ events with leptonic decays*, JHEP **10** (2021), 216, [arXiv:2102.08267 [hep-ph]].
- [63] S. Catani, S. Devoto, M. Grazzini, S. Kallweit and J. Mazzitelli, *Top-quark pair production at the LHC: Fully differential QCD predictions at NNLO*, JHEP **07** (2019), 100, [arXiv:1906.06535 [hep-ph]].
- [64] M. V. Garzelli, J. Mazzitelli, S. O. Moch and O. Zenaiev, *Top-quark pole mass extraction at NNLO accuracy, from total, single- and double-differential cross sections for $t\bar{t} + X$ production at the LHC*, JHEP **05** (2024), 321, [arXiv:2311.05509 [hep-ph]].
- [65] W. Bernreuther and Z.-G. Si, *Distributions and correlations for top quark pair production and decay at the Tevatron and LHC.*, Nucl. Phys. B **837** (2010), 90–121, [arXiv:1003.3926 [hep-ph]].
- [66] J. H. Kuhn, A. Scharf and P. Uwer, *Electroweak effects in top-quark pair production at hadron colliders*, Eur. Phys. J. C **51** (2007), 37–53, [hep-ph/0610335].
- [67] W. Bernreuther, M. Fuecker and Z.-G. Si, *Weak interaction corrections to hadronic top quark pair production*, Phys. Rev. D **74** (2006), 113005, [hep-ph/0610334].
- [68] J. H. Kühn, A. Scharf and P. Uwer, *Weak Interactions in Top-Quark Pair Production at Hadron Colliders: An Update*, Phys. Rev. D **91** (2015), no. 1, 014020, [arXiv:1305.5773 [hep-ph]].
- [69] W. Hollik and D. Pagani, *The electroweak contribution to the top quark forward-backward asymmetry at the Tevatron*, Phys. Rev. D **84** (2011), 093003, [arXiv:1107.2606 [hep-ph]].

- [70] D. Pagani, I. Tsiniikos and M. Zaro, *The impact of the photon PDF and electroweak corrections on $t\bar{t}$ distributions*, Eur. Phys. J. C **76** (2016), no. 9, 479, [arXiv:1606.01915 [hep-ph]].
- [71] C. Gütschow, J. M. Lindert and M. Schönherr, *Multi-jet merged top-pair production including electroweak corrections*, Eur. Phys. J. C **78** (2018), no. 4, 317, [arXiv:1803.00950 [hep-ph]].
- [72] A. Denner and M. Pellen, *NLO electroweak corrections to off-shell top-antitop production with leptonic decays at the LHC*, JHEP **08** (2016), 155, [arXiv:1607.05571 [hep-ph]].
- [73] W. Bernreuther, L. Chen and Z.-G. Si, *Binned top quark spin correlation and polarization observables for the LHC at 13.6 TeV*, Phys. Rev. D **109** (2024), no. 11, 116016, [arXiv:2403.04371 [hep-ph]].
- [74] R. Frederix, I. Tsiniikos and T. Vitos, *Probing the spin correlations of $t\bar{t}$ production at NLO QCD+EW*, Eur. Phys. J. C **81** (2021), no. 9, 817, [arXiv:2105.11478 [hep-ph]].
- [75] J. Gao, C. S. Li and H. X. Zhu, *Top Quark Decay at Next-to-Next-to Leading Order in QCD*, Phys. Rev. Lett. **110** (2013), no. 4, 042001, [arXiv:1210.2808 [hep-ph]].
- [76] M. Brucherseifer, F. Caola and K. Melnikov, *$\mathcal{O}(\alpha_s^2)$ corrections to fully-differential top quark decays*, JHEP **04** (2013), 059, [arXiv:1301.7133 [hep-ph]].
- [77] A. Behring, M. Czakon, A. Mitov, A. S. Papanastasiou and R. Poncelet, *Higher order corrections to spin correlations in top quark pair production at the LHC*, Phys. Rev. Lett. **123** (2019), no. 8, 082001, [arXiv:1901.05407 [hep-ph]].
- [78] M. Czakon, A. Mitov and R. Poncelet, *NNLO QCD corrections to leptonic observables in top-quark pair production and decay*, JHEP **05** (2021), 212, [arXiv:2008.11133 [hep-ph]].
- [79] D. Stremmer and M. Worek, *Complete NLO corrections to top-quark pair production with isolated photons*, JHEP **07** (2024), 091, [arXiv:2403.03796 [hep-ph]].
- [80] A. Ablat, M. Guzzi, K. Xie, S. Dulat, T.-J. Hou, I. Sitiwaldi and C. P. Yuan, *Exploring the impact of high-precision top-quark pair production data on the structure of the proton at the LHC*, Phys. Rev. D **109** (2024), no. 5, 054027, [arXiv:2307.11153 [hep-ph]].
- [81] R.-Q. Meng, S.-Q. Wang, T. Sun, C.-Q. Luo, J.-M. Shen and X.-G. Wu, *QCD improved top-quark decay at next-to-next-to-leading order*, Eur. Phys. J. C **83** (2023), no. 1, 59, [arXiv:2202.09978 [hep-ph]].
- [82] N. Kidonakis, *NNLO soft-gluon corrections for the top-quark p_T and rapidity distributions*, Phys. Rev. D **91** (2015), no. 3, 031501, [arXiv:1411.2633 [hep-ph]].
- [83] N. Kidonakis, M. Guzzi and A. Tonerio, *Top-quark cross sections and distributions at approximate N³LO*, Phys. Rev. D **108** (2023), no. 5, 054012, [arXiv:2306.06166 [hep-ph]].
- [84] N. Kidonakis, *Next-to-next-to-leading soft-gluon corrections for the top quark cross section and transverse momentum distribution*, Phys. Rev. D **82** (2010), 114030, [arXiv:1009.4935 [hep-ph]].
- [85] N. Kidonakis, *Two-loop soft anomalous dimensions and NNLL resummation for heavy quark production*, Phys. Rev. Lett. **102** (2009), 232003, [arXiv:0903.2561 [hep-ph]].
- [86] N. Kidonakis, *NNLO soft-gluon corrections for the top-antitop pair production cross section*, Phys. Rev. D **90** (2014), no. 1, 014006, [arXiv:1405.7046 [hep-ph]].
- [87] N. Kidonakis, *Top-quark double-differential distributions at approximate N³LO*, Phys. Rev. D **101** (2020), no. 7, 074006, [arXiv:1912.10362 [hep-ph]].
- [88] V. Ahrens, A. Ferroglia, M. Neubert, B. D. Pecjak and L. L. Yang, *Renormalization-Group Improved Predictions for Top-Quark Pair Production at Hadron Colliders*, JHEP **09** (2010), 097, [arXiv:1003.5827 [hep-ph]].
- [89] A. Ferroglia, B. D. Pecjak and L. L. Yang, *Soft-gluon resummation for boosted top-quark production at hadron colliders*, Phys. Rev. D **86** (2012), 034010, [arXiv:1205.3662 [hep-ph]].

- [90] A. Ferroglia, S. Marzani, B. D. Pecjak and L. L. Yang, *Boosted top production: factorization and resummation for single-particle inclusive distributions*, JHEP **01** (2014), 028, [[arXiv:1310.3836](#) [hep-ph]].
- [91] B. D. Pecjak, D. J. Scott, X. Wang and L. L. Yang, *Resummed differential cross sections for top-quark pairs at the LHC*, Phys. Rev. Lett. **116** (2016), no. 20, 202001, [[arXiv:1601.07020](#) [hep-ph]].
- [92] M. Czakon, A. Ferroglia, D. Heymes, A. Mitov, B. D. Pecjak, D. J. Scott, X. Wang and L. L. Yang, *Resummation for (boosted) top-quark pair production at NNLO+NNLL' in QCD*, JHEP **05** (2018), 149, [[arXiv:1803.07623](#) [hep-ph]].
- [93] L. G. Almeida, G. F. Sterman and W. Vogelsang, *Threshold Resummation for the Top Quark Charge Asymmetry*, Phys. Rev. D **78** (2008), 014008, [[arXiv:0805.1885](#) [hep-ph]].
- [94] B. D. Pecjak, D. J. Scott, X. Wang and L. L. Yang, *Resummation for rapidity distributions in top-quark pair production*, JHEP **03** (2019), 060, [[arXiv:1811.10527](#) [hep-ph]].
- [95] K. Hagiwara, Y. Sumino and H. Yokoya, *Bound-state Effects on Top Quark Production at Hadron Colliders*, Phys. Lett. B **666** (2008), 71–76, [[arXiv:0804.1014](#) [hep-ph]].
- [96] Y. Kiyo, J. H. Kuhn, S. Moch, M. Steinhauser and P. Uwer, *Top-quark pair production near threshold at LHC*, Eur. Phys. J. C **60** (2009), 375–386, [[arXiv:0812.0919](#) [hep-ph]].
- [97] W.-L. Ju, G. Wang, X. Wang, X. Xu, Y. Xu and L. L. Yang, *Top quark pair production near threshold: single/double distributions and mass determination*, JHEP **06** (2020), 158, [[arXiv:2004.03088](#) [hep-ph]].
- [98] W.-L. Ju, G. Wang, X. Wang, X. Xu, Y. Xu and L. L. Yang, *Invariant-mass distribution of top-quark pairs and top-quark mass determination*, Chin. Phys. C **44** (2020), no. 9, 091001, [[arXiv:1908.02179](#) [hep-ph]].
- [99] M. Beneke, M. Czakon, P. Falgari, A. Mitov and C. Schwinn, *Threshold expansion of the $gg(q\bar{q}) \rightarrow Q\bar{Q} + X$ cross section at $O(\alpha_s^4)$* , Phys. Lett. B **690** (2010), 483–490, [[arXiv:0911.5166](#) [hep-ph]], [Erratum: Phys.Lett.B 778, 464–464 (2018)].
- [100] M. Beneke, P. Falgari and C. Schwinn, *Threshold resummation for pair production of coloured heavy (s)particles at hadron colliders*, Nucl. Phys. B **842** (2011), 414–474, [[arXiv:1007.5414](#) [hep-ph]].
- [101] M. Beneke, P. Falgari, S. Klein and C. Schwinn, *Hadronic top-quark pair production with NNLL threshold resummation*, Nucl. Phys. B **855** (2012), 695–741, [[arXiv:1109.1536](#) [hep-ph]].
- [102] M. Cacciari, M. Czakon, M. Mangano, A. Mitov and P. Nason, *Top-pair production at hadron colliders with next-to-next-to-leading logarithmic soft-gluon resummation*, Phys. Lett. B **710** (2012), 612–622, [[arXiv:1111.5869](#) [hep-ph]].
- [103] J. Piclum and C. Schwinn, *Soft-gluon and Coulomb corrections to hadronic top-quark pair production beyond NNLO*, JHEP **03** (2018), 164, [[arXiv:1801.05788](#) [hep-ph]].
- [104] H. X. Zhu, C. S. Li, H. T. Li, D. Y. Shao and L. L. Yang, *Transverse-momentum resummation for top-quark pairs at hadron colliders*, Phys. Rev. Lett. **110** (2013), no. 8, 082001, [[arXiv:1208.5774](#) [hep-ph]].
- [105] H. T. Li, C. S. Li, D. Y. Shao, L. L. Yang and H. X. Zhu, *Top quark pair production at small transverse momentum in hadronic collisions*, Phys. Rev. D **88** (2013), 074004, [[arXiv:1307.2464](#) [hep-ph]].
- [106] S. Catani, M. Grazzini and A. Torre, *Transverse-momentum resummation for heavy-quark hadroproduction*, Nucl. Phys. B **890** (2014), 518–538, [[arXiv:1408.4564](#) [hep-ph]].
- [107] S. Catani, M. Grazzini and H. Sargsyan, *Azimuthal asymmetries in QCD hard scattering: infrared safe but divergent*, JHEP **06** (2017), 017, [[arXiv:1703.08468](#) [hep-ph]].
- [108] S. Catani, M. Grazzini and H. Sargsyan, *Transverse-momentum resummation for top-quark pair production at the LHC*, JHEP **11** (2018), 061, [[arXiv:1806.01601](#) [hep-ph]].

- [109] S. Alioli, A. Broggio and M. A. Lim, *Zero-jettiness resummation for top-quark pair production at the LHC*, JHEP **01** (2022), 066, [arXiv:2111.03632 [hep-ph]].
- [110] W.-L. Ju and M. Schönherr, *Projected transverse momentum resummation in top-antitop pair production at LHC*, JHEP **02** (2023), 075, [arXiv:2210.09272 [hep-ph]].
- [111] J. Mazzeiti, P. F. Monni, P. Nason, E. Re, M. Wiesemann and G. Zanderighi, *Next-to-Next-to-Leading Order Event Generation for Top-Quark Pair Production*, Phys. Rev. Lett. **127** (2021), no. 6, 062001, [arXiv:2012.14267 [hep-ph]].
- [112] J. Mazzeiti, P. F. Monni, P. Nason, E. Re, M. Wiesemann and G. Zanderighi, *Top-pair production at the LHC with MINNLO_{PS}*, JHEP **04** (2022), 079, [arXiv:2112.12135 [hep-ph]].
- [113] T. Ježo, J. M. Lindert and S. Pozzorini, *Resonance-aware NLOPS matching for off-shell $t\bar{t} + tW$ production with semileptonic decays*, JHEP **10** (2023), 008, [arXiv:2307.15653 [hep-ph]].
- [114] J. C. Collins, D. E. Soper and G. F. Sterman, *Transverse Momentum Distribution in Drell-Yan Pair and W and Z Boson Production*, Nucl. Phys. B **250** (1985), 199–224.
- [115] T. Becher and M. Neubert, *Drell-Yan Production at Small q_T , Transverse Parton Distributions and the Collinear Anomaly*, Eur. Phys. J. C **71** (2011), 1665, [arXiv:1007.4005 [hep-ph]].
- [116] G. Bozzi, S. Catani, G. Ferrera, D. de Florian and M. Grazzini, *Production of Drell-Yan lepton pairs in hadron collisions: Transverse-momentum resummation at next-to-next-to-leading logarithmic accuracy*, Phys. Lett. B **696** (2011), 207–213, [arXiv:1007.2351 [hep-ph]].
- [117] M. G. Echevarria, A. Idilbi and I. Scimemi, *Factorization Theorem For Drell-Yan At Low q_T And Transverse Momentum Distributions On-The-Light-Cone*, JHEP **07** (2012), 002, [arXiv:1111.4996 [hep-ph]].
- [118] T. Becher, M. Neubert and D. Wilhelm, *Electroweak Gauge-Boson Production at Small q_T : Infrared Safety from the Collinear Anomaly*, JHEP **02** (2012), 124, [arXiv:1109.6027 [hep-ph]].
- [119] A. Banfi, M. Dasgupta and S. Marzani, *QCD predictions for new variables to study dilepton transverse momenta at hadron colliders*, Phys. Lett. B **701** (2011), 75–81, [arXiv:1102.3594 [hep-ph]].
- [120] A. Banfi, M. Dasgupta, S. Marzani and L. Tomlinson, *Probing the low transverse momentum domain of Z production with novel variables*, JHEP **01** (2012), 044, [arXiv:1110.4009 [hep-ph]].
- [121] A. Banfi, M. Dasgupta, S. Marzani and L. Tomlinson, *Predictions for Drell-Yan ϕ^* and Q_T observables at the LHC*, Phys. Lett. B **715** (2012), 152–156, [arXiv:1205.4760 [hep-ph]].
- [122] S. Catani, D. de Florian, G. Ferrera and M. Grazzini, *Vector boson production at hadron colliders: transverse-momentum resummation and leptonic decay*, JHEP **12** (2015), 047, [arXiv:1507.06937 [hep-ph]].
- [123] I. Scimemi and A. Vladimirov, *Analysis of vector boson production within TMD factorization*, Eur. Phys. J. C **78** (2018), no. 2, 89, [arXiv:1706.01473 [hep-ph]].
- [124] W. Bizoń, X. Chen, A. Gehrmann-De Ridder, T. Gehrmann, N. Glover, A. Huss, P. F. Monni, E. Re, L. Rottoli and P. Torrielli, *Fiducial distributions in Higgs and Drell-Yan production at $N^3LL+NNLO$* , JHEP **12** (2018), 132, [arXiv:1805.05916 [hep-ph]].
- [125] A. Bacchetta, V. Bertone, C. Bissolotti, G. Bozzi, F. Delcarro, F. Piacenza and M. Radici, *Transverse-momentum-dependent parton distributions up to N^3LL from Drell-Yan data*, JHEP **07** (2020), 117, [arXiv:1912.07550 [hep-ph]].
- [126] W. Bizon, A. Gehrmann-De Ridder, T. Gehrmann, N. Glover, A. Huss, P. F. Monni, E. Re, L. Rottoli and D. M. Walker, *The transverse momentum spectrum of weak gauge bosons at $N^3LL + NNLO$* , Eur. Phys. J. C **79** (2019), no. 10, 868, [arXiv:1905.05171 [hep-ph]].
- [127] T. Becher and T. Neumann, *Fiducial q_T resummation of color-singlet processes at $N^3LL+NNLO$* , JHEP **03** (2021), 199, [arXiv:2009.11437 [hep-ph]].

- [128] M. A. Ebert, J. K. L. Michel, I. W. Stewart and F. J. Tackmann, *Drell-Yan q_T resummation of fiducial power corrections at N^3LL* , JHEP **04** (2021), 102, [[arXiv:2006.11382](#) [hep-ph]].
- [129] E. Re, L. Rottoli and P. Torrielli, *Fiducial Higgs and Drell-Yan distributions at $N^3LL'+NNLO$ with RadISH*, [arXiv:2104.07509](#) [hep-ph].
- [130] S. Camarda, L. Cieri and G. Ferrera, *Drell-Yan lepton-pair production: q_T resummation at N^3LL accuracy and fiducial cross sections at N^3LO* , Phys. Rev. D **104** (2021), no. 11, L111503, [[arXiv:2103.04974](#) [hep-ph]].
- [131] W.-L. Ju and M. Schönherr, *The q_T and $\Delta\phi$ spectra in W and Z production at the LHC at $N^3LL'+N^2LO$* , JHEP **10** (2021), 088, [[arXiv:2106.11260](#) [hep-ph]].
- [132] S. Camarda, L. Cieri and G. Ferrera, *Drell-Yan lepton-pair production: q_T resummation at N^4LL accuracy*, Phys. Lett. B **845** (2023), 138125, [[arXiv:2303.12781](#) [hep-ph]].
- [133] T. Neumann and J. Campbell, *Fiducial Drell-Yan production at the LHC improved by transverse-momentum resummation at N^4LLp+N^3LO* , Phys. Rev. D **107** (2023), no. 1, L011506, [[arXiv:2207.07056](#) [hep-ph]].
- [134] V. Moos, I. Scimemi, A. Vladimirov and P. Zurita, *Extraction of unpolarized transverse momentum distributions from the fit of Drell-Yan data at N^4LL* , JHEP **05** (2024), 036, [[arXiv:2305.07473](#) [hep-ph]].
- [135] A. Belyaev, P. M. Nadolsky and C. P. Yuan, *Transverse momentum resummation for Higgs boson produced via b anti- b fusion at hadron colliders*, JHEP **04** (2006), 004, [[hep-ph/0509100](#)].
- [136] G. Bozzi, S. Catani, D. de Florian and M. Grazzini, *Transverse-momentum resummation and the spectrum of the Higgs boson at the LHC*, Nucl. Phys. B **737** (2006), 73–120, [[hep-ph/0508068](#)].
- [137] G. Bozzi, S. Catani, D. de Florian and M. Grazzini, *Higgs boson production at the LHC: Transverse-momentum resummation and rapidity dependence*, Nucl. Phys. B **791** (2008), 1–19, [[arXiv:0705.3887](#) [hep-ph]].
- [138] P. F. Monni, E. Re and P. Torrielli, *Higgs Transverse-Momentum Resummation in Direct Space*, Phys. Rev. Lett. **116** (2016), no. 24, 242001, [[arXiv:1604.02191](#) [hep-ph]].
- [139] T. Becher, M. Neubert and D. Wilhelm, *Higgs-Boson Production at Small Transverse Momentum*, JHEP **05** (2013), 110, [[arXiv:1212.2621](#) [hep-ph]].
- [140] D. Neill, I. Z. Rothstein and V. Vaidya, *The Higgs Transverse Momentum Distribution at NNLL and its Theoretical Errors*, JHEP **12** (2015), 097, [[arXiv:1503.00005](#) [hep-ph]].
- [141] W. Bizon, P. F. Monni, E. Re, L. Rottoli and P. Torrielli, *Momentum-space resummation for transverse observables and the Higgs p_\perp at $N^3LL+NNLO$* , JHEP **02** (2018), 108, [[arXiv:1705.09127](#) [hep-ph]].
- [142] X. Chen, T. Gehrmann, E. W. N. Glover, A. Huss, Y. Li, D. Neill, M. Schulze, I. W. Stewart and H. X. Zhu, *Precise QCD Description of the Higgs Boson Transverse Momentum Spectrum*, Phys. Lett. B **788** (2019), 425–430, [[arXiv:1805.00736](#) [hep-ph]].
- [143] D. Gutierrez-Reyes, S. Leal-Gomez, I. Scimemi and A. Vladimirov, *Linearly polarized gluons at next-to-next-to leading order and the Higgs transverse momentum distribution*, JHEP **11** (2019), 121, [[arXiv:1907.03780](#) [hep-ph]].
- [144] R. V. Harlander, A. Tripathi and M. Wiesemann, *Higgs production in bottom quark annihilation: Transverse momentum distribution at NNLO+NNLL*, Phys. Rev. D **90** (2014), no. 1, 015017, [[arXiv:1403.7196](#) [hep-ph]].
- [145] G. Billis, B. Dehnadi, M. A. Ebert, J. K. L. Michel and F. J. Tackmann, *Higgs p_T Spectrum and Total Cross Section with Fiducial Cuts at Third Resummed and Fixed Order in QCD*, Phys. Rev. Lett. **127** (2021), no. 7, 072001, [[arXiv:2102.08039](#) [hep-ph]].

- [146] P. Cal, R. von Kuk, M. A. Lim and F. J. Tackmann, *qT spectrum for Higgs boson production via heavy quark annihilation at N³LL'+aN³LO*, Phys. Rev. D **110** (2024), no. 7, 076005, [arXiv:2306.16458 [hep-ph]].
- [147] C. W. Bauer, D. Pirjol and I. W. Stewart, *Soft collinear factorization in effective field theory*, Phys. Rev. D **65** (2002), 054022, [hep-ph/0109045].
- [148] C. W. Bauer and I. W. Stewart, *Invariant operators in collinear effective theory*, Phys. Lett. B **516** (2001), 134–142, [hep-ph/0107001].
- [149] C. W. Bauer, S. Fleming, D. Pirjol and I. W. Stewart, *An Effective field theory for collinear and soft gluons: Heavy to light decays*, Phys. Rev. D **63** (2001), 114020, [hep-ph/0011336].
- [150] C. W. Bauer, S. Fleming and M. E. Luke, *Summing Sudakov logarithms in $B \rightarrow X_s \gamma$ in effective field theory.*, Phys. Rev. D **63** (2000), 014006, [hep-ph/0005275].
- [151] C. W. Bauer, S. Fleming, D. Pirjol, I. Z. Rothstein and I. W. Stewart, *Hard scattering factorization from effective field theory*, Phys. Rev. D **66** (2002), 014017, [hep-ph/0202088].
- [152] M. Beneke, A. P. Chapovsky, M. Diehl and T. Feldmann, *Soft collinear effective theory and heavy to light currents beyond leading power*, Nucl. Phys. B **643** (2002), 431–476, [hep-ph/0206152].
- [153] M. Beneke and T. Feldmann, *Multipole expanded soft collinear effective theory with nonAbelian gauge symmetry*, Phys. Lett. B **553** (2003), 267–276, [hep-ph/0211358].
- [154] C. W. Bauer, D. Pirjol and I. W. Stewart, *Factorization and endpoint singularities in heavy to light decays*, Phys. Rev. D **67** (2003), 071502, [hep-ph/0211069].
- [155] B. O. Lange and M. Neubert, *Factorization and the soft overlap contribution to heavy to light form-factors*, Nucl. Phys. B **690** (2004), 249–278, [hep-ph/0311345], [Erratum: Nucl.Phys.B 723, 201–202 (2005)].
- [156] M. Beneke and T. Feldmann, *Factorization of heavy to light form-factors in soft collinear effective theory*, Nucl. Phys. B **685** (2004), 249–296, [hep-ph/0311335].
- [157] E. Eichten and B. R. Hill, *An Effective Field Theory for the Calculation of Matrix Elements Involving Heavy Quarks*, Phys. Lett. B **234** (1990), 511–516.
- [158] H. Georgi, *An Effective Field Theory for Heavy Quarks at Low-energies*, Phys. Lett. B **240** (1990), 447–450.
- [159] B. Grinstein, *The Static Quark Effective Theory*, Nucl. Phys. B **339** (1990), 253–268.
- [160] M. Neubert, *Heavy quark symmetry*, Phys. Rept. **245** (1994), 259–396, [hep-ph/9306320].
- [161] A. Pineda and J. Soto, *Effective field theory for ultrasoft momenta in NRQCD and NRQED*, Nucl. Phys. B Proc. Suppl. **64** (1998), 428–432, [hep-ph/9707481].
- [162] N. Brambilla, A. Pineda, J. Soto and A. Vairo, *Potential NRQCD: An Effective theory for heavy quarkonium*, Nucl. Phys. B **566** (2000), 275, [hep-ph/9907240].
- [163] M. Beneke, *Perturbative heavy quark - anti-quark systems*, PoS **hf8** (1999), 009, [hep-ph/9911490].
- [164] M. Beneke, A. Signer and V. A. Smirnov, *Top quark production near threshold and the top quark mass*, Phys. Lett. B **454** (1999), 137–146, [hep-ph/9903260].
- [165] M. E. Luke, A. V. Manohar and I. Z. Rothstein, *Renormalization group scaling in nonrelativistic QCD*, Phys. Rev. D **61** (2000), 074025, [hep-ph/9910209].
- [166] A. V. Manohar and I. W. Stewart, *Renormalization group analysis of the QCD quark potential to order v^{**2}* , Phys. Rev. D **62** (2000), 014033, [hep-ph/9912226].
- [167] A. V. Manohar and I. W. Stewart, *The QCD heavy quark potential to order v^{**2} : One loop matching conditions*, Phys. Rev. D **62** (2000), 074015, [hep-ph/0003032].

- [168] A. V. Manohar and I. W. Stewart, *Running of the heavy quark production current and $1/v$ potential in QCD*, Phys. Rev. D **63** (2001), 054004, [hep-ph/0003107].
- [169] A. H. Hoang, *Heavy quarkonium dynamics*, hep-ph/0204299.
- [170] A. Pineda and A. Signer, *Heavy Quark Pair Production near Threshold with Potential Non-Relativistic QCD*, Nucl. Phys. B **762** (2007), 67–94, [hep-ph/0607239].
- [171] A. Pineda and J. Soto, *The Renormalization group improvement of the QCD static potentials*, Phys. Lett. B **495** (2000), 323–328, [hep-ph/0007197].
- [172] W.-L. Ju and L. L. Yang, *Resummation of soft and Coulomb corrections for $t\bar{t}h$ production at the LHC*, JHEP **06** (2019), 050, [arXiv:1904.08744 [hep-ph]].
- [173] I. Balitsky and A. Tarasov, *Power corrections to TMD factorization for Z-boson production*, JHEP **05** (2018), 150, [arXiv:1712.09389 [hep-ph]].
- [174] I. Balitsky, *Gauge-invariant TMD factorization for Drell-Yan hadronic tensor at small x* , JHEP **05** (2021), 046, [arXiv:2012.01588 [hep-ph]].
- [175] I. Balitsky, *Drell-Yan angular lepton distributions at small x from TMD factorization.*, JHEP **09** (2021), 022, [arXiv:2105.13391 [hep-ph]].
- [176] I. Balitsky and A. Tarasov, *Higher-twist corrections to gluon TMD factorization*, JHEP **07** (2017), 095, [arXiv:1706.01415 [hep-ph]].
- [177] A. Vladimirov, V. Moos and I. Scimemi, *Transverse momentum dependent operator expansion at next-to-leading power*, JHEP **01** (2022), 110, [arXiv:2109.09771 [hep-ph]].
- [178] M. A. Ebert, A. Gao and I. W. Stewart, *Factorization for azimuthal asymmetries in SIDIS at next-to-leading power*, JHEP **06** (2022), 007, [arXiv:2112.07680 [hep-ph]], [Erratum: JHEP **07**, 096 (2023)].
- [179] L. Gamberg, Z.-B. Kang, D. Y. Shao, J. Terry and F. Zhao, *Transverse-momentum-dependent factorization at next-to-leading power*, arXiv:2211.13209 [hep-ph].
- [180] S. Rodini and A. Vladimirov, *Factorization for quasi-TMD distributions of sub-leading power*, JHEP **09** (2023), 117, [arXiv:2211.04494 [hep-ph]].
- [181] S. Rodini and A. Vladimirov, *Transverse momentum dependent factorization for SIDIS at next-to-leading power*, Phys. Rev. D **110** (2024), no. 3, 034009, [arXiv:2306.09495 [hep-ph]].
- [182] A. Vladimirov, *Kinematic power corrections in TMD factorization theorem*, JHEP **12** (2023), 008, [arXiv:2307.13054 [hep-ph]].
- [183] S. Rodini, A. C. Alvaro and B. Pasquini, *Collinear matching for next-to-leading power transverse-momentum distributions*, Phys. Lett. B **845** (2023), 138163, [arXiv:2306.15052 [hep-ph]].
- [184] M. A. Ebert, I. Moulton, I. W. Stewart, F. J. Tackmann, G. Vita and H. X. Zhu, *Subleading power rapidity divergences and power corrections for q_T* , JHEP **04** (2019), 123, [arXiv:1812.08189 [hep-ph]].
- [185] M. Inglis-Whalen, M. Luke, J. Roy and A. Spourdalakis, *Factorization of power corrections in the Drell-Yan process in EFT*, Phys. Rev. D **104** (2021), no. 7, 076018, [arXiv:2105.09277 [hep-ph]].
- [186] M. Inglis-Whalen, *Power Corrections and Rapidity Logarithms in Soft-collinear Effective Theory*, Ph.D. thesis, Toronto U., 2022.
- [187] G. Ferrera, W.-L. Ju and M. Schönherr, *Zero-bin subtraction and the q_T spectrum beyond leading power*, JHEP **04** (2024), 005, [arXiv:2312.14911 [hep-ph]].
- [188] J. Campbell, T. Neumann and G. Vita, *Projection-to-Born-improved Subtractions at NNLO*, arXiv:2408.05265 [hep-ph].
- [189] M. Beneke, A. P. Chapovsky, A. Signer and G. Zanderighi, *Effective theory approach to unstable particle production*, Phys. Rev. Lett. **93** (2004), 011602, [hep-ph/0312331].

- [190] M. Beneke, A. P. Chapovsky, A. Signer and G. Zanderighi, *Effective theory calculation of resonant high-energy scattering*, Nucl. Phys. B **686** (2004), 205–247, [[hep-ph/0401002](#)].
- [191] A. H. Hoang and C. J. Reisser, *Electroweak absorptive parts in NRQCD matching conditions*, Phys. Rev. D **71** (2005), 074022, [[hep-ph/0412258](#)].
- [192] A. H. Hoang and C. J. Reisser, *On electroweak matching conditions for top pair production at threshold*, Phys. Rev. D **74** (2006), 034002, [[hep-ph/0604104](#)].
- [193] M. Beneke, B. Jantzen and P. Ruiz-Femenia, *Electroweak non-resonant NLO corrections to $e^+e^- \rightarrow W^+W^-b\bar{b}$ in the $t\bar{t}$ resonance region*, Nucl. Phys. B **840** (2010), 186–213, [[arXiv:1004.2188](#)] [[hep-ph](#)].
- [194] A. A. Penin and J. H. Piclum, *Threshold production of unstable top*, JHEP **01** (2012), 034, [[arXiv:1110.1970](#)] [[hep-ph](#)].
- [195] B. Jantzen and P. Ruiz-Femenia, *Next-to-next-to-leading order nonresonant corrections to threshold top-pair production from e^+e^- collisions: Endpoint-singular terms*, Phys. Rev. D **88** (2013), no. 5, 054011, [[arXiv:1307.4337](#)] [[hep-ph](#)].
- [196] M. Beneke, A. Maier, T. Rauh and P. Ruiz-Femenia, *Non-resonant and electroweak NNLO correction to the e^+e^- top anti-top threshold*, JHEP **02** (2018), 125, [[arXiv:1711.10429](#)] [[hep-ph](#)].
- [197] T. Becher, N. Schalch and X. Xu, *Resummation of Next-to-Leading Nonglobal Logarithms at the LHC*, Phys. Rev. Lett. **132** (2024), no. 8, 081602, [[arXiv:2307.02283](#)] [[hep-ph](#)].
- [198] T. Becher, M. Neubert, D. Y. Shao and M. Stillger, *Factorization of non-global LHC observables and resummation of super-leading logarithms*, JHEP **12** (2023), 116, [[arXiv:2307.06359](#)] [[hep-ph](#)].
- [199] T. Becher, P. Hager, G. Martinelli, M. Neubert, D. Schwienbacher and M. Stillger, *Super-Leading Logarithms in $pp \rightarrow 2$ Jets*, [arXiv:2411.12742](#) [[hep-ph](#)].
- [200] N. Kidonakis and G. F. Sterman, *Resummation for QCD hard scattering*, Nucl. Phys. B **505** (1997), 321–348, [[hep-ph/9705234](#)].
- [201] R. Bonciani, S. Catani, M. L. Mangano and P. Nason, *NLL resummation of the heavy quark hadroproduction cross-section*, Nucl. Phys. B **529** (1998), 424–450, [[hep-ph/9801375](#)], [Erratum: Nucl.Phys.B 803, 234 (2008)].
- [202] N. Kidonakis, E. Laenen, S. Moch and R. Vogt, *Sudakov resummation and finite order expansions of heavy quark hadroproduction cross-sections*, Phys. Rev. D **64** (2001), 114001, [[hep-ph/0105041](#)].
- [203] A. Broggio, A. Ferroglia, B. D. Pecjak, A. Signer and L. L. Yang, *Associated production of a top pair and a Higgs boson beyond NLO*, JHEP **03** (2016), 124, [[arXiv:1510.01914](#)] [[hep-ph](#)].
- [204] A. Broggio, A. Ferroglia, B. D. Pecjak and L. L. Yang, *NNLL resummation for the associated production of a top pair and a Higgs boson at the LHC*, JHEP **02** (2017), 126, [[arXiv:1611.00049](#)] [[hep-ph](#)].
- [205] A. Broggio, A. Ferroglia, G. Ossola, B. D. Pecjak and R. D. Sameshima, *Associated production of a top pair and a Z boson at the LHC to NNLL accuracy*, JHEP **04** (2017), 105, [[arXiv:1702.00800](#)] [[hep-ph](#)].
- [206] A. Kulesza, L. Motyka, T. Stebel and V. Theeuwes, *Associated $t\bar{t}H$ production at the LHC: Theoretical predictions at NLO+NNLL accuracy*, Phys. Rev. D **97** (2018), no. 11, 114007, [[arXiv:1704.03363](#)] [[hep-ph](#)].
- [207] A. Kulesza, L. Motyka, T. Stebel and V. Theeuwes, *Improving predictions for associated $t\bar{t}H$ production at the LHC: soft gluon resummation through NNLL accuracy*, PoS **EPS-HEP2017** (2017), 339, [[arXiv:1710.06358](#)] [[hep-ph](#)].
- [208] A. Kulesza, L. Motyka, D. Schwartzländer, T. Stebel and V. Theeuwes, *Associated production of a top quark pair with a heavy electroweak gauge boson at NLO+NNLL accuracy*, Eur. Phys. J. C **79** (2019), no. 3, 249, [[arXiv:1812.08622](#)] [[hep-ph](#)].

- [209] M. van Beekveld, A. Kulesza and L. M. Valero, *Threshold Resummation for the Production of Four Top Quarks at the LHC*, Phys. Rev. Lett. **131** (2023), no. 21, 211901, [arXiv:2212.03259 [hep-ph]].
- [210] A. J. Buras, M. Jamin, M. E. Lautenbacher and P. H. Weisz, *Effective Hamiltonians for $\Delta S = 1$ and $\Delta B = 1$ nonleptonic decays beyond the leading logarithmic approximation*, Nucl. Phys. B **370** (1992), 69–104, [Addendum: Nucl.Phys.B 375, 501 (1992)].
- [211] G. Buchalla, A. J. Buras and M. E. Lautenbacher, *Weak decays beyond leading logarithms*, Rev. Mod. Phys. **68** (1996), 1125–1144, [hep-ph/9512380].
- [212] A. Ferroglia, M. Neubert, B. D. Pecjak and L. L. Yang, *Two-loop divergences of massive scattering amplitudes in non-abelian gauge theories*, JHEP **11** (2009), 062, [arXiv:0908.3676 [hep-ph]].
- [213] A. Ferroglia, M. Neubert, B. D. Pecjak and L. L. Yang, *Two-loop divergences of scattering amplitudes with massive partons*, Phys. Rev. Lett. **103** (2009), 201601, [arXiv:0907.4791 [hep-ph]].
- [214] J. C. Collins, D. E. Soper and G. F. Sterman, *Factorization of Hard Processes in QCD*, Adv. Ser. Direct. High Energy Phys. **5** (1989), 1–91, [hep-ph/0409313].
- [215] R. Bonciani, S. Catani, M. Grazzini, H. Sargsyan and A. Torre, *The q_T subtraction method for top quark production at hadron colliders*, Eur. Phys. J. C **75** (2015), no. 12, 581, [arXiv:1508.03585 [hep-ph]].
- [216] S. Catani, I. Fabre, M. Grazzini and S. Kallweit, *$t\bar{t}H$ production at NNLO: the flavour off-diagonal channels*, Eur. Phys. J. C **81** (2021), no. 6, 491, [arXiv:2102.03256 [hep-ph]].
- [217] S. Catani, S. Devoto, M. Grazzini, S. Kallweit, J. Mazzitelli and C. Savoini, *Higgs Boson Production in Association with a Top-Antitop Quark Pair in Next-to-Next-to-Leading Order QCD*, Phys. Rev. Lett. **130** (2023), no. 11, 111902, [arXiv:2210.07846 [hep-ph]].
- [218] L. Buonocore, S. Devoto, S. Kallweit, J. Mazzitelli, L. Rottoli and C. Savoini, *Associated production of a W boson and massive bottom quarks at next-to-next-to-leading order in QCD*, Phys. Rev. D **107** (2023), no. 7, 074032, [arXiv:2212.04954 [hep-ph]].
- [219] S. Catani, S. Devoto, M. Grazzini, S. Kallweit and J. Mazzitelli, *Bottom-quark production at hadron colliders: fully differential predictions in NNLO QCD*, JHEP **03** (2021), 029, [arXiv:2010.11906 [hep-ph]].
- [220] L. Buonocore, S. Devoto, M. Grazzini, S. Kallweit, J. Mazzitelli, L. Rottoli and C. Savoini, *Precise Predictions for the Associated Production of a W Boson with a Top-Antitop Quark Pair at the LHC*, Phys. Rev. Lett. **131** (2023), no. 23, 231901, [arXiv:2306.16311 [hep-ph]].
- [221] J. Mazzitelli, A. Ratti, M. Wiesemann and G. Zanderighi, *B -hadron production at the LHC from bottom-quark pair production at NNLO+PS*, Phys. Lett. B **843** (2023), 137991, [arXiv:2302.01645 [hep-ph]].
- [222] J. Mazzitelli, V. Sotnikov and M. Wiesemann, *Next-to-next-to-leading order event generation for Z -boson production in association with a bottom-quark pair*, arXiv:2404.08598 [hep-ph].
- [223] M. Beneke and V. A. Smirnov, *Asymptotic expansion of Feynman integrals near threshold*, Nucl. Phys. B **522** (1998), 321–344, [hep-ph/9711391].
- [224] V. A. Smirnov, *Applied asymptotic expansions in momenta and masses*, Springer Tracts Mod. Phys. **177** (2002), 1–262.
- [225] V. A. Smirnov, *Analytic tools for Feynman integrals*, vol. 250, 2012.
- [226] B. Jantzen, *Foundation and generalization of the expansion by regions*, JHEP **12** (2011), 076, [arXiv:1111.2589 [hep-ph]].
- [227] J. C. Collins, *INTRINSIC TRANSVERSE MOMENTUM. 1. NONGAUGE THEORIES*, Phys. Rev. D **21** (1980), 2962.

- [228] J. C. Collins and D. E. Soper, *Back-To-Back Jets in QCD*, Nucl. Phys. B **193** (1981), 381, [Erratum: Nucl.Phys.B 213, 545 (1983)].
- [229] Y.-T. Chien, D. Y. Shao and B. Wu, *Resummation of Boson-Jet Correlation at Hadron Colliders*, JHEP **11** (2019), 025, [arXiv:1905.01335 [hep-ph]].
- [230] L. Chen, G.-Y. Qin, L. Wang, S.-Y. Wei, B.-W. Xiao, H.-Z. Zhang and Y.-Q. Zhang, *Study of Isolated-photon and Jet Momentum Imbalance in pp and PbPb collisions*, Nucl. Phys. B **933** (2018), 306–319, [arXiv:1803.10533 [hep-ph]].
- [231] Y.-T. Chien, R. Rahn, S. Schrijnder van Velzen, D. Y. Shao, W. J. Waalewijn and B. Wu, *Recoil-free azimuthal angle for precision boson-jet correlation*, Phys. Lett. B **815** (2021), 136124, [arXiv:2005.12279 [hep-ph]].
- [232] H. Bouaziz, Y. Delenda and K. Khelifa-Kerfa, *Azimuthal decorrelation between a jet and a Z boson at hadron colliders*, JHEP **10** (2022), 006, [arXiv:2207.10147 [hep-ph]].
- [233] Y.-T. Chien, R. Rahn, D. Y. Shao, W. J. Waalewijn and B. Wu, *Precision boson-jet azimuthal decorrelation at hadron colliders*, JHEP **02** (2023), 256, [arXiv:2205.05104 [hep-ph]].
- [234] R. F. del Castillo, M. G. Echevarria, Y. Makris and I. Scimemi, *Transverse momentum dependent distributions in dijet and heavy hadron pair production at EIC*, JHEP **03** (2022), 047, [arXiv:2111.03703 [hep-ph]].
- [235] A. Banfi, M. Dasgupta and Y. Delenda, *Azimuthal decorrelations between QCD jets at all orders*, Phys. Lett. B **665** (2008), 86–91, [arXiv:0804.3786 [hep-ph]].
- [236] C. Zhang, Q.-S. Dai and D. Y. Shao, *Azimuthal decorrelation for photon induced dijet production in ultra-peripheral collisions of heavy ions*, JHEP **2023** (2023), no. 02, 002, [arXiv:2211.07071 [hep-ph]].
- [237] M.-S. Gao, Z.-B. Kang, D. Y. Shao, J. Terry and C. Zhang, *QCD resummation of dijet azimuthal decorrelations in pp and pA collisions*, JHEP **10** (2023), 013, [arXiv:2306.09317 [hep-ph]].
- [238] Y. Li, D. Neill and H. X. Zhu, *An exponential regulator for rapidity divergences*, Nucl. Phys. B **960** (2020), 115193, [arXiv:1604.00392 [hep-ph]].
- [239] Y. Li and H. X. Zhu, *Bootstrapping Rapidity Anomalous Dimensions for Transverse-Momentum Resummation*, Phys. Rev. Lett. **118** (2017), no. 2, 022004, [arXiv:1604.01404 [hep-ph]].
- [240] R. Angeles-Martinez, M. Czakon and S. Sapeta, *NNLO soft function for top quark pair production at small transverse momentum*, JHEP **10** (2018), 201, [arXiv:1809.01459 [hep-ph]].
- [241] T. Gehrmann, T. Lubbert and L. L. Yang, *Transverse parton distribution functions at next-to-next-to-leading order: the quark-to-quark case*, Phys. Rev. Lett. **109** (2012), 242003, [arXiv:1209.0682 [hep-ph]].
- [242] T. Gehrmann, T. Luebbert and L. L. Yang, *Calculation of the transverse parton distribution functions at next-to-next-to-leading order*, JHEP **06** (2014), 155, [arXiv:1403.6451 [hep-ph]].
- [243] T. Becher and G. Bell, *Analytic Regularization in Soft-Collinear Effective Theory*, Phys. Lett. B **713** (2012), 41–46, [arXiv:1112.3907 [hep-ph]].
- [244] S. Catani and M. Grazzini, *Higgs Boson Production at Hadron Colliders: Hard-Collinear Coefficients at the NNLO*, Eur. Phys. J. C **72** (2012), 2013, [arXiv:1106.4652 [hep-ph]], [Erratum: Eur.Phys.J.C 72, 2132 (2012)].
- [245] S. Catani and P. K. Dhani, *Collinear functions for QCD resummations*, JHEP **03** (2023), 200, [arXiv:2208.05840 [hep-ph]].
- [246] S. Catani, S. Devoto, M. Grazzini and J. Mazzitelli, *Soft-parton contributions to heavy-quark production at low transverse momentum*, JHEP **04** (2023), 144, [arXiv:2301.11786 [hep-ph]].

- [247] M. Beneke, P. Falgari and C. Schwinn, *Soft radiation in heavy-particle pair production: All-order colour structure and two-loop anomalous dimension*, Nucl. Phys. B **828** (2010), 69–101, [[arXiv:0907.1443](#) [hep-ph]].
- [248] S. Actis, A. Denner, L. Hofer, A. Scharf and S. Uccirati, *Recursive generation of one-loop amplitudes in the Standard Model*, JHEP **04** (2013), 037, [[arXiv:1211.6316](#) [hep-ph]].
- [249] S. Actis, A. Denner, L. Hofer, J.-N. Lang, A. Scharf and S. Uccirati, *RECOLA: REcursive Computation of One-Loop Amplitudes*, Comput. Phys. Commun. **214** (2017), 140–173, [[arXiv:1605.01090](#) [hep-ph]].
- [250] W. Beenakker, S. Dittmaier, M. Kramer, B. Plumper, M. Spira and P. M. Zerwas, *NLO QCD corrections to t anti- t H production in hadron collisions*, Nucl. Phys. B **653** (2003), 151–203, [[hep-ph/0211352](#)].
- [251] L. Chen, M. Czakon and R. Poncelet, *Polarized double-virtual amplitudes for heavy-quark pair production*, JHEP **03** (2018), 085, [[arXiv:1712.08075](#) [hep-ph]].
- [252] S. Di Vita, T. Gehrmann, S. Laporta, P. Mastrolia, A. Primo and U. Schubert, *Master integrals for the NNLO virtual corrections to $q\bar{q} \rightarrow t\bar{t}$ scattering in QCD: the non-planar graphs*, JHEP **06** (2019), 117, [[arXiv:1904.10964](#) [hep-ph]].
- [253] S. Badger, E. Chaubey, H. B. Hartanto and R. Marzucca, *Two-loop leading colour QCD helicity amplitudes for top quark pair production in the gluon fusion channel*, JHEP **06** (2021), 163, [[arXiv:2102.13450](#) [hep-ph]].
- [254] M. K. Mandal, P. Mastrolia, J. Ronca and W. J. Bobadilla Torres, *Two-loop scattering amplitude for heavy-quark pair production through light-quark annihilation in QCD*, JHEP **09** (2022), 129, [[arXiv:2204.03466](#) [hep-ph]].
- [255] G. Wang, T. Xia, L. L. Yang and X. Ye, *On the high-energy behavior of massive QCD amplitudes*, JHEP **05** (2024), 082, [[arXiv:2312.12242](#) [hep-ph]].
- [256] M.-x. Luo, T.-Z. Yang, H. X. Zhu and Y. J. Zhu, *Unpolarized quark and gluon TMD PDFs and FFs at N^3LO* , JHEP **06** (2021), 115, [[arXiv:2012.03256](#) [hep-ph]].
- [257] M.-x. Luo, T.-Z. Yang, H. X. Zhu and Y. J. Zhu, *Quark Transverse Parton Distribution at the Next-to-Next-to-Next-to-Leading Order*, Phys. Rev. Lett. **124** (2020), no. 9, 092001, [[arXiv:1912.05778](#) [hep-ph]].
- [258] M.-X. Luo, T.-Z. Yang, H. X. Zhu and Y. J. Zhu, *Transverse Parton Distribution and Fragmentation Functions at NNLO: the Gluon Case*, JHEP **01** (2020), 040, [[arXiv:1909.13820](#) [hep-ph]].
- [259] J.-y. Chiu, A. Jain, D. Neill and I. Z. Rothstein, *The Rapidity Renormalization Group*, Phys. Rev. Lett. **108** (2012), 151601, [[arXiv:1104.0881](#) [hep-ph]].
- [260] J.-Y. Chiu, A. Jain, D. Neill and I. Z. Rothstein, *A Formalism for the Systematic Treatment of Rapidity Logarithms in Quantum Field Theory*, JHEP **05** (2012), 084, [[arXiv:1202.0814](#) [hep-ph]].
- [261] S. Moch, J. A. M. Vermaseren and A. Vogt, *The Three loop splitting functions in QCD: The Nonsinglet case*, Nucl. Phys. B **688** (2004), 101–134, [[hep-ph/0403192](#)].
- [262] J. M. Henn, G. P. Korchemsky and B. Mistlberger, *The full four-loop cusp anomalous dimension in $\mathcal{N} = 4$ super Yang-Mills and QCD*, JHEP **04** (2020), 018, [[arXiv:1911.10174](#) [hep-th]].
- [263] A. von Manteuffel, E. Panzer and R. M. Schabinger, *Cusp and collinear anomalous dimensions in four-loop QCD from form factors*, Phys. Rev. Lett. **124** (2020), no. 16, 162001, [[arXiv:2002.04617](#) [hep-ph]].
- [264] F. Herzog, S. Moch, B. Ruijl, T. Ueda, J. A. M. Vermaseren and A. Vogt, *Five-loop contributions to low- N non-singlet anomalous dimensions in QCD*, Phys. Lett. B **790** (2019), 436–443, [[arXiv:1812.11818](#) [hep-ph]].

- [265] M.-X. Luo, X. Wang, X. Xu, L. L. Yang, T.-Z. Yang and H. X. Zhu, *Transverse Parton Distribution and Fragmentation Functions at NNLO: the Quark Case*, JHEP **10** (2019), 083, [[arXiv:1908.03831 \[hep-ph\]](#)].
- [266] A. A. Vladimirov, *Correspondence between Soft and Rapidity Anomalous Dimensions*, Phys. Rev. Lett. **118** (2017), no. 6, 062001, [[arXiv:1610.05791 \[hep-ph\]](#)].
- [267] M. A. Ebert, B. Mistlberger and G. Vita, *Transverse momentum dependent PDFs at N^3LO* , JHEP **09** (2020), 146, [[arXiv:2006.05329 \[hep-ph\]](#)].
- [268] G. Das, S.-O. Moch and A. Vogt, *Soft corrections to inclusive deep-inelastic scattering at four loops and beyond*, JHEP **03** (2020), 116, [[arXiv:1912.12920 \[hep-ph\]](#)].
- [269] C. Duhr, B. Mistlberger and G. Vita, *Soft integrals and soft anomalous dimensions at N^3LO and beyond*, JHEP **09** (2022), 155, [[arXiv:2205.04493 \[hep-ph\]](#)].
- [270] C. Duhr, B. Mistlberger and G. Vita, *Four-Loop Rapidity Anomalous Dimension and Event Shapes to Fourth Logarithmic Order*, Phys. Rev. Lett. **129** (2022), no. 16, 162001, [[arXiv:2205.02242 \[hep-ph\]](#)].
- [271] I. Moulton, H. X. Zhu and Y. J. Zhu, *The four loop QCD rapidity anomalous dimension*, JHEP **08** (2022), 280, [[arXiv:2205.02249 \[hep-ph\]](#)].
- [272] B. A. Kniehl, A. A. Penin, V. A. Smirnov and M. Steinhauser, *Potential NRQCD and heavy quarkonium spectrum at next-to-next-to-next-to-leading order*, Nucl. Phys. B **635** (2002), 357–383, [[hep-ph/0203166](#)].
- [273] T. Hahn, *Generating Feynman diagrams and amplitudes with FeynArts 3*, Comput. Phys. Commun. **140** (2001), 418–431, [[hep-ph/0012260](#)].
- [274] R. Mertig, M. Bohm and A. Denner, *FEYN CALC: Computer algebraic calculation of Feynman amplitudes*, Comput. Phys. Commun. **64** (1991), 345–359.
- [275] V. Shtabovenko, R. Mertig and F. Orellana, *New Developments in FeynCalc 9.0*, Comput. Phys. Commun. **207** (2016), 432–444, [[arXiv:1601.01167 \[hep-ph\]](#)].
- [276] V. Shtabovenko, R. Mertig and F. Orellana, *FeynCalc 9.3: New features and improvements*, Comput. Phys. Commun. **256** (2020), 107478, [[arXiv:2001.04407 \[hep-ph\]](#)].
- [277] V. Shtabovenko, *FeynHelpers: Connecting FeynCalc to FIRE and Package-X*, Comput. Phys. Commun. **218** (2017), 48–65, [[arXiv:1611.06793 \[physics.comp-ph\]](#)].
- [278] N. Brambilla, H. S. Chung, V. Shtabovenko and A. Vairo, *FeynOnium: Using FeynCalc for automatic calculations in Nonrelativistic Effective Field Theories*, JHEP **11** (2020), 130, [[arXiv:2006.15451 \[hep-ph\]](#)].
- [279] T. Becher and M. Neubert, *Infrared singularities of scattering amplitudes in perturbative QCD*, Phys. Rev. Lett. **102** (2009), 162001, [[arXiv:0901.0722 \[hep-ph\]](#)], [Erratum: Phys.Rev.Lett. **111**, 199905 (2013)].
- [280] P. Bärnreuther, M. Czakon and P. Fiedler, *Virtual amplitudes and threshold behaviour of hadronic top-quark pair-production cross sections*, JHEP **02** (2014), 078, [[arXiv:1312.6279 \[hep-ph\]](#)].
- [281] M. Czakon and P. Fiedler, *The soft function for color octet production at threshold*, Nucl. Phys. B **879** (2014), 236–255, [[arXiv:1311.2541 \[hep-ph\]](#)].
- [282] G. Wang, X. Xu, L. L. Yang and H. X. Zhu, *The next-to-next-to-leading order soft function for top quark pair production*, JHEP **06** (2018), 013, [[arXiv:1804.05218 \[hep-ph\]](#)].
- [283] V. A. Smirnov, *Analytical result for dimensionally regularized massless on shell double box*, Phys. Lett. B **460** (1999), 397–404, [[hep-ph/9905323](#)].
- [284] J. B. Tausk, *Nonplanar massless two loop Feynman diagrams with four on-shell legs*, Phys. Lett. B **469** (1999), 225–234, [[hep-ph/9909506](#)].

- [285] T. Hahn, *Routines for the diagonalization of complex matrices*, physics/0607103.
- [286] T. van Ritbergen, J. A. M. Vermaseren and S. A. Larin, *The Four loop beta function in quantum chromodynamics*, Phys. Lett. B **400** (1997), 379–384, [hep-ph/9701390].
- [287] M. Czakon, *The Four-loop QCD beta-function and anomalous dimensions*, Nucl. Phys. B **710** (2005), 485–498, [hep-ph/0411261].
- [288] A. Banfi, P. F. Monni, G. P. Salam and G. Zanderighi, *Higgs and Z-boson production with a jet veto*, Phys. Rev. Lett. **109** (2012), 202001, [arXiv:1206.4998 [hep-ph]].
- [289] A. Banfi, G. P. Salam and G. Zanderighi, *NLL+NNLO predictions for jet-veto efficiencies in Higgs-boson and Drell-Yan production*, JHEP **06** (2012), 159, [arXiv:1203.5773 [hep-ph]].
- [290] T. Gleisberg, S. Hoeche, F. Krauss, A. Schalicke, S. Schumann and J.-C. Winter, *SHERPA 1. alpha: A Proof of concept version*, JHEP **02** (2004), 056, [hep-ph/0311263].
- [291] T. Gleisberg, S. Hoeche, F. Krauss, M. Schonherr, S. Schumann, F. Siegert and J. Winter, *Event generation with SHERPA 1.1*, JHEP **02** (2009), 007, [arXiv:0811.4622 [hep-ph]].
- [292] E. Bothmann et al., Sherpa collaboration, *Event Generation with Sherpa 2.2*, SciPost Phys. **7** (2019), no. 3, 034, [arXiv:1905.09127 [hep-ph]].
- [293] E. Bothmann et al., Sherpa collaboration, *Event generation with Sherpa 3*, arXiv:2410.22148 [hep-ph].
- [294] A. Buckley, J. Ferrando, S. Lloyd, K. Nordström, B. Page, M. Rüfenacht, M. Schönherr and G. Watt, *LHAPDF6: parton density access in the LHC precision era*, Eur. Phys. J. C **75** (2015), 132, [arXiv:1412.7420 [hep-ph]].
- [295] E. Bothmann, A. Buckley, I. A. Christidi, C. Gütschow, S. Höche, M. Knobbe, T. Martin and M. Schönherr, *Accelerating LHC event generation with simplified pilot runs and fast PDFs*, Eur. Phys. J. C **82** (2022), no. 12, 1128, [arXiv:2209.00843 [hep-ph]].
- [296] R. D. Ball et al., NNPDF collaboration, *Parton distributions from high-precision collider data*, Eur. Phys. J. C **77** (2017), no. 10, 663, [arXiv:1706.00428 [hep-ph]].
- [297] T. Hahn, *CUBA: A Library for multidimensional numerical integration*, Comput. Phys. Commun. **168** (2005), 78–95, [hep-ph/0404043].
- [298] T. Hahn, *Concurrent Cuba*, J. Phys. Conf. Ser. **608** (2015), no. 1, 012066, [arXiv:1408.6373 [physics.comp-ph]].
- [299] F. Krauss, R. Kuhn and G. Soff, *AMEGIC++ 1.0: A Matrix element generator in C++*, JHEP **02** (2002), 044, [hep-ph/0109036].
- [300] A. Buckley, J. Butterworth, D. Grellscheid, H. Hoeth, L. Lonnblad, J. Monk, H. Schulz and F. Siegert, *Rivet user manual*, Comput. Phys. Commun. **184** (2013), 2803–2819, [arXiv:1003.0694 [hep-ph]].
- [301] C. Bierlich et al., *Robust Independent Validation of Experiment and Theory: Rivet version 3*, SciPost Phys. **8** (2020), 026, [arXiv:1912.05451 [hep-ph]].
- [302] C. Bierlich, A. Buckley, J. M. Butterworth, C. Gütschow, L. Lonnblad, T. Procter, P. Richardson and Y. Yeh, *Robust independent validation of experiment and theory: Rivet version 4 release note*, SciPost Phys. Codeb. **36** (2024), 1, [arXiv:2404.15984 [hep-ph]].
- [303] F. Cascioli, P. Maierhofer and S. Pozzorini, *Scattering Amplitudes with Open Loops*, Phys. Rev. Lett. **108** (2012), 111601, [arXiv:1111.5206 [hep-ph]].
- [304] S. Kallweit, J. M. Lindert, P. Maierhöfer, S. Pozzorini and M. Schönherr, *NLO electroweak automation and precise predictions for W+multijet production at the LHC*, JHEP **04** (2015), 012, [arXiv:1412.5157 [hep-ph]].

- [305] F. Buccioni, S. Pozzorini and M. Zoller, *On-the-fly reduction of open loops*, Eur. Phys. J. C **78** (2018), no. 1, 70, [[arXiv:1710.11452](#) [hep-ph]].
- [306] F. Buccioni, J.-N. Lang, J. M. Lindert, P. Maierhöfer, S. Pozzorini, H. Zhang and M. F. Zoller, *OpenLoops 2*, Eur. Phys. J. C **79** (2019), no. 10, 866, [[arXiv:1907.13071](#) [hep-ph]].
- [307] S. Catani and M. H. Seymour, *A General algorithm for calculating jet cross-sections in NLO QCD*, Nucl. Phys. B **485** (1997), 291–419, [[hep-ph/9605323](#)], [Erratum: Nucl.Phys.B 510, 503–504 (1998)].
- [308] S. Catani, S. Dittmaier, M. H. Seymour and Z. Trocsanyi, *The Dipole formalism for next-to-leading order QCD calculations with massive partons*, Nucl. Phys. B **627** (2002), 189–265, [[hep-ph/0201036](#)].
- [309] T. Gleisberg and F. Krauss, *Automating dipole subtraction for QCD NLO calculations*, Eur. Phys. J. C **53** (2008), 501–523, [[arXiv:0709.2881](#) [hep-ph]].
- [310] M. Schönherr, *An automated subtraction of NLO EW infrared divergences*, Eur. Phys. J. C **78** (2018), no. 2, 119, [[arXiv:1712.07975](#) [hep-ph]].
- [311] V. Ahrens, A. Ferroglia, M. Neubert, B. D. Pecjak and L.-L. Yang, *RG-improved single-particle inclusive cross sections and forward-backward asymmetry in $t\bar{t}$ production at hadron colliders*, JHEP **09** (2011), 070, [[arXiv:1103.0550](#) [hep-ph]].